Berichte
zur Polar-
und Meeresforschung

629
2011

Reports
on Polar and Marine Research

Russian-German Cooperation SYSTEM LAPTEV SEA:
The expedition Eastern Laptev Sea - Buor Khaya Peninsula 2010

Edited by
Sebastian Wetterich, Pier Paul Overduin
and Mikhail Grigoriev
with contributions of the participants

HELMHOLTZ
GEMEINSCHAFT

ALFRED-WEGENER-INSTITUT FÜR
POLAR- UND MEERESFORSCHUNG
in der Helmholtz-Gemeinschaft
D-27570 BREMERHAVEN
Bundesrepublik Deutschland

ISSN 1866-3192

Hinweis

Die Berichte zur Polar- und Meeresforschung werden vom Alfred-Wegener-Institut für Polar-und Meeresforschung in Bremerhaven* in unregelmäßiger Abfolge herausgegeben.

Sie enthalten Beschreibungen und Ergebnisse der vom Institut (AWI) oder mit seiner Unterstützung durchgeführten Forschungsarbeiten in den Polargebieten und in den Meeren.

Es werden veröffentlicht:

— Expeditionsberichte (inkl. Stationslisten und Routenkarten)
— Expeditionsergebnisse (inkl. Dissertationen)
— wissenschaftliche Ergebnisse der Antarktis-Stationen und anderer Forschungs-Stationen des AWI
— Berichte wissenschaftlicher Tagungen

Die Beiträge geben nicht notwendigerweise die Auffassung des Instituts wieder.

Notice

The Reports on Polar and Marine Research are issued by the Alfred Wegener Institute for Polar and Marine Research in Bremerhaven*, Federal Republic of Germany. They appear in irregular intervals.

They contain descriptions and results of investigations in polar regions and in the seas either conducted by the Institute (AWI) or with its support.

The following items are published:

— expedition reports (incl. station lists and route maps)
— expedition results (incl. Ph.D. theses)
— scientific results of the Antarctic stations and of other AWI research stations
— reports on scientific meetings

The papers contained in the Reports do not necessarily reflect the opinion of the Institute.

The „Berichte zur Polar- und Meeresforschung” continue the former „Berichte zur Polarforschung”

* Anschrift / Address
Alfred-Wegener-Institut
für Polar- und Meeresforschung
D-27570 Bremerhaven
Germany
www.awi.de

Editor in charge:
Dr. Horst Bornemann

Assistant editor:
Birgit Chiaventone

Die "Berichte zur Polar- und Meeresforschung" (ISSN 1866-3192) werden ab 2008 ausschließlich als Open-Access-Publikation herausgegeben (URL: http://epic.awi.de).

Since 2008 the "Reports on Polar and Marine Research" (ISSN 1866-3192) are only available as web-based open-access publications (URL: http://epic.awi.de)

Russian-German Cooperation SYSTEM LAPTEV SEA:

The expedition Eastern Laptev Sea - Buor Khaya Peninsula 2010

Sebastian Wetterich, Pier Paul Overduin and Mikhail Grigoriev

with contributions of the participants

Please cite or link this publication using the identifier hdl:10013/epic.37743 or http://hdl.handle.net/10013/epic.37743

ISSN 1866-3192

July 25 – August 25, 2010

Eastern Laptev Sea, Buor Khaya Peninsula

Russian expedition leaders:
Dr. Mikhail Grigoriev
Melnikov Permafrost Institute Yakutsk, SB RAS
Vice-Director for Science
Merzlotnaya St. 36, 677010 Yakutsk, Russia

Dr. Aleksandr Makarov
Arctic and Antarctic Research Institute
Beringa st. 38, 199397 St.Petersburg, Russia

German expedition leader:
Dr. Pier Paul Overduin
Alfred Wegener Institute for Polar and Marine Research
Department of Periglacial Research
Telegrafenberg A5, 14473 Potsdam, Germany

CONTENT

1. INTRODUCTION

Sebastian Wetterich & Aleksandr Makarov

1.1 Scientific rationale

The fieldwork in summer 2010 was undertaken by a joint Russian-German team on Buor Khaya Peninsula in the Eastern Laptev Sea (Fig. 1-1) in a transdisciplinary approach that combined the fields of coastal research, geophysics, geodesy, sedimentology, geocryology, Quaternary geology and modern ecology. The overall aim was to study coastal and nearshore permafrost, its surface features and the biological inventory in a region where such studies have not been performed so far. Doing so, a spatial gap was filled between the intensively studied Central Laptev Sea region (including the Lena Delta) to the west and the Dmitry Laptev Strait region to the east which have been the subject of the Russian-German research programs LAPTEV SEA and LAPTEV 2000 since 1998.

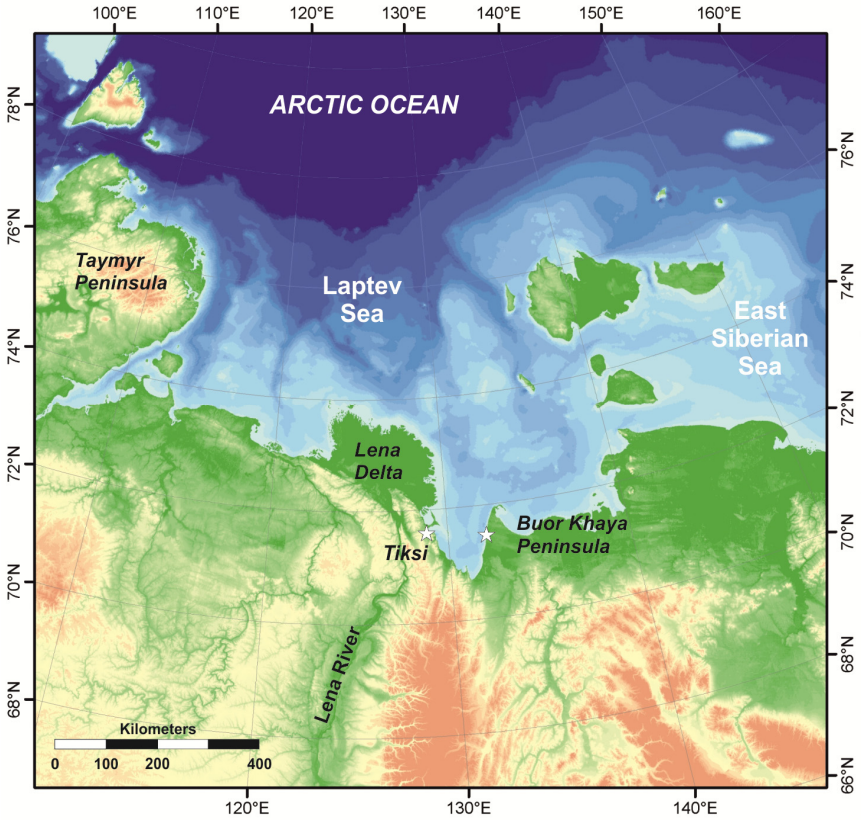

Figure 1-1: Position of the Buor Khaya Peninsula in the Eastern Laptev Sea. DEM compiled by G. Grosse (University of Alaska, Fairbanks, AK).

Buor Khaya Peninsula, located east of the settlement Tiksi, offers a variety of permafrost-related features on land and in the near shore zone. For the first time, botanic (chapter 2) and limnological (chapter 3) inventories were undertaken in order to obtain modern reference data for further palaeoecological applications.
A survey of the coastal stratigraphy and geomorphology (chapters 4 and 5) was undertaken to improve coastal classification, to determine today's coastline position for change rate determination and comparison with remote sensing products. The measurement of shoreface profiles on land and on sea supplies information on the stability of the coast and current mass fluxes. In addition, measurements of the thermokarst topography in the coastal hinterland was undertaken to capture the processes of the landscape dynamics by permafrost degradation as completely as possible. Supported by remote sensing data (ALOS, KOMPSAT, SPOT, RapidEye), the survey data will be used to create large-area digital elevation models. Such DEM help to estimate volume changes as a result of offshore mass movements and ice melt can be calculated.
Sediment samples from the onshore and submarine areas (chapter 6) allow direct comparison between the original source material and redeposited material and allow analysis of fossil carbon transformations and environmental indicators.
Geophysical measurements (Geoelectrical Resistivity Tomography, ERT) was used to capture the depth of the ice-bonded permafrost below seafloor (chapter 7) in preparation for a future subsea permafrost drilling campaign. The state of permafrost, its submarine environment and the degradation rate can be determined by the seafloor topography, and the temperature and salinity regimes, both in the water column and sediment. Since the occurrence of freshwater in the coastal area is determined by river water input and coastal erosion, we expect results at Buor Khaya to be broadly valid for large parts of the ice-rich Arctic permafrost coasts.
We obtained important information on baseline and sensitivity of the terrestrial permafrost from the structure and composition of the frozen coastal sequences exposed at the shoreline. The comparison of original, Late Pleistocene permafrost deposits with sediments accumulated in thermokarst depressions and with submarine deposits covers various stages of recent permafrost dynamics.

1.2 Expedition itinerary and general logistics

The fieldwork on Buor Khaya Peninsula was carried out between August 3rd and 19th, 2010 (Tab. 1-1). In total, nine participants (Fig. 1-2, Tab. 1-2) from four institutions took part in this campaign which was carried out within the framework of the expedition 'Laptev - Lena 2010' of the Russian-German Science Cooperation 'System Laptev Sea'.

The success of the expedition 'Laptev 2010 - Buor Khaya' would not have been possible without the support of several Russian and German institutions and authorities. In particular, we would like to express our appreciation to the Tiksi Hydrobase (Dmitry Melnichenko), the Lena Delta Reserve (Aleksandr Gukov), the Arctic Antarctic Research Institute St. Petersburg (Dmitry Bol'shiyanov) and AWI Potsdam logistics (Waldemar Schneider).

Figure 1-2: Participants from left to right; back row: I. Yakshina, A. Sandakov, S. Wetterich; middle row: J. Strauss, F. Guenther, L. Schirrmeister, A. Makarov; front row: M. Grigoriev, P.P. Overduin.

Table 1-1: Time table of the expedition Laptev 2010 - Buor Khaya.

Date	Location	Task
2011-07-25	Berlin	Departure
2011-07-28	Tiksi	Arrival
2011-07-28 to 2011-08-03	Tiksi	Preparation work
2011-08-03 to 2011-08-19	Buor Khaya Peninsula	Fieldwork
2011-08-19 to 2011-08-25	Tiksi	After-field logistics
2011-08-25	Tiksi	Departure
2011-08-25	Berlin	Arrival

Table 1-2: List of participants in alphabetical order.

Participant	Competence	Affiliation	e-mail
Grigoriev, Mikhail	1st Russian expedition leader, coastal dynamics	Permafrost Institute Yakutsk, RAS SB	grigoriev[at]mpi.ysn.ru
Guenther, Frank	coastal dynamics	AWI Potsdam	frank.guenther[at]awi.de
Makarov, Aleksandr	2nd Russian expedition leader, geomorphology	AARI St. Petersburg	makarov[at]aari.nw.ru
Overduin, Pier Paul	German expedition leader, geophysics	AWI Potsdam	paul.overduin[at]awi.de
Sandakov, Aleksandr	coastal dynamics	Permafrost Institute Yakutsk, RAS SB	alecsanderus[at]rambler.ru
Schirrmeister, Lutz	permafrost, limnology	AWI Potsdam	lutz.schirrmeister[at]awi.de
Strauss, Jens	permafrost	AWI Potsdam	jens.strauss[at]awi.de
Wetterich, Sebastian	limnology, geophysics	AWI Potsdam	sebastian.wetterich[at]awi.de
Yakshina, Irina	soil science, botany	Lena Delta Reserve Tiksi	i_yakshina[at]rambler.ru

2. STUDY OF SOILS AND FLORA OF THE WESTERN COAST OF THE BUOR KHAYA PENINSULA

Irina Yakshina

2.1 Scientific background and objectives

During the 2010 field season, research focussed on the area around the mouth of Ortho Stan River on the western coast of the Buor Khaya Peninsula. This research seeks to characterize the soil cover and vegetation of the peninsula, which is located in a ecological subzone of typical tundras.

2.2 Material and methods

Thirteen basic soil profiles were described, including full geobotanical descriptions of each pit. Soil pits were excavated and prepared following generally accepted methods (e.g. Desyatkin et al., 2009; Dobrovol'sky, 1979). Forty eight soil samples were taken from the pits for standard chemical analysis (Tab. 2-1). The samples will be processed in the Institute of Soil Science, Hamburg University, Germany (Tab. 2-2). The positions of the pits are shown in Figure 2-1.

Based on the results of this work, a soil map of the area of work is in preparation. Drawing up to a soil map on the basis of a geomorphologic map will be more rational and correct (Tab. 2-2). For classifying soils we stuck to the classification of Yelovskaya (1987).

In addition to soil and geobotanical research, the following works are made: (1) assembling a herbarium that contains 140 sheets of 77 species of vascular plants (Tab. 2-3); (2) sampling soils for microbiological research; (3) collecting seeds of 45 plant species (Tab. 2-4), (4) taking part in collection of palaeontological remains; (5) bird and animal watching; (6) littoral benthos collecting; (7) photographing.

The seed collection was sent to AWI. Soil samples for microbiological research were sent to Russian Research Institute of Vegetable Breeding and Seed Production. All other materials have been added to the academic and museum collections of the reserve.

Expected outcome are (1) classification and systematic description of the types of Buor Khaya Peninsula soils; (2) characterisation of the chemical composition of investigated soils; (3) mapping a soil cover of key sites on Buor Khaya Peninsula; (4) drawing up of the list of vascular plants of work area.

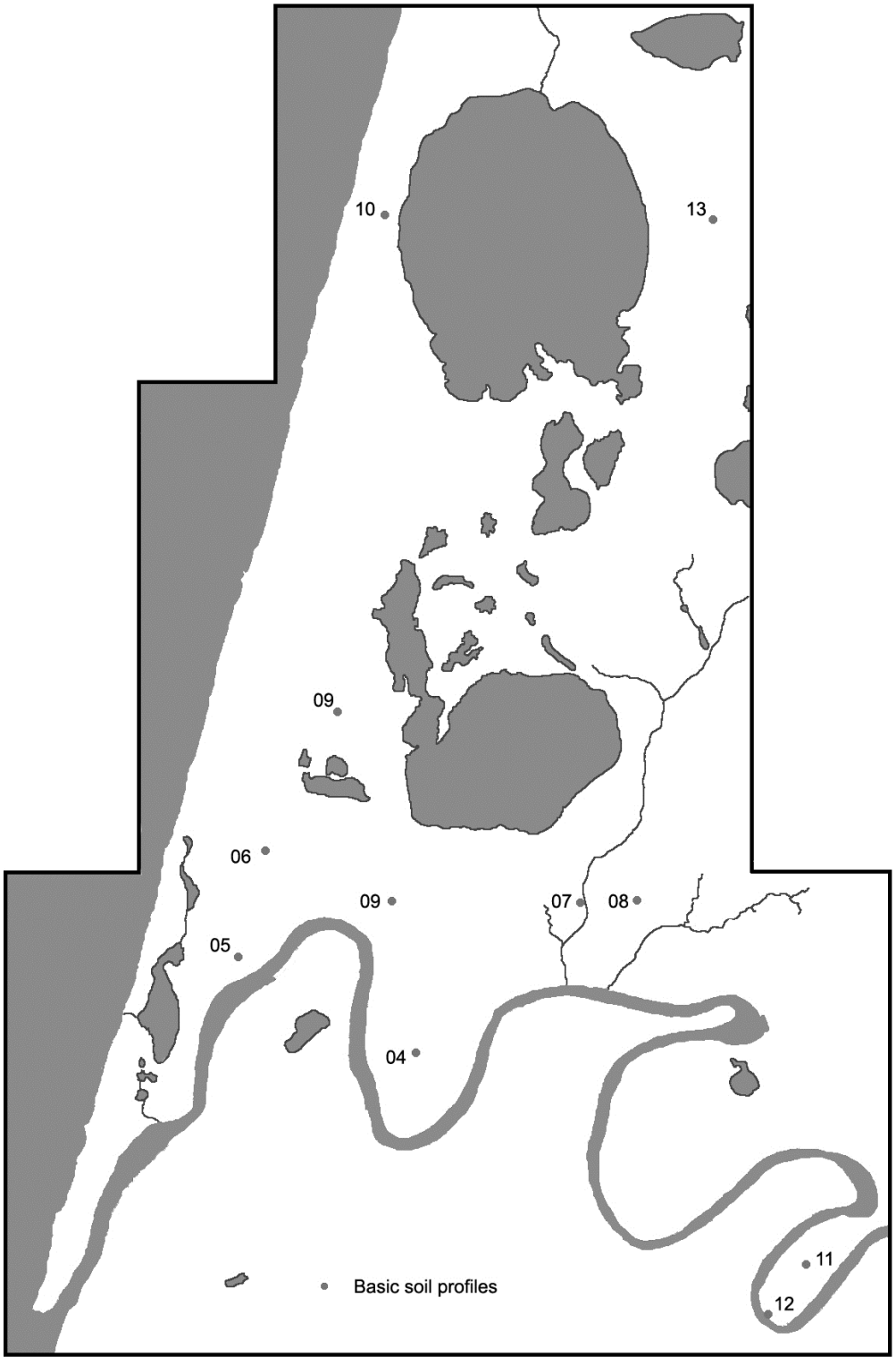

Figure 2-1: Scheme of location of basic soil pits ob Buor Khaya Peninsula (Eastern Laptev Sea).

Table 2-1: Sample list of soil pits.

Sample №	Sample depth [cm b.s.]	Profile ID (coordinates) and location
1	4-11	**BKh01.06.08.2010 (71° 25,168' N; 132° 06,591' E)**
2	15-25	Southern research site. The top part of the watershed
3	30-40	plateau
4	1-8	**BKh02.06.08.2010 (71° 24,877' N; 132° 06,399' E)**
5	10-20	Southern research site. Alas
6	25-35	
7	4-11	**BKh03.09.08.2010 (71° 34,447' N; 132° 13,790' E)**
8	13-23	Surface between the Ortho Stan River and the lake
9	26-34	
10	1-6	**BKh04.09.08.2010 (71° 34,096' N; 132° 13,955' E)**
11	7-17	Floodplain of Ortho-Stan River, 2nd from the sea meander
12	20-30	
13	35-40	
14	5-10	**BKh05.10.08.2010 (71° 34,315' N; 132° 12,663' E)**
15	10-15	Floodplain of Ortho-Stan River, 1st from the sea meander,
16	20-30	alluvial-marine terrace
17	32-40	
18	2-8	**BKh06.10.08.2010 (71° 34,563' N; 132° 12,849' E)**
19	10-20	The top part of the watershed
20	22-30	
21	32-42	
22	44-51	
23	4-14	**BKh07.11.08.2010 (71° 34,439' N; 132° 15,183' E)**
24	20-30	The broad gully - inflow of the river
25	3-12	**BKh08.11.08.2010 (71° 34,443' N; 132° 15,596' E)**
26	15-25	The upper part of the watershed
27	31-38	
28	1-7	**BKh09.12.08.2010 (71° 34,886' N; 132° 13,392' E)**
29	8-17	Alas
30	19-24	
31	26-33	
32	35-43	
33	4-14	**BKh10.13.08.2010 (71° 36,039' N; 132° 13,736' E)**
34	25-35	The western slope of a watershed to the lake, baydzherakh
35	50-60	
36	80-90	
37	2-10	**BKh11.14.08.2010 (71° 33,600' N; 132° 16,829' E)**
38	10-20	The high floodplain. The central part of a meander
39	20-30	
40	30-34	
41	1-9	**BKh12.14.08.2010 (71° 33,483' N; 132° 16,549' E)**
42	15-25	The middle floodplain
43	35-45	
44	60-70	
45	3-13	**BKh13.16.08.2010 (71° 36,025' N; 132°16,171' E)**
46	15-25	Watershed slope
47	30-40	
48	50-60	

Table 2-2: Pending tasks.

№	Task	Responsible persons
1	Standard set of chemical analysis of soil samples	Lars Kutzbach, Hamburg University
2	Microbiological research of soil samples	Daria Shumilina, Russian Research Institute of Vegetable Breeding and Seed Production
3	Geomorphologic map that will serve as a basis for the soil map	Alexander Makarov, AARI
4	Determination of some plant species	Lyudmila Mikhaleva, Lyudmila Kuznetzova, IBPC, Yakutsk

Table 2-3: Herbarium specimen.

Family	Species	№
Equisetaceae	*Equisetum arvense L. ssp.boreale (Bong.) Rupr.*	1
Poaceae (Gramineae)	(Gramineae) sp.	2 to 5
	Alopecurus alpinus Smith	6
	Poa alpigena (Fries) Lindm.	7
Cyperaceae	*Carex* sp.	8 to 9
	Eriophorum sp.	10 to 11
	Eriophorum polystachion L.	12
Juncaceae	*Juncus sp.*	13
	Lusula sp.	14 to 15
Salicaceae	*Salix* sp.	16 to 18
	Salix myrtilloides L.	19
	Salix polaris Wahlenb.	20
Betulaceae	*Betula exilis Sukacz.*	21
Polygonaceae	*Oxyria digyna (L.) Hill.*	22
	Polygonum ellipticum Willd. ex Spreng.	23
	Polygonum tripterocarpum A.Gray.	24
	Polygonum viviparum L.	25
	Rumex arcticus Trautv.	26
Caryophyllaceae	*Cerastium maximum L.*	27
	Cerastium Regelii Ostenf.	28
	Gastrolychnis apetala (L.) Tolm. et Kozh.	29
	Honckenya oblongifolia Torr. et A. Gray	30
	Minuartia macrocarpa (Pursch.) Ostenf.	31
	Stellaria Edwardsii R.Br.	32
	Stellaria humifusa Rottb.	33
	Stellaria peduncularis Bunge	34
Ranunculaceae	*Delphinium chamissonis G.Pritz. et Walp.*	35
	Ranunculus hyperboreus Rottb.	36
	Ranunculus lapponicus L.	37
	Ranunculus Pallasii Schlecht.	38
Papaveraceae	*Papaver angustifolium Tolm.*	39

Table 2-3: Herbarium specimen (continuation).

Family	Species	№
Brassicaceae (Cruciferae)	*Cardamine pratensis L.*	40
	Cochlearia arctica Schlecht.	41
	Descurainia sophioides (Fisch. ex Hook) O.E.Schulz	42
	Draba sp.	43
	Draba sp.	44
	Draba sp.	45
	Neuroloma nudicaule (L.) DC.	46
Saxifragaceae	*Chrysosplenium alternifolium L.*	47
	Saxifraga cernua L.	48
	Saxifraga hieracifolia Waldst. et Kit.	49
	Saxifraga hirculus L.	50
	Saxifraga Nelsoniana D.Don	51
Rosaceae	*Comarum palustre L.*	52
	Dryas punctata Juz.	53
	Rubus chamaemorus L.	54
	Potentilla hyparctica Malte	55
	Potentilla pulchella R.Br.	56
Fabaceae (Leguminaceae)	*Astragalus alpinus L.*	57
Empetraceae	*Empetrum subholarcticum V.Vassil.*	58
Hippuridaceae	*Hippuris vulgaris L.*	59
Ericaceae	*Arctous alpina (L.) Nied.*	60
	Cassiope tetragona (L.) D.Don	61
	Ledum decumbens (Ait.) Hult.	62
	Vaccinium uliginosum L.	63
	Vaccinium vitis-idaea L.	64
Polemoniaceae	*Polemonium acutiflorum Willd. ex Roem. et Schult*	65
Boraginaceae	*Myosotis alpestris F.W.Schmidt ssp. asiatica Vestergr. ex Hult.*	66
Scrophulariaceae	*Lagotis minor (Willd.) Standley*	67
	Pedicularis sudetica Willd.	68
	Pedicularis verticillata L.	69
Valerianaceae	*Valeriana capitata Pall. ex Link*	70
Asteraceae (Compositae)	*Artemisia sp.*	71
	Artemisia Tilesii Ledeb.	72
	Petasites frigidus (L.) Cass.	73
	Senecio congestus (R.Br.) DC.	74
	Senecio tundricola Tolm.	75
	Taraxacum arcticum (Trautv.) Dahlst.	76
	Tripleurospermum hookeri Sch. Bip.	77

Table 2-4: Collected seeds.

№	Species
1	*Alopecurus alpinus Smith*
2	*Arctophila fulva (Trin.) Anderss.*
3	*Arctous alpina (L.) Nied.*
4	*Artemisia Tilesii Ledeb.*
5	*Betula exilis Sukacz.*
6	*Caltha arctica R.Br.*
7	*Cardamine pratensis L.*
8	*Cerastium maximum L.*
9	*Chrysosplenium alternifolium L.*
10	*Cochlearia arctica Schlecht.*
11	*Comarum palustre L.*
12	*Draba parvisiliquosa Tolm.*
13	*Dryas punctata Juz.*
14	*Empetrum subholarcticum V.Vassil.*
15	*Eriophorum Scheuchzeri Hoppe*
16	*Gastrolychnis apetala (L.) Tolm. et Kozh.*
17	*Honckenya oblongifolia Torr et Gray*
18	*Ranunculus hyperboreus Rottb.*
19	*Ranunculus lapponicus L.*
20	*Lagotis minor (Willd.) Standley*
21	*Luzula tundricola Gorodk. ex V.Vassil.*
22	*Minuartia macrocarpa (Pursch.) Ostenf.*
23	*Myosotis asiatica (Vestergren) Schischk. et Serg.*
24	*Neuroloma nudicaule (L.) DC.*
25	*Papaver angustifolium Tolm.*
26	*Pedicularis sudetica Willd.*
27	*Polemonium acutiflorum Willd. ex Roem. et Schult.*
28	*Polygonum tripterocarpum A.Gray.*
29	*Polygonum viviparum L.*
30	*Potentilla hyparctica Malte*
31	*Rumex arcticus Trautv.*
32	*Salix glauca L.*
33	*Salix polaris Wahlenb.*
34	*Saxifraga cernua L.*
35	*Saxifraga hieracifolia Waldst. et Kit.*
36	*Saxifraga hirculus L.*
37	*Saxifraga Nelsoniana D.Don*
38	*Senecio atropurpureus (Ledeb.) B.Fedtsch.*
39	*Stellaria peduncularis Bunge*
40	*Taraxacum arcticum (Trautv.) Dahlst.*
41	*Vaccinium uliginosum L.*
42	*Valeriana capitata Pall. ex Link.*
43	*Poaceae (Gramineae) sp. + gerb. sample*
44	*Poaceae (Gramineae) sp. + gerb. sample*
45	*Poaceae (Gramineae) sp. + gerb. sample*

3. LIMNOLOGICAL STUDIES ON POLYGONAL WATERS OF BUOR KHAYA PENINSULA

Sebastian Wetterich & Lutz Schirrmeister

3.1 Scientific background and objectives

The intention of our limnological fieldwork on polygonal waters (Fig. 3-1) in summer 2010 on Buor Khaya Peninsula (Eastern Laptev Sea) was the record and monitoring of abiotic parameters such as climate conditions, temperature fluctuations, ionic and stable isotope composition in polygonal waters in relation to bioindicators such as pollen, diatoms, chironomids, rhizopods and ostracods. The investigation of the present-day conditions in the waters allows the quantification of influencing parameters, which control the modern occurrence of these indicator organisms. In future, results of the study can be useful for interpretation of fossil data from sediment cores and outcrops and also for quantitative palaeo-environmental reconstructions of the region using several palaeo-bioindicators.

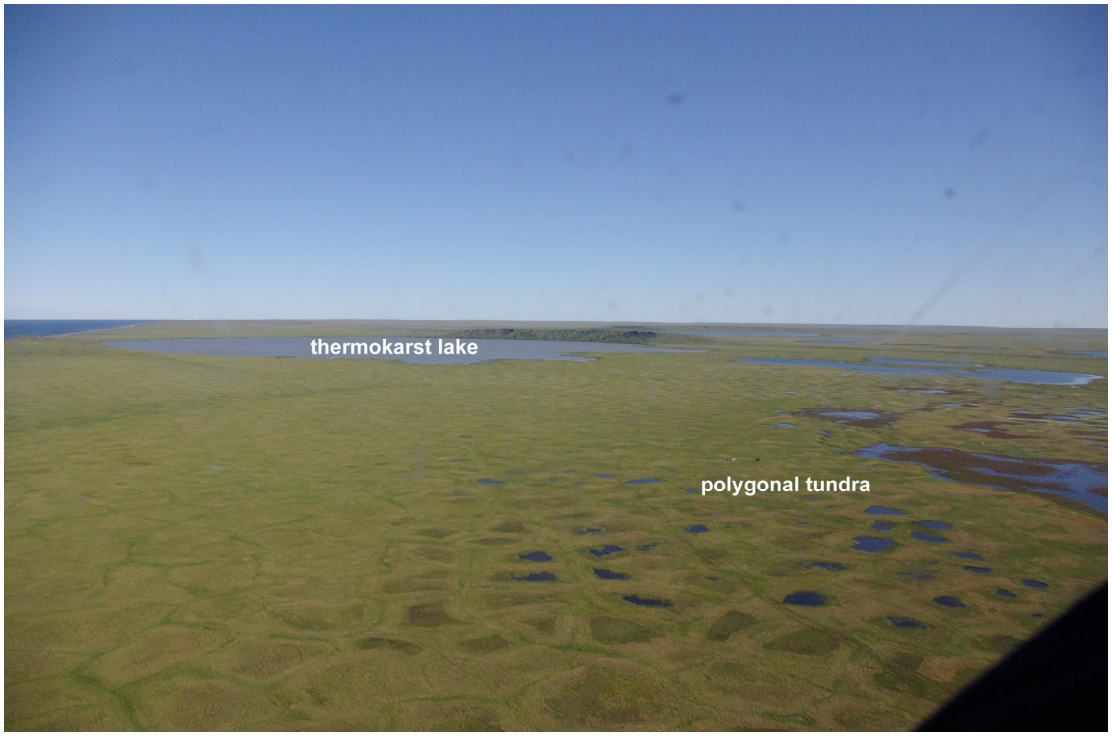

Figure 3-1: Landscape overview from Buor Khaya Peninsula. Photograph taken during helicopter flight on August 2, 2010 by J. Strauss (AWI Potsdam).

3.2 Study sites

Limnological studies were undertaken in different landscape units around the camp (71,56667 °N, 132,19631°E) in August 2010, i.e. on the floodplain of the Orto-Stan River where polygons were represented as high-center-type with interpolygonal ponds (Fig. 3-2a) or as low-center type with intrapolygonal ponds, in thermokarst depressions (alas) with intrapolygonal ponds (Fig. 3-2b), and on the top of Yedoma hills with interpolygon ponds between baydzherakhs (Fig. 3-2c). Additionally, south of Tiksi (71,65°N, 128,8°E) near the Geophysical Observatory several waters have also been sampled after the fieldwork on Buor Khaya Peninsula.

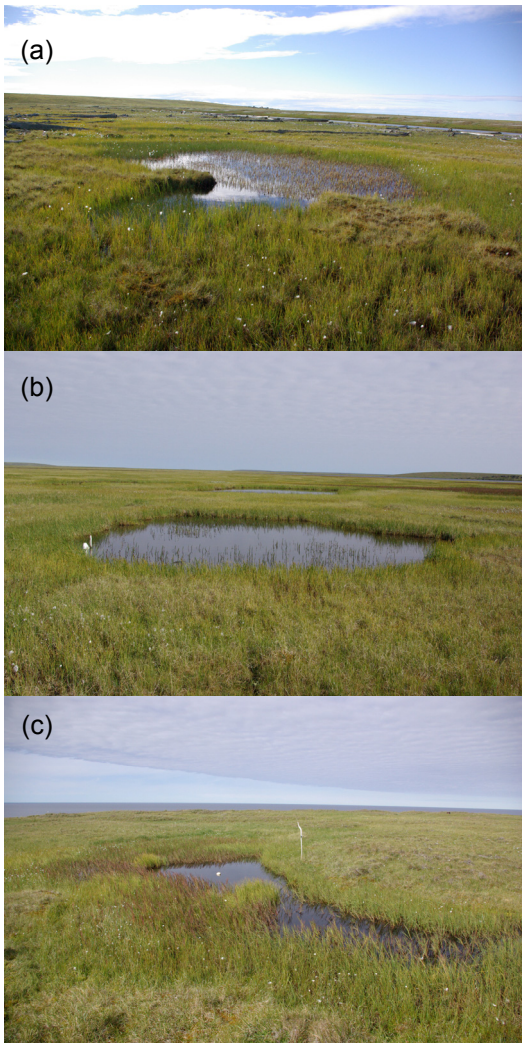

Figure 3-2: Exemplary polygon types on Buor Khaya Peninsula (a) interpolygonal ponds on the floodplain of the Orto-Stan River, (b) intrapolygon pond in a thermokarst depression, and (c) interpolygon pond on the top of a Yedoma hill. Photographs taken in August 2010 by J. Strauss (AWI Potsdam).

3.3 Material and methods

Investigations on properties of water chemistry and physics in the waters were undertaken in order to describe the recent life conditions for organisms. Our investigations included the estimation of water depth and size. We quantified pH, electrical conductivity (EC) and temperature using a WTW pocket meter. Still in the field, the determination of total hardness, alkalinity and acidity was performed by means of titrimetric test kits (Viscolor).

For hydrochemical analyses in the lab, the pond water was sampled above the sediment surface from each site. Samples for cation analyses (15 ml) were acidified with 200 µl HNO_3, whereas samples for anion analysis and residue samples were cool stored. Before conservation, samples for cation and anion analyses were filtered by a cellulose-acetate filtration set (pore size 0.45 µm). Additionally, precipitation and pond water samples for $\delta^{18}O$ and δD isotope analyses (30 ml) were preserved without any conservation.
Surface sediments of the ponds were sampled for sedimentological and botanical and zoological analyses. For these purposes, studies on pollen, diatoms, chironomids, rhizopods and ostracods are planned. Living ostracods were caught in surface sediment samples from different pond zones using an exhaustor system (Viehberg, 2002) and preserved in 70 % alcohol. Further taxonomical work using soft body characteristics will provide the first description of modern ostracod assemblages from the study area.

A similar approach has already been applied on periglacial waters in the Lena Delta (Wetterich et al. 2008), in the coastal area of the Dmitry Laptev Strait (Wetterich & Schirrmeister, 2009), and in the Kolyma lowland (Wetterich & Schirrmeister, submitted).

One interpolygon pond on the top a Yedoma hill (BK-01, Fig. 3-2c) was selected as monitoring site. Here, we performed continuous temperature measurements at three levels using temperature logging (MinidanTemp 0.1, ESYS). The loggers were placed in two different water depths (1 m and 0.05 m below the water surface) and in the air (1 m above the water surface). Additionally, every four days repeated hydrochemical measurements and sampling of water and ostracods were performed in order to obtain temporal dynamics of the studied parameters and proxy as well as their relationships among each other.

3.4 Field results

All studied waters belong to the polygon water type in different stages of their development as they were situated in different geomorphological units (Fig. 3-2; Tab. 3-1). The size of the ponds reaches from 3 x 4 m up to 15 x 20 m (Tab. 3-2).

Table 3-1: Geographical features of the studied waters.

Sample №	Date yy/mm/dd	Time	Region	Locality	Coordinates °N	°E
BK-01a	10/08/06	12:00	Buor Khaya	Yedoma top	71,57713	132,20976
BK-02	10/08/06	13:30	Buor Khaya	alas	71,57970	132,21661
BK-01b	10/08/10	18:00	Buor Khaya	Yedoma top	71,57713	132,20976
BK-03	10/08/11	14:00	Buor Khaya	floodplain	71,57108	132,22993
BK-04	10/08/11	14:30	Buor Khaya	floodplain	71,56965	132,23225
BK-05	10/08/11	18:00	Buor Khaya	Yedoma top	71,56348	132,29807
BK-01c	10/08/14	14:00	Buor Khaya	Yedoma top	71,57713	132,20976
BK-06	10/08/14	15:00	Buor Khaya	alas	71,57915	132,21826
BK-07	10/08/14	16:00	Buor Khaya	alas	71,58003	132,22261
BK-01d	10/08/18	15:00	Buor Khaya	Yedoma top	71,57713	132,20976
Tiksi-01	10/08/21	17:00	Tiksi	valley bottom	71,35888	128,47652
Tiksi-01	10/08/21	18:00	Tiksi	valley bottom	71,35859	128,47857
Tiksi-03	10/08/23	17:00	Tiksi	valley bottom	71,56445	128,80246
Tiksi-04	10/08/23	18:00	Tiksi	valley bottom	71,55963	128,80632

The ground substrates of polygons are built up by coarse to fine disperse organic mud and rich in more or less decomposed plant detritus. Two small and very shallow tributary waters sampled near Tiksi had a pebbly ground overgrown with water mosses. Results of the finger-print hydrochemistry during the fieldwork are presented in Table 3-3. In general, the studied polygon ponds are characterised by slightly acidic pH (pH 5.5 to 6 according to the Viscolor test) and low EC (147 to 285 µS/cm). The tributaries near Tiksi show very low EC (15 to 131 µS/cm). The acidity for most of the waters varies between 0.2 and 0.4 mmol/l. The alkalinity ranges from 0.2 up to 1.2 mmol/l.
Trends in hydrochemical parameters are not obvious and do not show distinct gradients over the monitored period in repeatedly sampled pond BK-01.

Table 3-2: Morphological and sedimentological features of the studied waters.

Sample №	Water type	Substrate	Size [m x m]	Depth [m] maximal	Sample depth [m] water	ostracods
BK-01a	interpolygon	organic mud	12 x 16	1	0.5	0.3 - 0.7
BK-02	intrapolygon	organic mud	10 x 12	0.5	0.3	0.1 - 0.3
BK-01b	interpolygon	organic mud	12 x 16	1	0.5	0.3 - 0.7
BK-03	interpolygon	organic mud	6 x 8	0.5	0.4	0.4
BK-04	intrapolygon	organic mud	15 x 20	0.5	0.5	0.5
BK-05	interpolygon	organic mud	2 x 7	0.5	0.5	0.5
BK-01c	interpolygon	organic mud	12 x 16	1	0.5	0.3 - 0.7
BK-06	intrapolygon	organic mud	10 x 10	0.7	0.5	0.5-0.7
BK-07	intrapolygon	organic mud	7 x 8	0.6	0.5	0.5 - 0.6
BK-01d	interpolygon	organic mud	12 x 16	1	0.5	0.3 - 0.7
Tiksi-01	interpolygon	organic mud	3 x 4	0.7	0.5	0.3 - 0.5
Tiksi-02	interpolygon	organic mud	10 x 20	> 1	0.5	0.5
Tiksi-03	small tributary	moss, pebbles	2 (broad)	0.15	0.15	0.15
Tiksi-04	small tributary	moss, pebbles	2 - 4 (broad)	0.1	0.1	0.1

Table 3-3: Physico-chemical features of the studied waters.

Sample №	T_{Air} [°C]	T_{water} [°C]	EC* [µS/cm]	pH Viscolor	pH WTW	Alk* [mmol/l]	Aci* [mmol/l]	TH* [°dH]	TH* [mmol/l]
BK-01a	12.5	7.9	148	6	6.8	0.2	0.4	2	0.4
BK-02	14.6	13.8	206	6	7	0.6	0.4	2.5	0.5
BK-01b	16	8.4	153	6	6.2	0.4	0.4	2	0.4
BK-03	12.9	11.1	285	5.5	6.3	0.7	0.8	2.5	0.5
BK-04	14.3	13.6	234	6	6.5	0.4	0.3	2	0.4
BK-05	14.4	12.5	147	6	6.1	0.7	1.8	> 20	> 3.5
BK-01c	6.3	6.7	150	6	7.3	0.3	0.2	3.2	0.6
BK-06	6.6	7.5	228	6	7.2	0.4	0.2	4	0.7
BK-07	7.1	7.6	275	6	7.1	0.6	0.2	3.5	0.6
BK-01d	12.5	8.2	153	6	6.1	0.2	0.4	1.5	0.3
Tiksi-01	16.2	10.1	38	6	6	0.4	0.6	1.5	0.3
Tiksi-02	18.6	13.3	15	6	6.3	0.3	0.2	0.5	0.1
Tiksi-03	14.3	12	131	6.5	7.1	1.2	0.4	4	0.7
Tiksi-04	13.7	11.5	43	6.5	6.8	0.4	0.4	2.5	0.5

* EC – electrical conductivity; Alk – Alkalinity; Aci – Acidity; TH – Total hardness

The temperature monitoring was performed during the fieldwork from August 6 until August 18 in pond BK-01 (Fig. 3-2c). Surface ($T_{surface}$) water temperatures are co-varying in lower amplitude with air temperature (T_{air}) variations whereas the bottom water temperatures (T_{bottom}) remain unchanged at about 1 °C most probably due to cooling from the shallow permafrost table below the pond (Fig. 3-3).

High daily maximum values of T_{air} during the early evening hours seem to be overestimated due to the direct sun radiation during the mostly cloudless days.

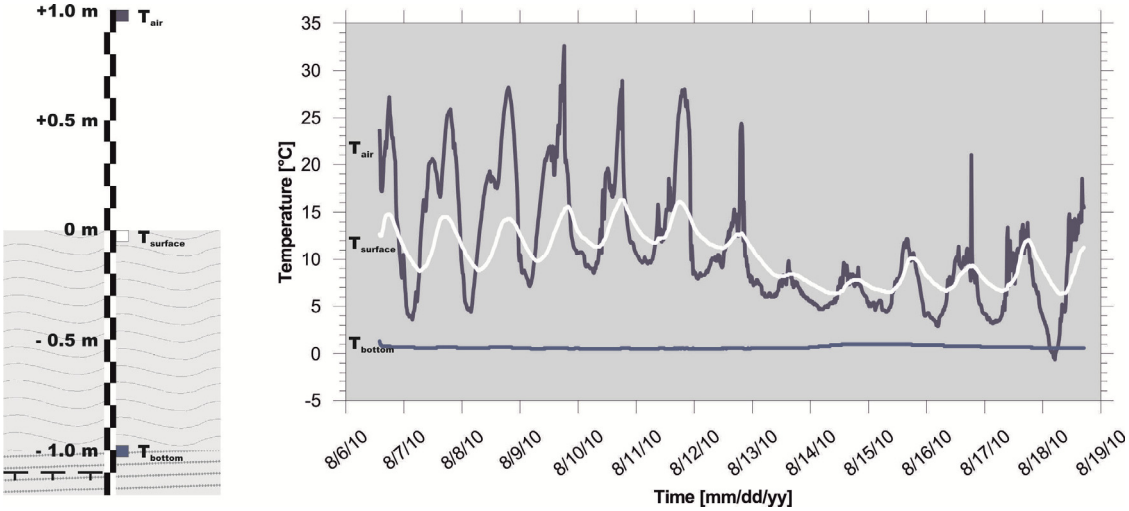

Figure 3-3: Daily temperature variations at the monitored pond BK-01. Three levels are figured out. T_{bottom}: above the sediments in 1 m water depth; $T_{surface}$: directly below the water surface; T_{air}: 1 m above the water surface.

3.5 Outlook

Pollen, diatoms, chironomids, rhizopods from sediments and live caught ostracods will be investigated to illuminate their relationship to environmental factors such as temperature, pH, and conductivity in polygon waters. Later, this information will be applied to fossil assemblages obtained from sediment cores and permafrost deposits in order to infer quantitative environmental changes via organism-environment transfer-functions.
In the laboratory, water samples will be analysed for element content by means of an ICP-OES and anion content by Ion Chromatography. Furthermore, analyses of $\delta^{18}O$ and δD isotopes on water and precipitation samples will be performed in order to compare these data with isotope values in calcareous ostracod valves.
The understanding of the recent relationship between isotope ratios in waters and in ostracod valves will lead to an interpretation tool for palaeoenvironmental information preserved in fossil ostracods. For the same purpose element analyses (e.g. Ca, Mg, Sr) in waters and ostracod valves will be undertaken. Analyses of nitrogen organic and total carbon contents on surface sediment samples by CN-Analyzer as well as grain-size distribution by laser particle analyzer will be carried out in order to characterize the sedimentological setting of the investigated ponds. Such investigations on polygon waters will contribute to the current joint Russian-German POLYGON project funded by the Russian Foundation for Basic Research (RFBR) and the Deutsche Forschungs-gemeinschaft (DFG).

4. TOPOGRAPHICAL SURVEYS FOR COASTAL DYNAMICS STUDIES

Frank Guenther, Paul Overduin & Aleksandr Sandakov

4.1 Introduction

The combination of accelerated coastal erosion during summer and a high net sea ice production over the winter time affects other regions of the world ocean. Clastic and organic materials released to the sea from the East Siberian coast are transported with the Transpolar Drift Stream across the Arctic Basin to the North Atlantic. Understanding the impacts of accelerating coastal erosion on this environment and the role it plays in feedbacks to climatic change requires estimates of mass fluxes and how they are controlled by the interaction of driving forces and coastal geomorphology. This field campaign focuses on coastal erosion on the Buor Khaya Peninsula and aims to produce a basic dataset of topographic reference measurements for analyses of coastal dynamics. According to previous local studies (Are et al., 2000) and our own preliminary estimations, the coastline of the peninsula retreats at rates of 1 – 4 m per year.

The main objectives are:

- to identify different spatial erosional patterns
- to determine the intensity of key parameters for geomorphodynamics and associated processes

For this purpose several processing steps and analyses were performed:

- Monitoring of shoreline position changes and change rate determination by comparison of field measurements with space-borne imagery and aerial photographs taken at various times
- Calculation of volumetric coastal erosion using multitemporal digital elevation models
- Geomorphometrical coastline characterization by measuring shoreface profiles
- Geomorphological classification of relief units along the Buor Khaya and Yana Bay coasts

The area around the northern cape “Mys Buor Khaya” has been identified as a key site of the International Polar Year (IPY) coastal monitoring programme “Arctic Circumpolar Coastal Observatory Network” (ACCO-Net) and is representative for Northeast Siberian lowlands. During the last few years various remote sensing data have been acquired for coastal erosion studies and more were acquired during this field campaign. Remote sensing data will be used to generate digital elevation models (DEM) and ortho images. In order to take advantage of the possibilities available from new optical high resolution satellite imagery, reliable and well distributed ground reference data is essential. The elongated coastline of the Buor Khaya Peninsula reveals a high heterogeneity of geomorphological units, such as alasses, Yedoma hills and

transition zones. The research challenge here is to create estimates of mass fluxes due to coastal erosion for each unit considering changing terrain heights and the heterogeneity and complexity of the upper shoreface profile using three-dimensional change detection.

4.2 Remote Sensing

Planned acquisition of ALOS PRISM stereographic imagery over the period of the expedition were unsuccessful. Three RapidEye multispectral images acquired for the period between 8. and 27. August 2010 (RapidEye AG, Brandenburg, Germany). RapidEye provides consistent datasets over large coastline sections at high temporal and geometric resolution. In order to span a long period of time, historical space-borne optical imagery of the CORONA and HEXAGON programs (1960s-1970s) were also made available for change detection analysis.

4.3 Field Methods

Topographic elevation data was collected by direct tacheometric field survey using a ZEISS ELTA C30 tacheometer. Measurements were taken with the corresponding reflector mirror KTR-1N, mounted on a telescopic bar with an adjustable length of up to 4 m. Because of the limited visual field of the tacheometer due to intervening baidzharakhs (remnants of polygon centers exposed by thawing of ground ice) or steep cliffs, the instrument position had to be changed several times to survey a whole thermoterrace or a specific coastline segment. To ensure regular positioning in a predefined local co-ordinate system, a network of well distributed anchor points, so called backside points, had to be set up, within which the “free-stationing” could be applied. All points of this network were marked with a plastic cap and a numbered wooden stick. Backside points which could be used repeatedly were instrumented with a stationary KTR-1N reflector on a tripod.

4.4 Field Results

Topographic surveys were conducted at six different sites (Tab. 4-1), covering the morphological spectrum from steep cliffs along alas-coasts and concave thermo-denudational terraces to convex Yedoma hills. Five sites extend over a 55 km north-south section along the Buor Khaya Gulf coast, one site was visited on the Yana Bay coast in the north of the Buor Khaya Peninsula. Inclination of the lower shoreface profile is thought to have an effect on the intensity of coastal erosion. The north-south transect along the west coast follows the changing bathymetry of the nearshore zone from steep slopes in the north to gentle slopes of the abrasion terrace in the south, while the Yana Bay around Cape Ostry is very shallow (Fig. 4-1).

The wide distribution of study sites allows identification of regional erosion patterns. The site name *1st to 2nd Yedoma* relates to the first and second Yedoma hills as seen from the field camp to the north. This site was easy to reach by a walk from the field camp. The sites *Are, 3rd Yedoma, Lagoon* and *North Cliff* were visited by zodiac. *Cape Ostry* was reached by a longer march from a temporary camp near *North Cliff*.

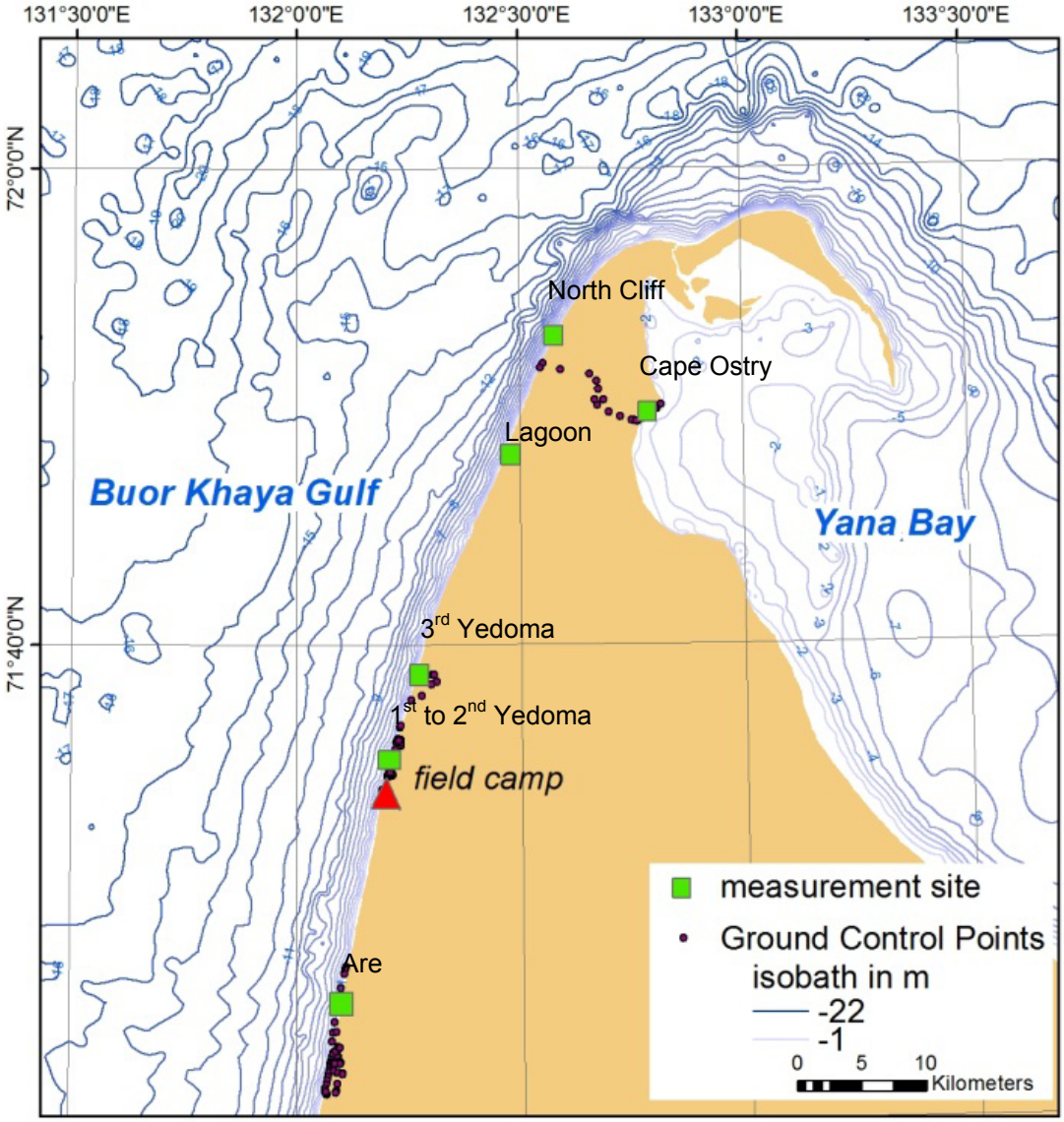

Figure 4-1: Study sites of tacheometric surveys and coverage of complementary GCPs.

Because of a high redundancy of backside points the mean horizontal and vertical accuracy of each stationing is less than 2 cm in local co-ordinates. For each backside point the absolute co-ordinate was determined. On the basis of the backside point network the point clouds of the separate survey projects were geocoded with a mean horizontal accuracy from 1.2 to 1.8 m (Tab. 4-1) into an absolute coordinate system. Finally, in this way each measuring point is

assigned with an absolute co-ordinate. This allows combination with any other geospatial data. The heights were converted into absolute values according to the factual sea level. For subsequent photogrammetric processing of stereo imagery, full GCPs, including accurate z-values, are essential. Therefore, topographic elevation data was collected also, where possible, for lakes and other distinct objects of the coastal hinterland. Measurement was primarily done for the upper coastline (cliff top) and the lower coastline (cliff bottom). Each separate topographic survey features an adequate number and density of irregular distributed points, allowing for interpolation to a high resolution DEM. In addition to 102 backside points, 98 ground control points (GCP) were collected for surface and coastline descriptions, but first and foremost for geo-referencing purposes. GCPs were marked on a set of ALOS AVNIR-2 (2009) printouts and documented in photographic form.

Table 4-1: Key data of the tacheometric survey.

Site	No. measurement points	No. backside points	Elevation range (m)	Accuracy of absolute geocoding (m)	Linear distance of coastal segment (m)
Are	150	15	0 – 34.3	1.3	989
1st to2nd Yedoma	633	31	0 – 30.7	1.3	3075
3rd Yedoma	264	11	0 – 38	1.6	376
Lagoon	86	18	0 – 7.8	1.5	595
North Cliff	137	8	0 – 25.5	1.2	373
Cape Ostry	186	19	0 - 33	1.8	1300
total	**1456**	**102**	**0 - 38**	**1.45**	**6708**

4.4.1 Site 1st to 2nd Yedoma

The survey project *1st to 2nd Yedoma* (Fig. 4-2) covers the longest segment of surveyed coast with over 3 km length (Tab. 4-1). Work was carried out on 05.08 and 14.-16.08.10. The 1st Yedoma hill is surrounded by extensive beaches and drift wood, which seem to protect this area from erosion. The slopes are convex and no outcrops of Ice Complex were observed. The upper seaward west-facing slope (Fig. 4-2a) exhibits a flatter terrace (6-12° inclination) and smoothly merges into the Yedoma surface. The lower slope is steeper (20-25°) and more dissected. The south facing slope of the 1st Yedoma (Fig. 4-2b) is of sloping form with an inclination of 7-15° and inactive. Between the two Yedoma hills along a stretch of 2 km, alas deposits (on average 10.5 m a.s.l.) are truncated by active erosion and form a steep cliff. Close to Xedoma hills, the polygonal surface is more dissected by cracks. Cliff top and cliff bottom positions were measured at irregular intervals.

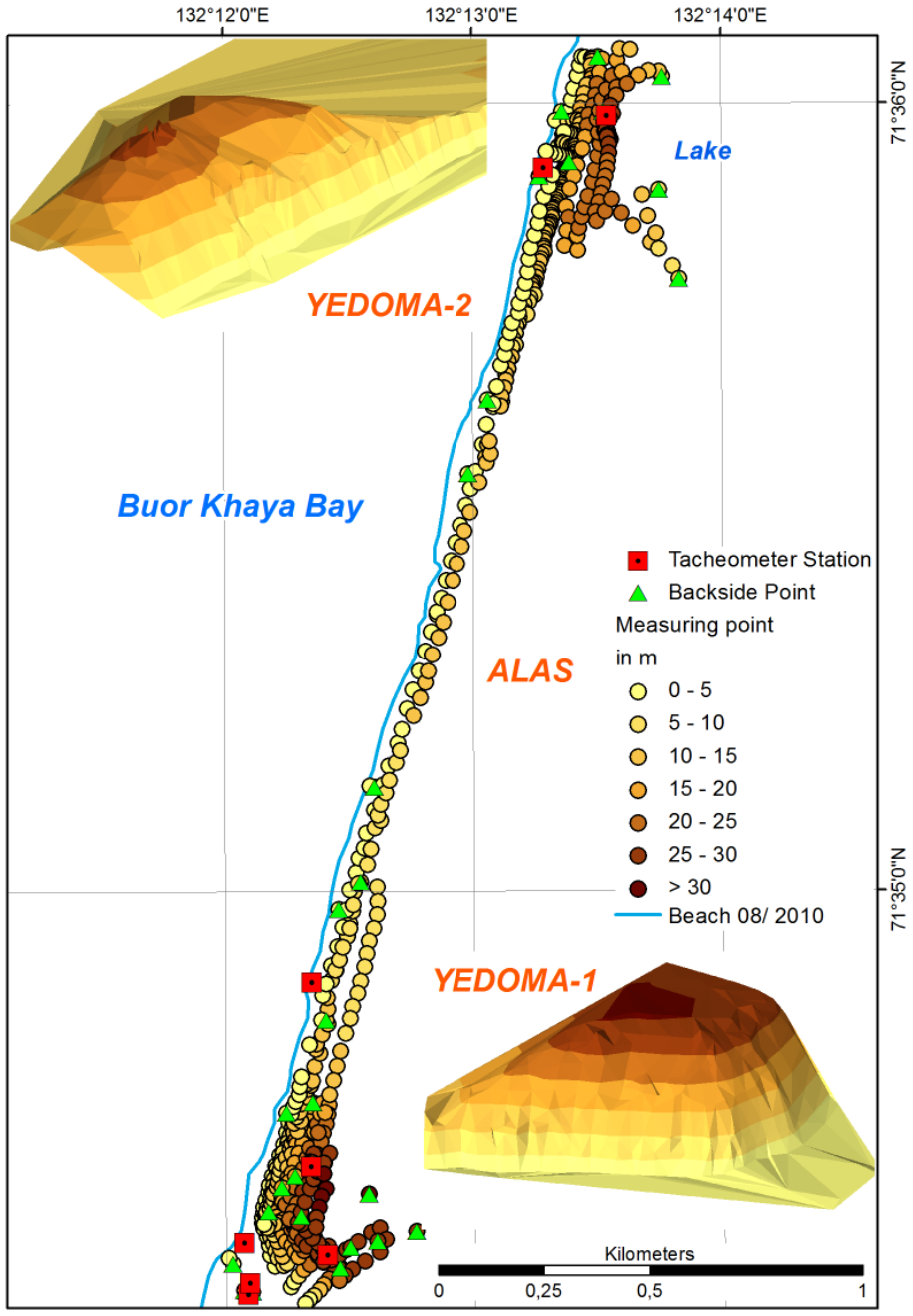

Figure 4-2: Map of the coast survey at 1st to 2nd Yedoma and oblique views of interpolated Triangulated Irregular Networks (TIN).

The morphology of the 2nd Yedoma is sloping-terraced. Eroding baidzharakhs characterize the < 40 m wide terrace, which goes up to 12 – 13 m a.s.l. The vertical Ice Complex outcrop is 2 – 6 m high, the outline of the retreating headwall in plan is wavy with some sharp breaks and propagates upslope.

Stabilized baidzharakhs are present on the undissected upper slope. Mean elevation of the Yedoma top is 25 -26 m a.s.l., on baidzharakhs up to

29.5 m a.s.l. The beach had an average height of 1.5 m a.s.l. at the cliff bottom. The thermokarst lake next to the 1st Yedoma is at a height of 7.6 m a.s.l.

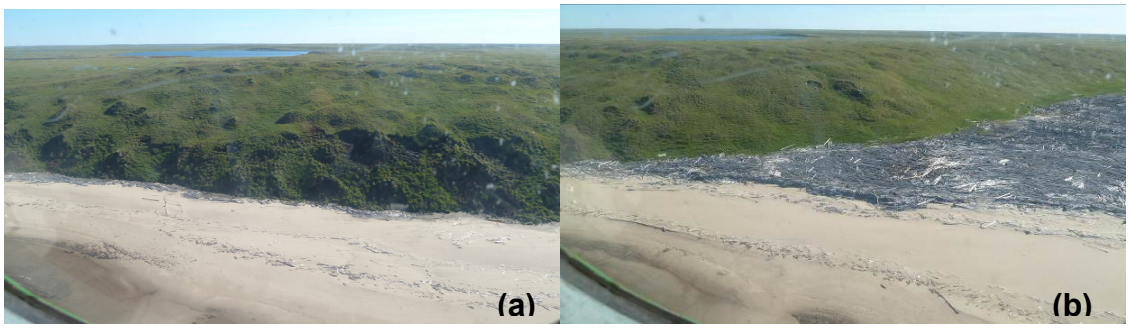

Figure 4-3: Photos from helicopter of the *1st Yedoma*; (a) seaward-facing slope (b) south-facing slope.

4.4.2 Site Are

This site was internally named after Feliks Are to underline the repetitive character of our tacheometric measurements at this site (Are et al., 2000). The survey (Fig. 4-4) was carried out on 06.08.10.

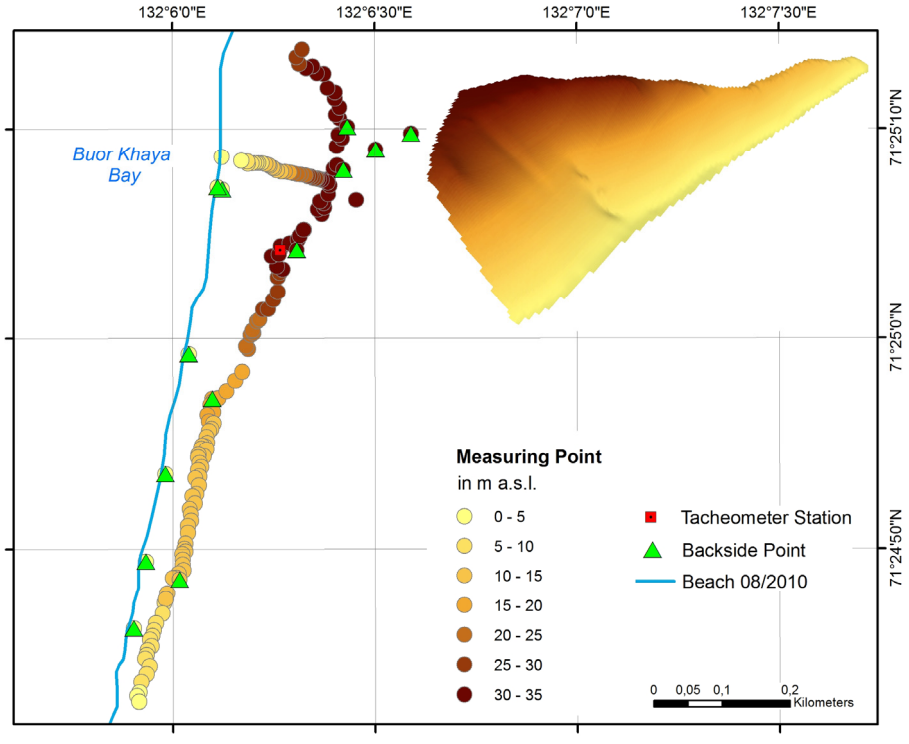

Figure 4-4: Map of the coast survey at Are and oblique view of interpolated raster.

The thermo-terrace is of a very self-contained shape and extends 130 m inland. Preliminary estimations indicate a mean annual retreat rate of the upper

coastline about 2.5 m a^{-1}, while the cliff bottom retreats only 1 m a^{-1}. The *Are* site is a typical example for an active coast of concave shape with prevailing thermo-denudational slope processes (Fig. 4-5a). Close to the cliff top, the extensive terrace vegetation cover is disturbed and a 1-2 m high, nearly vertical, retreating Ice Complex outcrop wall, which is in general smooth in plan, marks the transition to the undissected Yedoma top. Mainly this border and the cliff top of the adjacent steep alas coast (Fig. 4-5b) were measured here. According to our measurements, the distance from the current cliff top to two iron pipes (33.8 m a.s.l.) rammed into the ground earlier (the two easternmost backside points in the map), is about 54 m and 102 m. In addition, a slope profile through the central part of the thermo-terrace was measured. The mean slope is 12°. The cliff bottom of the Yedoma coast as well as for the alas coast is at 2 m a.s.l.

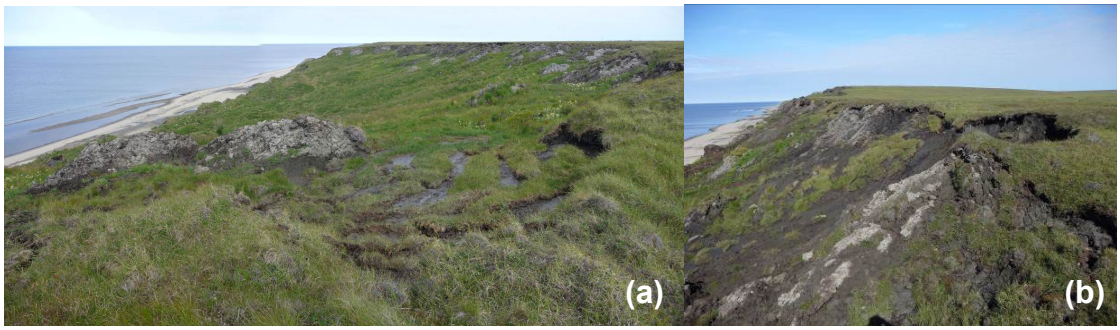

Figure 4-5: (a) Half-round thermo-terrace; (b) steep alas coast in the southern part.

4.4.3 Site Lagoon

The north-south oriented thermokarst lagoon was visited during an excursion on the way to the northern peninsula on 10.08.10. The lagoon is flooded during storms, so we expect coastal erosion to be active here as well. Measurements were taken for the northern margin of the lagoon (Fig. 4-6), where a 6-7 m high south-facing alas cliff is present (Fig. 4-7a).

In the area around the tacheometer station, the alas coast bordering the sea is 8 m a.s.l. high and strongly dissected along polygon cracks. The water level of the lagoon was 0.4 m above the factual sea level on 10.08.10. The lagoon itself is protected by a 1.5 m high sand embankment with drift wood on top (Fig. 4-7b). In the western part, where the cliff bordering the lagoon is higher and seems to be more active, mean slope is 13 - 17°. The slope decreases eastward down to 7-10°, where the cliff is less pronounced. At the eastern end of the lagoon a 250 m wide belt of drift wood has accumulated, protecting the hinterland from storm events. Close to the coast, the alas surface around the tacheometer station was dissected along polygonal cracks.

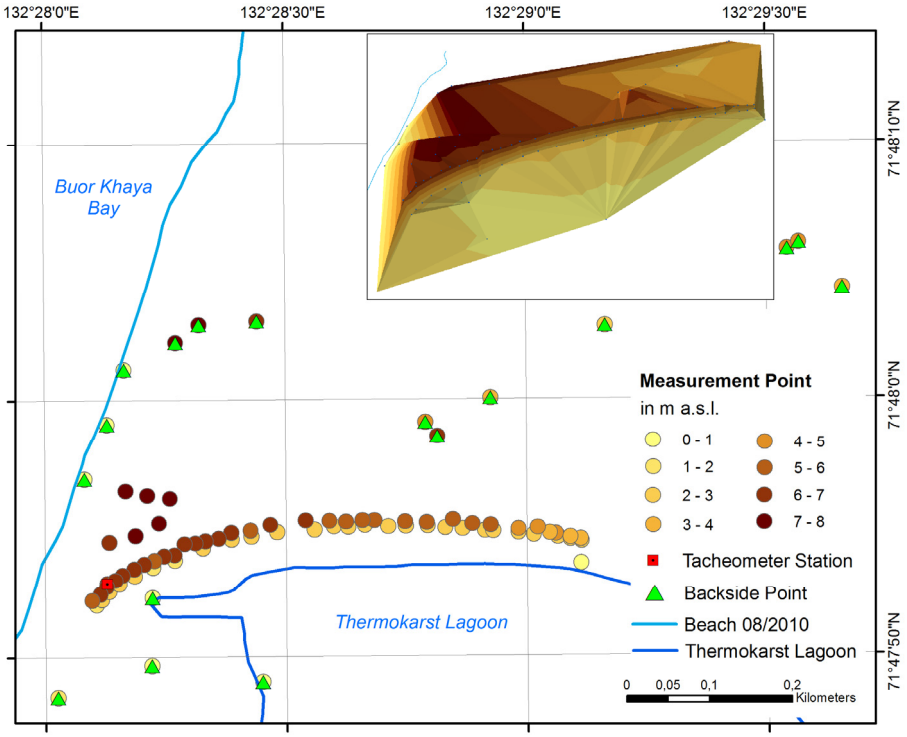

Figure 4-6: Map of the survey at Lagoon and oblique view of interpolated TIN.

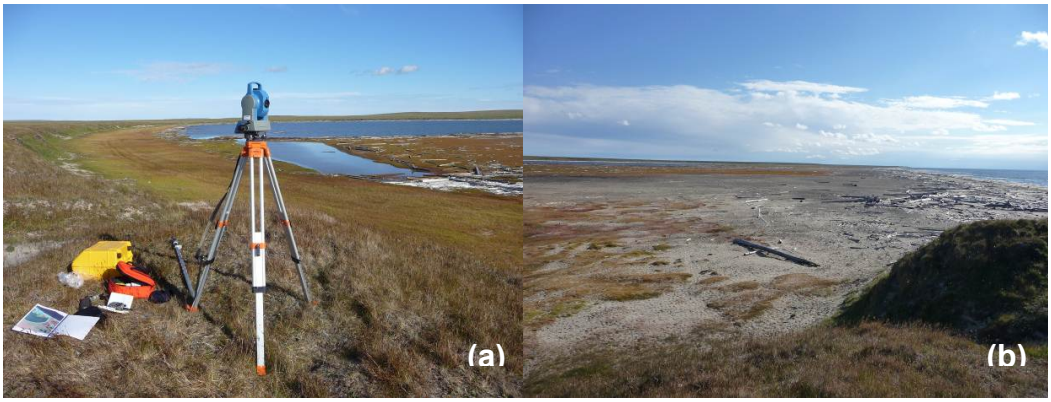

Figure 4-7: Tacheometer station at site Lagoon, view in eastern direction along the surveyed alas cliff, bordering the thermokarst-lagoon in the north; (b) view from the same point to the south, drift wood on top of the 1.5 m high sand embankment.

4.4.4 Site Cape Ostry

The site was chosen for a field measurement campaign based on preliminary studies, which indicated high erosion rates here. It turned out to be up to 3.5 m per year. In order understand the local process-structure and to start a coastline survey, on 11.08.10 the Yana Bay coast was visited as part of a one day expedition from a temporary outside camp (71,864°N; 132,551°E) near the Lena Yuryuege mouth. During the walk from the east to the west coast, along a

12 km transect 13 GCPs of easy to recognise ponds and other natural objects were collected for georeferencing purposes of remote sensing data. Lake margins are well suited to serve as homologous points in stereophotogrammetric processing. Therefore, it is advantageous to know the absolute lake level height. On the way to Cape Ostry the levels of three lakes were determined (Fig. 4-8). Small residual or secondary thermokarst lakes in alasses in this area are on a height of 7 – 8.5 m. The level of the large primary thermokarst lake near Cape Ostry is slightly higher (10.6 m). Judging from topographical maps, the high erosion rate observed on Cape Ostry is associated with eroding away a 17 m a.s.l. high Yedoma hill, which was protruding into the sea and exceptionally exposed to thermo-abrasion. Now the ice rich transition zone between Ice Complex and Alas deposits build up the cliff (Fig. 4-9 a). GCP 48 (71.83544°N; 132.81929°E) marks the easternmost position of the cliff top of Cape Ostry at that time. In contrast to the west coast, the Yana Bay coast had no sandy beach, but thermo-erosional niches were common, indicating strong thermo-abrasional activity (Fig. 4-9 b).

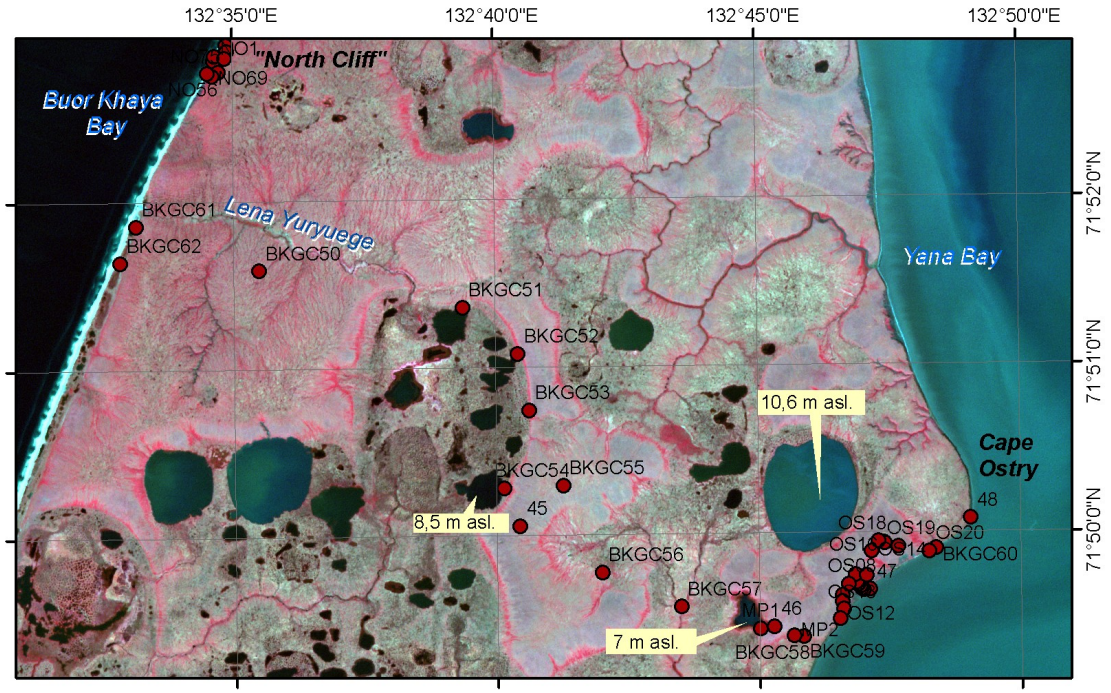

Figure 4-8: Map of GCPs collected during the excursion to Cape Ostry and measured lake elevations (image copyright is RapidEye).

A thermo-erosional section of the coast was surveyed, spanning over 1.3 km along the southern margin of Cape Ostry and forming a thermo-terrace within Ice Complex of 100 to 200 m width inland (Fig. 4-10). The thermo-terrace can be divided into a stabilized part east of the tacheometer station and a newly forming south-western part (Fig. 4-9 c). The eastern part exhibits baidzharakhs and successional vegetation communities, while the western part is presently active with a disturbed surface. Slope angle of the flat upper terrace floor increases downslope from 3 - 9°. The upslope propagating headwall in the

active part is well pronounced and less than 0.5 m high. As a result of the canalisation of the melt water from above, slopes close to the coast are steeper and more dissected.

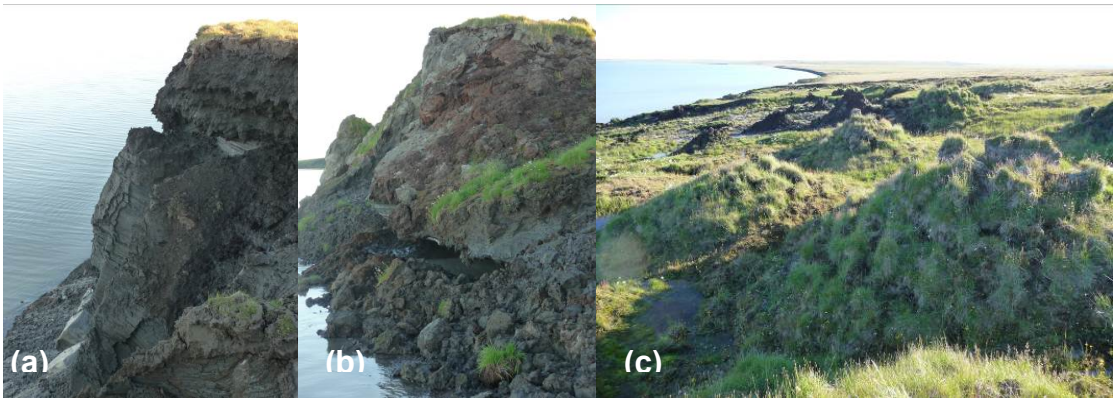

Figure 4-9: (a) The cliff of Cape Ostry, above which the land surface dips towards the southwest, corresponding to the slope of the former yedoma hill towards the alas basin; (b) thermo-erosional niche on the southern margin of Cape Ostry; (c) stabilised baidzharakhs near tacheometer station, active slumping in the background.

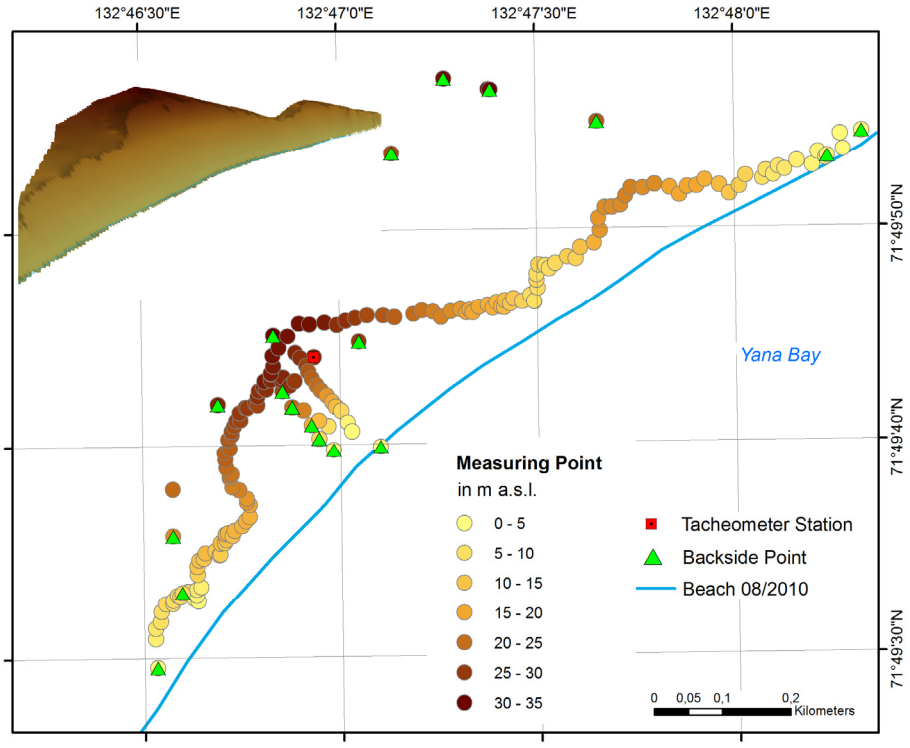

Figure 4-10: Map of the survey near Cape Ostry.

4.4.5 Site North Cliff

North Cliff is the northernmost site visited during the expedition. Field work was carried out on 12.08.10. Due to rainy weather tacheometric measurements (Fig. 4-11) were limited to a smaller spatial extent, but aimed to take into account important vertices of the coastal profile.

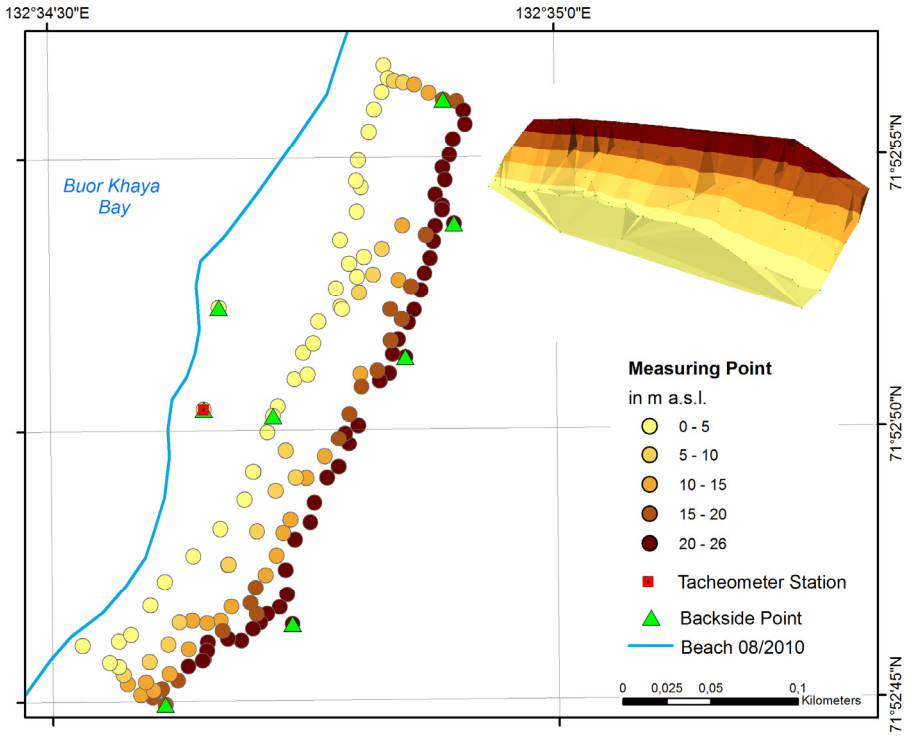

Figure 4-11: Map of the survey at North Cliff and oblique view of TIN.

Figure 4-12: (a) view from cliff top onto the terrace, tacheometer operator on the beach; (b) view along the cliff in northern direction.

The morphology here can be characterized as a steep, slightly rounded, inland, terraced, coastal profile of 25 m height with a continuous vertical Ice Complex outcrop (8 m high) in the upper part and deposits of eroded sediments at the cliff bottom. The comparatively thin terrace (< 35 m wide) indicates the active removal of the erosional products at the cliff bottom. This is confirmed by a comparison of our field data with space-borne imagery from 1968, which reveals that along the cliff, retreat rate of the lower coastline varies from 55 – 85 m (1.3 m a^{-1} – 2 m a^{-1}), while the retreat rates of the upper part rarely exceed 1.5 m a^{-1}, indicating prevailing thermo-abrasional activity here.

4.4.6 Site 3rd Yedoma

This site is the highest Yedoma hill (37.9 m a.s.l.) along the western coast of the Buor Khaya Peninsula and was visited on 17.08.10. Because of the complex cliff structure, point measurements were made very densely (Fig. 4-13).

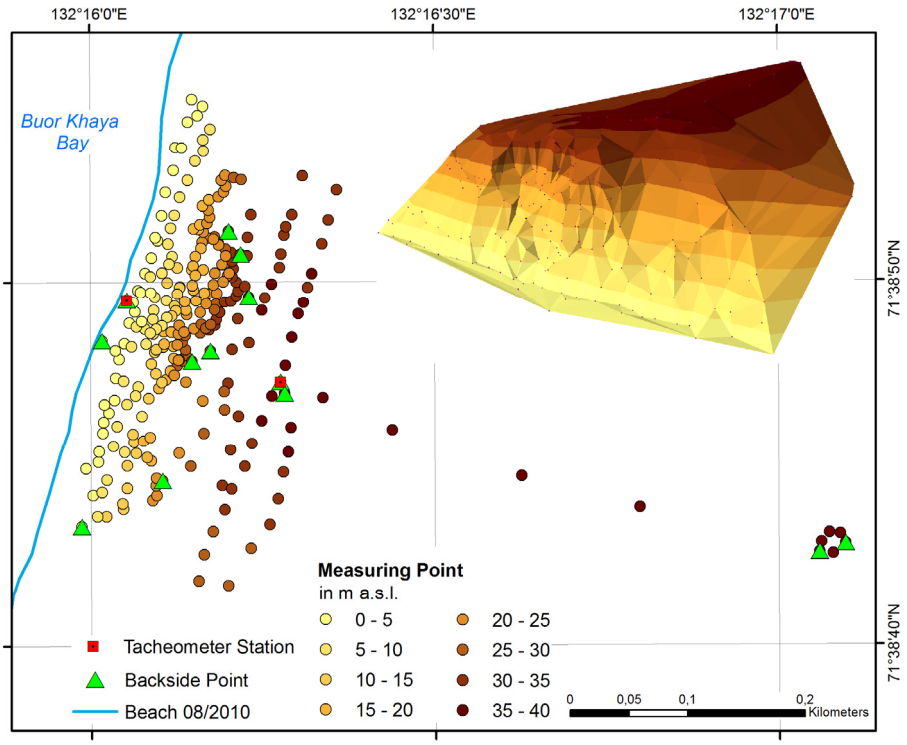

Figure 4-13: Map of the survey at 3rd Yedoma and interpolated TIN.

The small scale structure is two neigh-bouring and converging thermo-terraces (Fig. 4-14 a). The upslope and radially propagating headwall (reaching its highest level at 30 – 33 m a.s.l.) is curved inland in plan, with some sharp breaks (Fig. 4-14b). A flat, stabilized upper slope, consisting of baidzharakhs, merges into the undissected Yedoma surface with a trigonometric point of reference on top. Beside the main outcrop of Ice Complex (up to 10 m high) in the uppermost part of the active cliff, the terraced cliff exhibits in places a

secondary (currently developing) retreating headwall or older generation (currently inactive) sharp edge (Fig. 4-14b). This results in a hetero-
geneous, steplike profile of the coast. The beach is very narrow (<20 m). As a stable point in the hinterland, the outline of a polygonal pond (20 m in diameter, 37.2 m a.s.l.), situated 500 m eastward of the trigonometric landmark, was included in the local survey project.

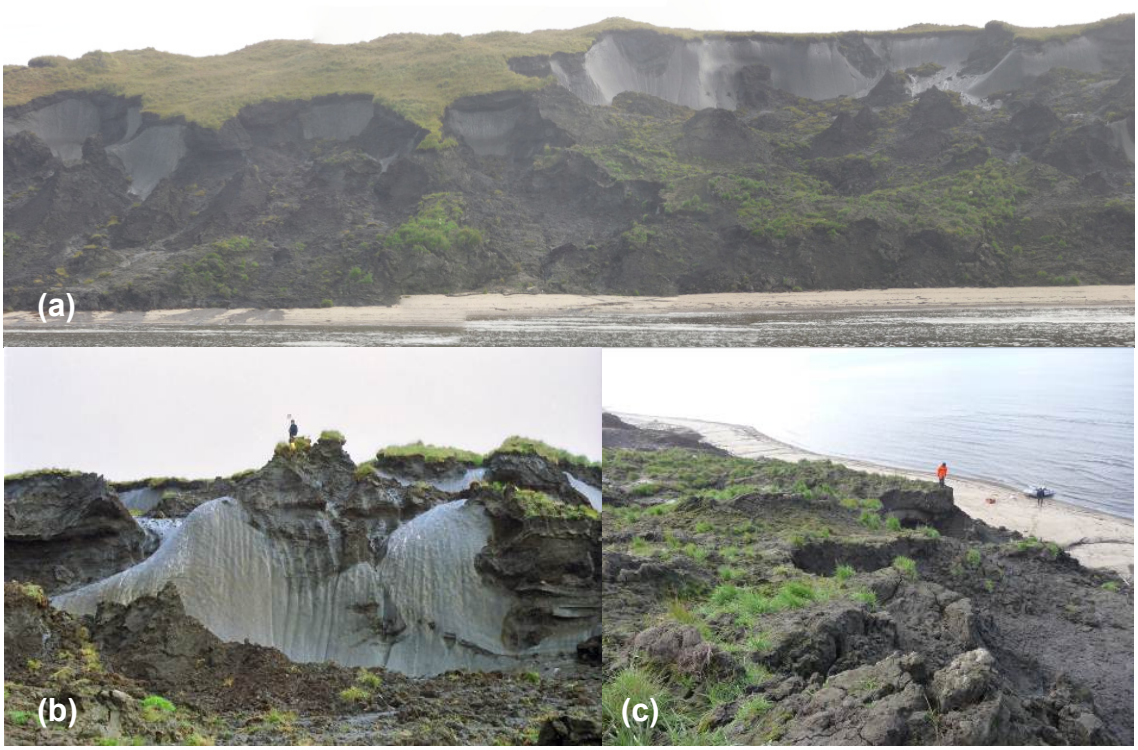

Figure 4-14: (a) Part of the coast of the 3rd Yedoma seen from the seaside; (b) protrusion of the active retreating headwall; (c) inactive scarp in the middle of the thermo-terrace; persons for scale.

4.5 Bathymetrical measurements

Erosion of the sea bottom and therefore change in the underwater portion of the shoreface exert control on the development of the coastline. Uncemented or thawed sediments above the ice-bearing subsea permafrost table are a source of easily erodible sediment. Erosion of this material, or subsidence of the seabed, create accommodation space in the submarine shoreface for material derived from the coast, and decrease damping of wave energy impinging on the shore. As a result of migration of the isobaths towards the coast and therefore increasing slope angle of the abrasion terrace, the upper coastline itself responds. Accordingly, repeat measurements of bathymetry are of particular interest. In order to create estimates of sea-bottom erosion our field data will be compared with nautical charts, which represent measurements made decades ago. Bathymetric measurements were carried out using a marine GPS echosounder on board a zodiac, used simultaneously with the geoelectric

system or as a stand-alone device. During geoelectrical surveys and excursions to coastal erosion and geological sampling sites (see chapter 6), extensive along shore bathymetric measurements were taken, tracing mainly the 2 to 4 m isobaths over a distance of about 100 km. Cross shore bathymetrical profiling was carried out for three key sites (*North Cliff*, *1st to 2nd Yedoma* and *Are*). Examples of the shoreface profiles are given in Figures 4-15 to 4-18. Generally the profiles are of concave to linear form, mean shoreface inclination varies from 0.003 (*Are*-1) to 0.006 (*North Cliff*). Close to the coastline, several sandbanks are often connected in series. The profiles of alas coasts do not differ in shape from the neighbouring Yedoma coasts.

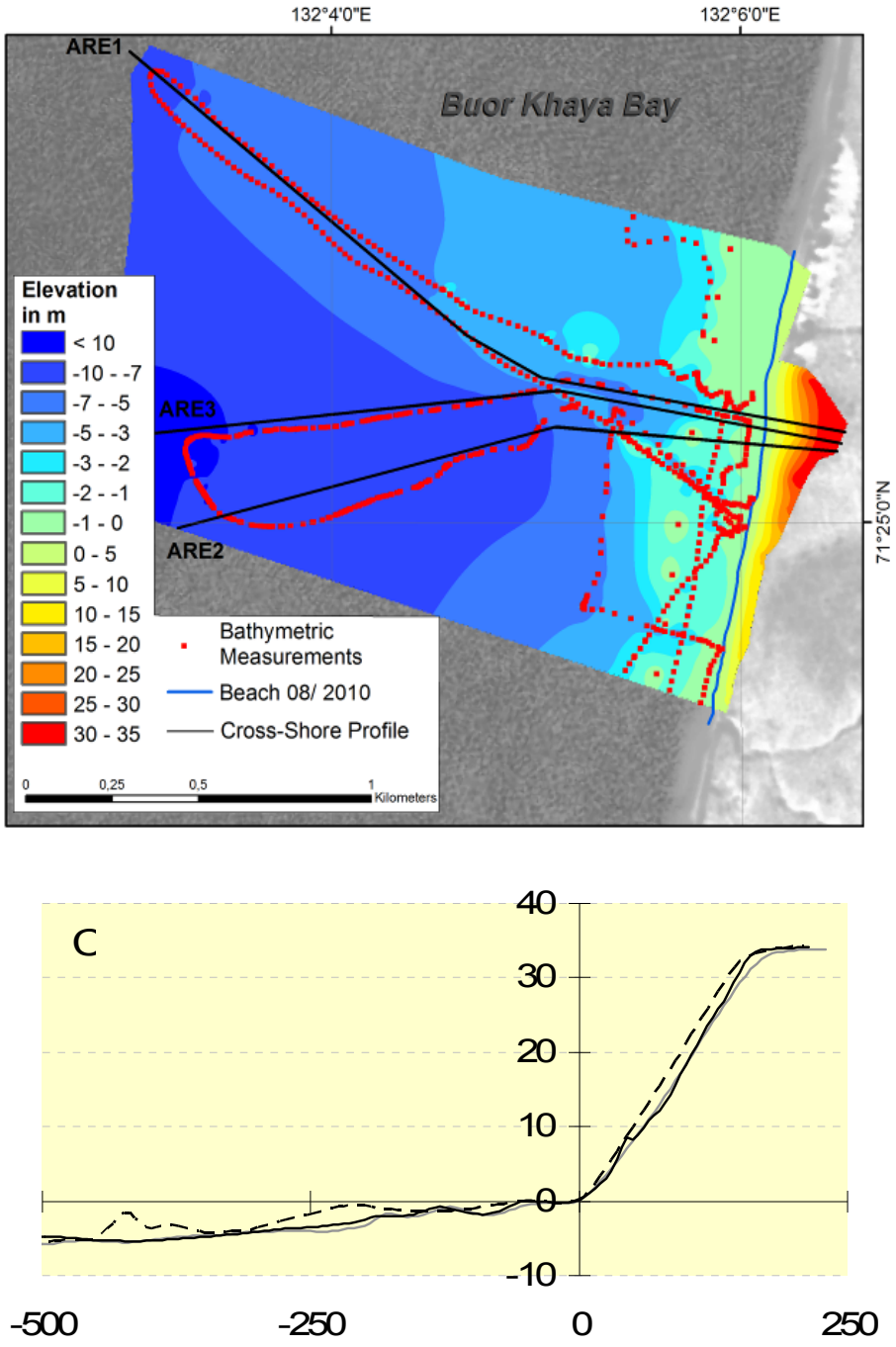

Figure 4-15: Map of the location and near shore diagrams (ARE1, ARE2, ARE3) of cross shore profiles at site *Are*, joint DEM of the shore face (bathymetric and tacheometric measurements).

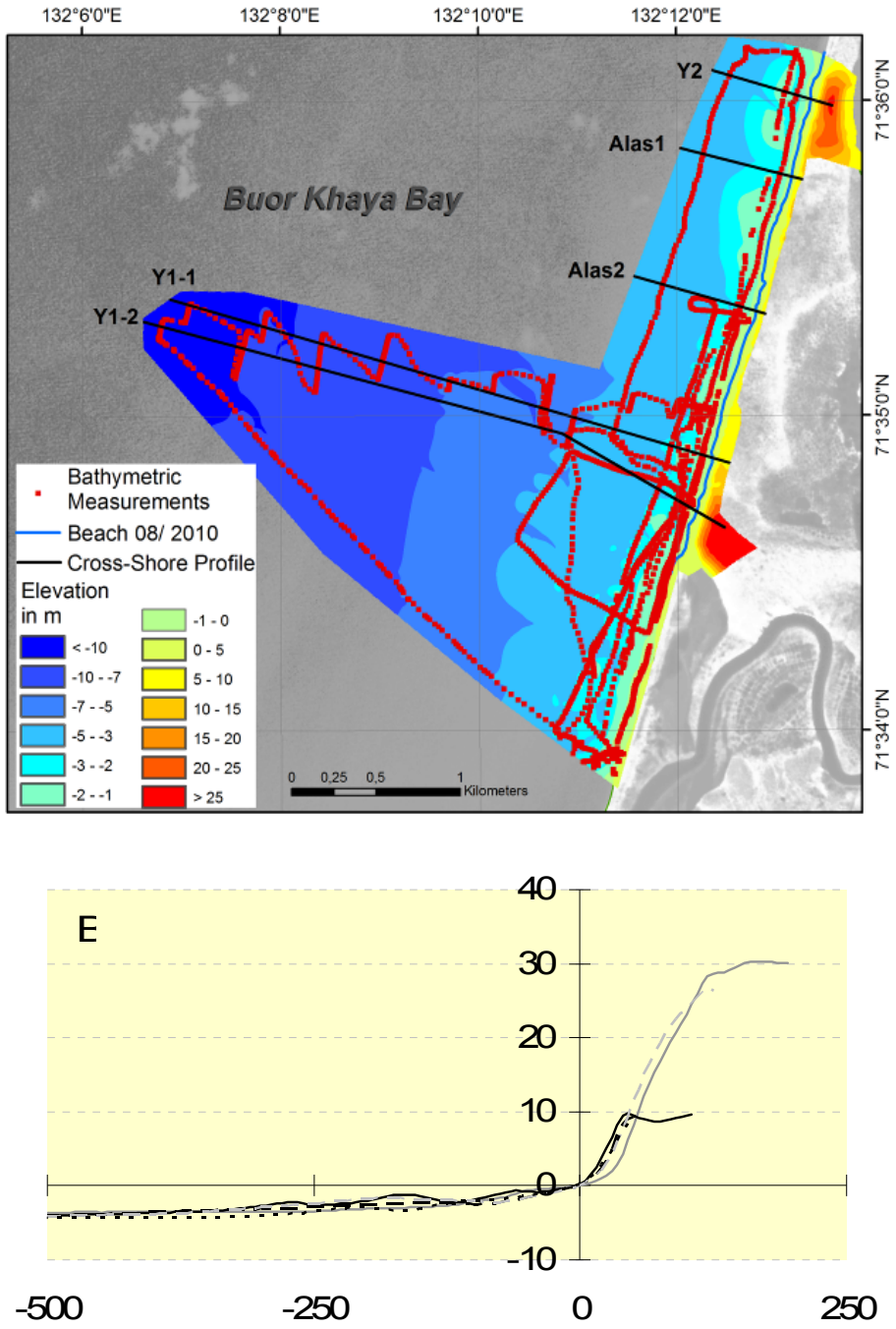

Figure 4-16: Map of the location and near shore diagrams (Y1-1, Y1-2, Y2, Alas1 and Alas2) of cross shore profiles at site *1st to 2nd Yedoma*, joint DEM of the shore face (bathymetric and tacheometric measurements).

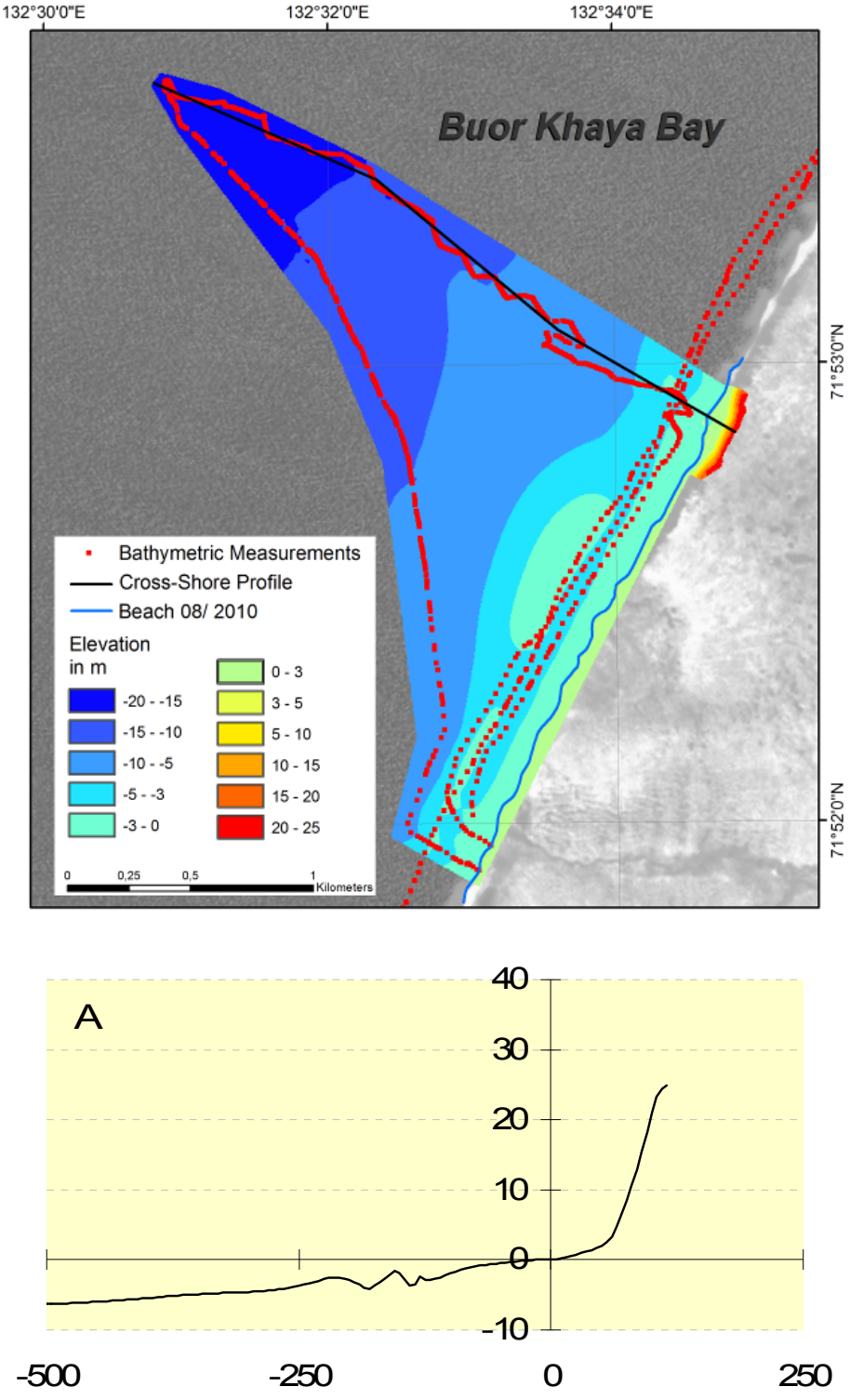

Figure 4-17: Map of the location and near shore diagram of cross shore profile at site *North Cliff* (NKLIF), joint DEM of the shore face (bathymetric and tacheometric measurements).

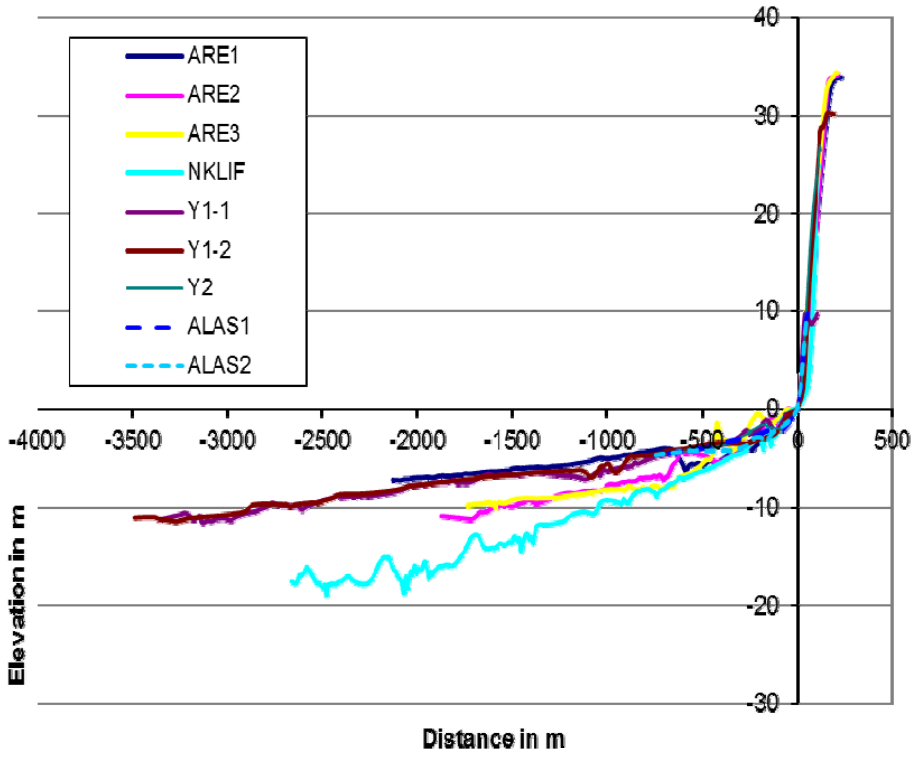

Figure 4-18: Diagram of the entire cross shore profiles.

5. PERMAFROST SEQUENCES OF BUOR KHAYA PENINSULA

Jens Strauss & Lutz Schirrmeister

5.1 Aims and objectives

This part of the expedition 'Laptev Sea - Buor Khaya 2010' was focused on studies of permafrost profiles using outcrops along the shore of the Buor Khaya Peninsula. The aim of the planned measurements are a development of a stratigraphic differentiated carbon balance and characteristic, relating the transformation of the organic matter with the permafrost dynamics during the last Late Quaternary climatic cycle, as well as examining the stability and/or degradation of the organic carbon matter fixed in permafrost.
Moreover, the expected results of cryolithological and stratigraphical studies will be used for paleoenvironmental reconstructions. In this context, the results will be compared and correlated with results of similar studies of around the Laptev and East Siberian Sea since 1998 (Russian-German Science Cooperation SYSTEM LAPTEV SEA).

5.2 Methods and field measurements

After first reconnaissance trips five selected sites were chosen for detailed studies (Fig. 5-1).

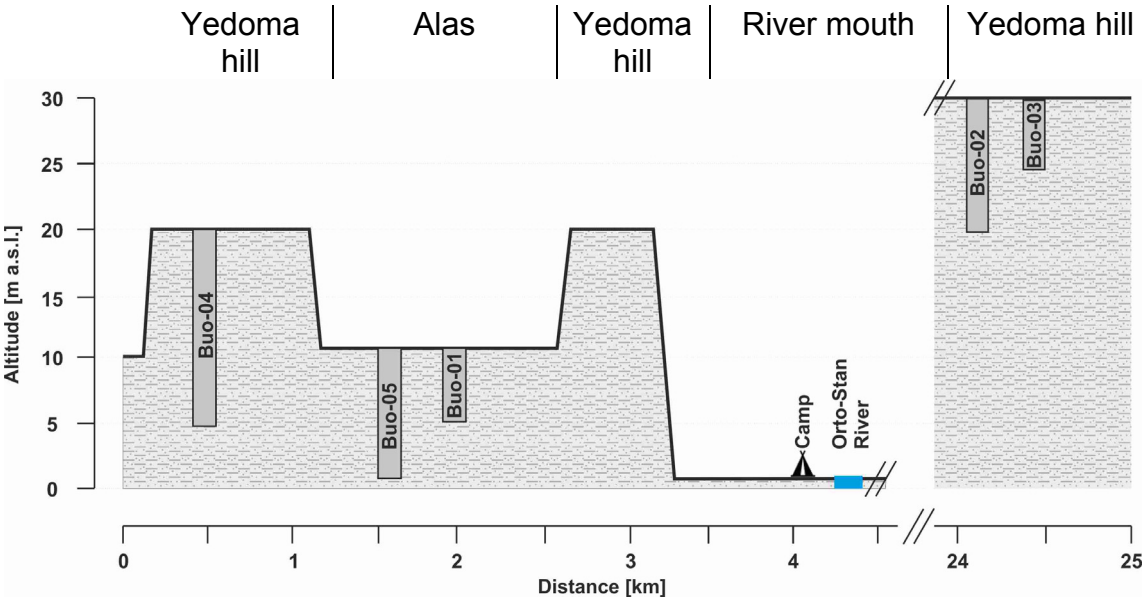

Figure 5-1: Scheme of the observed part of the shore at the Buor Khaya Peninsula with positions of the studied profiles.

The sediment of the profiles and sub profiles, partly exposed on thermokarst mounds (baydzherakhs) in thaw slumps were dug by spades and subsequently cleaned with hacks. After that the sediments and cryolithology of the chosen sequences were surveyed, described, photographed and sketched. Various sub profiles were stacked together to create composite profiles. The correlation of the sampling position in neighbouring sub profiles was done by height estimation using measuring tape. The upper edge of a profile was calibrated with tacheometer measurements (see chapter 4).
Frozen deposits were sampled for further multidisciplinary studies (sedimentology, paleoecology, geochronology, organic geochemistry) using hammers and small axes (Appendix 1). The sediment samples were packed in plastic bags. Some samples were collected unfrozen. The samples for biogeochemistry must kept cold and so these samples were stored in a thermo box. Two types of ground ice samples were taken as well (Appendix 2). Firstly, if the ice content in sediment samples was high enough, the supernatant water from the texture ice was separated for isotopic analyses. Secondly, selected ice wedges were sampled using ice screws. Furthermore, at two ice wedges, one near Buo-01 and the other next to Buo-04, larger samples of about 4 litres were taken for ^{36}Cl dating of ground ice (Gilichinsky et al., 2007).
Already in the field, the gravimetric ice content was determined according to van Everdingen (1998). Therefore frozen samples were taken in aluminium boxes, weighted and dried. For volume measurements, frozen sample material was used to determine the displacement. This is necessary for calculations of bulk density.

5.3 Outcrop description

The studied outcrops are situated at the shore of the Buor Khaya Peninsula. The permafrost sections consist of Yedoma hills and thermokarst depressions (Fig. 5-1). Bedrock outcrops are not observed but gravel (2 to 10 cm in diameter) indicates a short distance to the basement.
Two exposures of alas sequences (Buo-01 and Buo-05), two composite profiles of Ice Complex sections (Buo-02, Buo-04), and one small profile of lake deposits (Buo-03) next to the Ice Complex of Buo-02 were studied and sampled in detail.

5.3.1 Profile Buo-01

The exposure is located in a section of a thermokarst depression (alas) about 2 km north of the camp and close to the profile Buo-05. The cliff is about 9.5 m high (Fig. 5-2 and Fig. 5-3a) and the uppermost two meters are well-exposed.

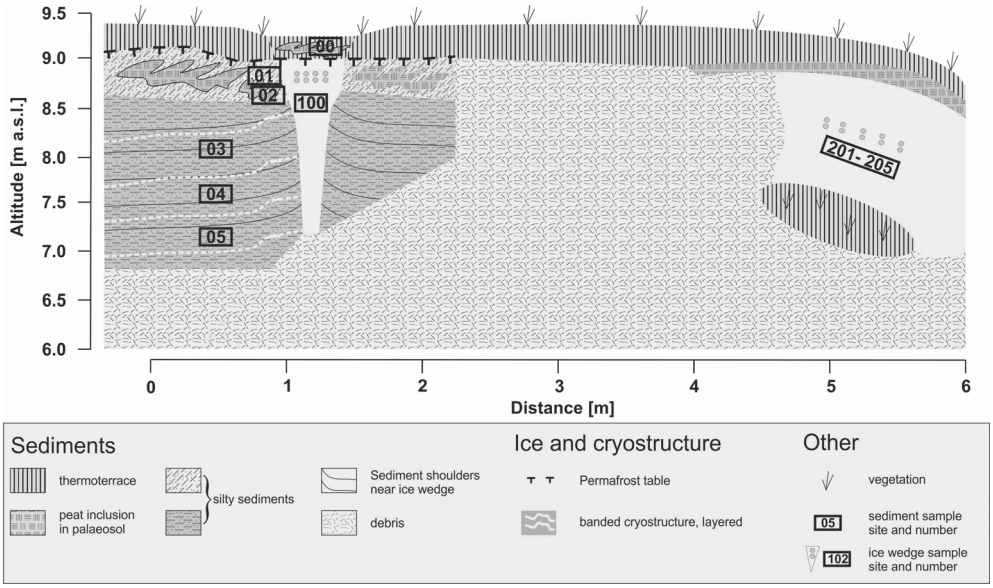

Figure 5-2: Scheme of the alas profile Buo-01.

The studied sequence starts at the surface with an unfrozen active layer (Fig. 5-4b). At this layer, recent roots penetrate the greyish-brown peaty soil horizon. Below the permafrost table a few ice veins and micro lens-like cryostructures were observed in grey silty fine-sand. At 8.7 m a.s.l. a peat inclusion was sampled. Here the sediment is ice supersaturated (646 wt % gravimetric ice content, Fig. 5-3b). The lowermost three samples are located in a horizon of greyish silty fine-sand with brownish iron-oxide patches.

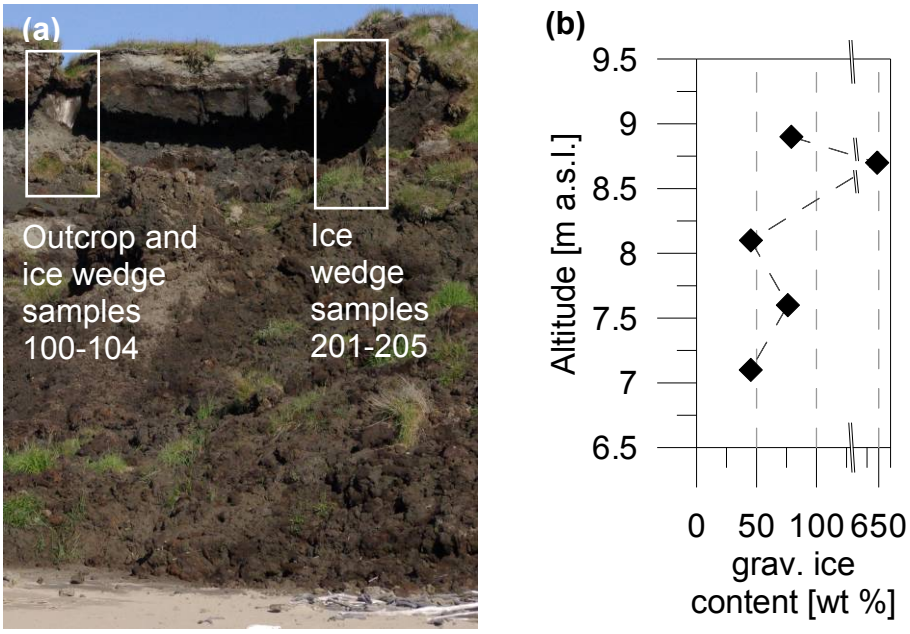

Figure 5-3: (a) Overview photo (by J. Strauss, August 2010) and (b) gravimetric ice content of profile Buo-01.

The cryostructure is characterised by bands parallel to the sediment structures. These ice bands are composed of compact fine lenses. In the interlayers, ice-bands (length 4-5 cm) are diagonal and perpendicular oriented to the sediment structures and the compact fine lens-like banding. Except the peaty sample, the gravimetric ice content varies between 45 to 79 wt % (Fig. 5-3b).

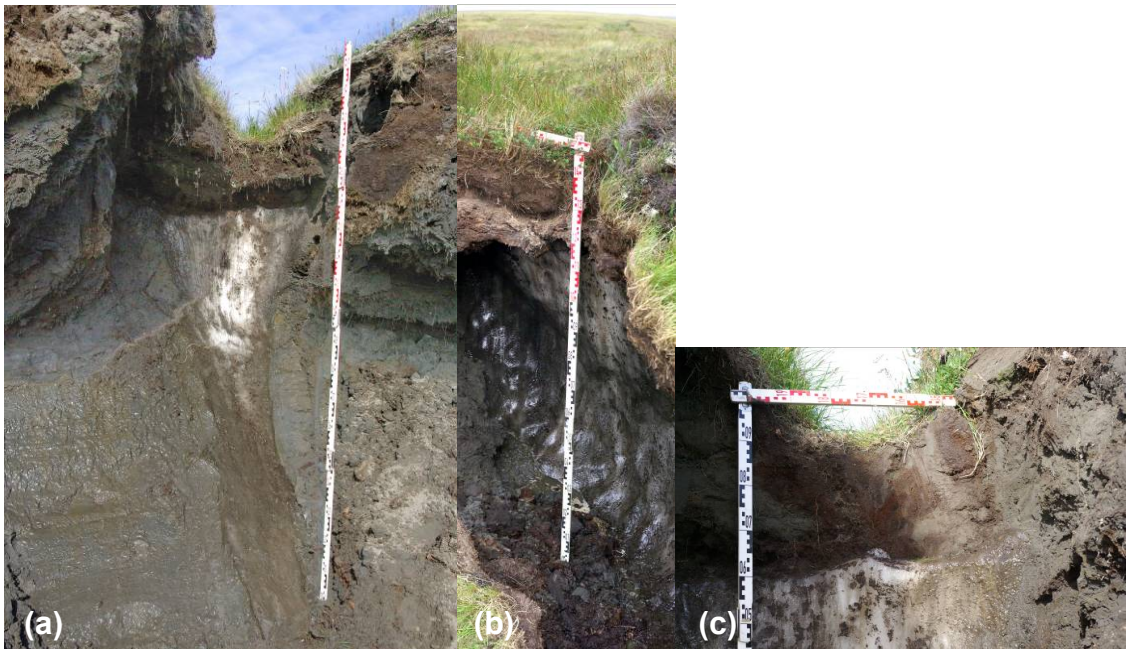

Figure 5-4: (a) Profile and (b) ice wedge overview and (c) detail photo of the active layer (Photos by J. Strauss, August 2010).

For stable water isotope measurements, four ice wedge samples in 0.15 m distance were taken next to the profile in 8.9 m a.s.l.. The ice wedge is vertical cut and consisted of milky-white ice with gas bubbles (< 1 mm). Only less sediment is included. The width on top was 0.9 m and in 1 m depth 0.3 m. The ice wedge has shoulders in which the ice bands of the sediments bended. From this ice wedge an additional large ice sample for $^{36}Cl/^{10}Be$ was taken.
On the opposite side of the small thaw slump 4 m right of Buo-01-A (Fig. 5-2 and Fig. 5-3a), another diagonal cut and 3 m wide ice wedge (Fig. 5-4b) was sampled. The ice was milky-white and on the surface high centre polygons appear.

5.3.2 Profile Buo-02

An Ice Complex exposure was studied in 24.5 km south of the campsite. The studied approximately 10 m long sequence reaches from the cliff edge down to a thermo-terrace where older permafrost deposits are buried by debris (Fig. 5-5a and b). Several 2-3 m wide and 5-7 m deep ice wedges are exposed at this ca 150 m wide thaw slump.

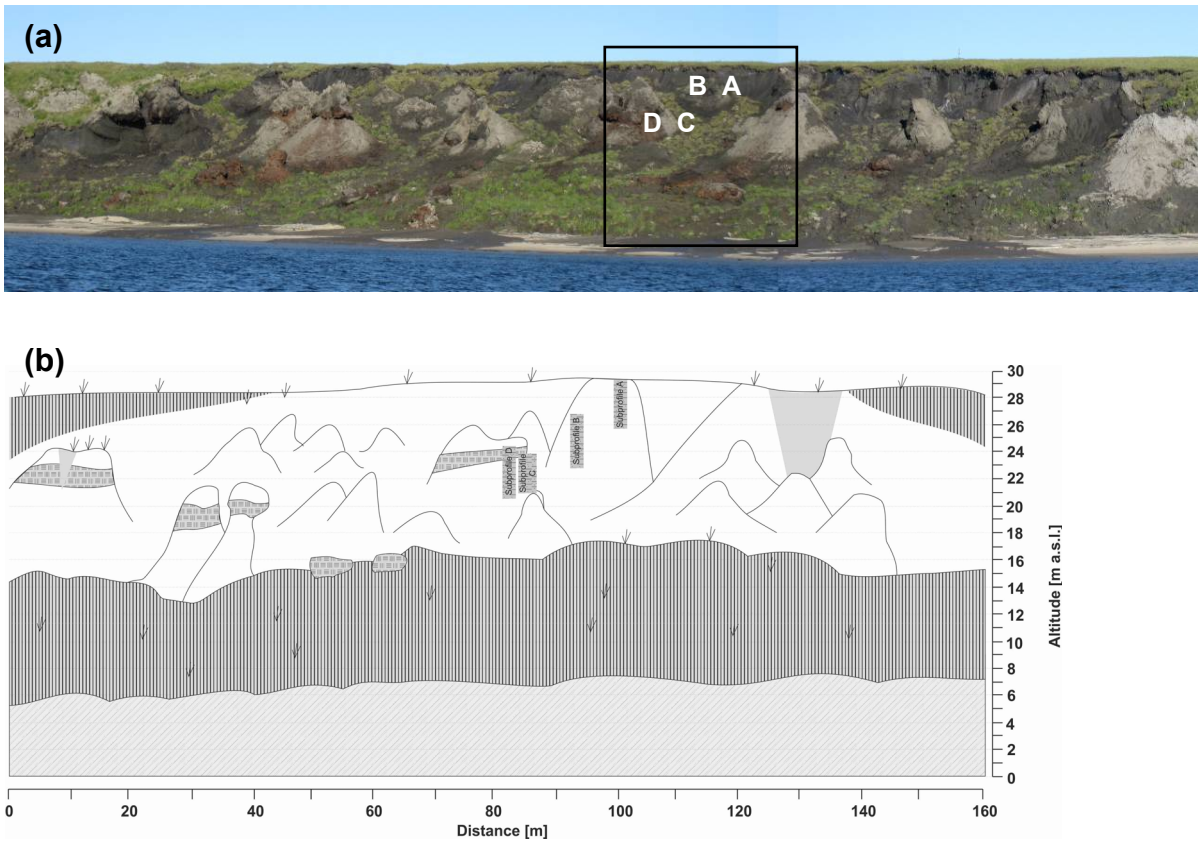

Figure 5-5: (a) Overview photo (by J. Strauss, August 2010) and (b) scheme of the Ice Complex profile Buo-02.

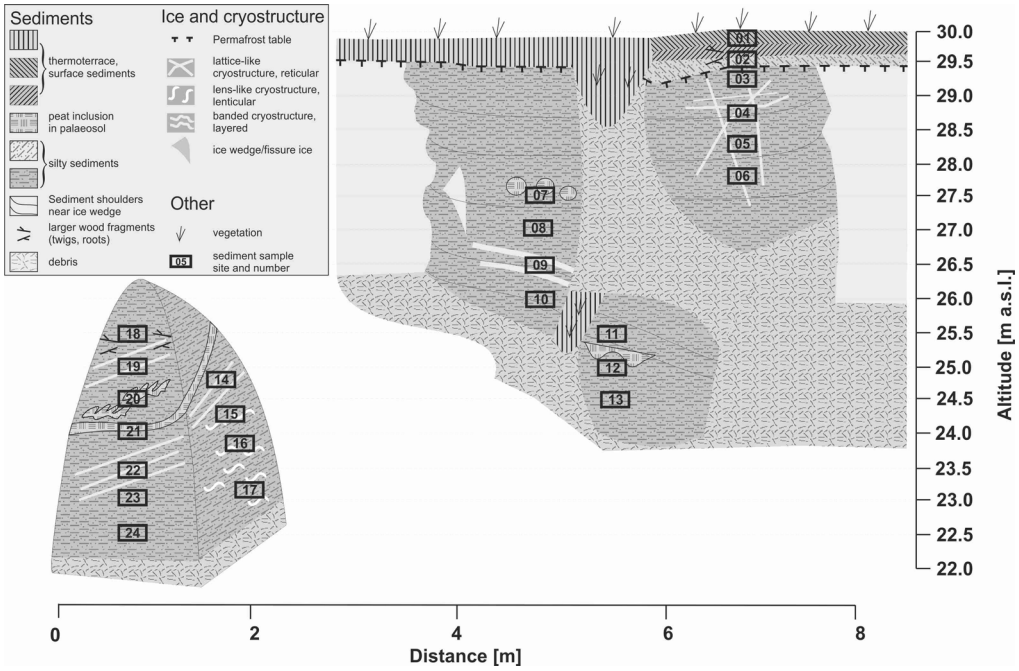

Figure 5-6: Scheme of the Ice Complex profile Buo-02.

The composite profile Buo-02 consists of four sub profiles (Buo-02-A to Buo-02-D, Fig. 5-6). The edge of the cliff is not the highest point of the Ice Complex sequence. The top of the Yedoma hill is marked with a trigonometric point in approximately 100 m distance. Here the hill is 7 to 10 m higher than at the cliff edge. Probably the studied exposure does not cover a stratigraphically complete sequence.
The first layer of Buo-02-A (Fig. 5-8a) is unfrozen with a matrix of brownish sandy deposits. Recent roots appeared.
At lower part of the active layer in 29.5 m height the sediment consists of grey and silty fine sand and is akin to the underlying frozen sediments. Several larger plant fragments occur. Under the permafrost table from 27.8 to 29.3 m, the cryostructure is horizontal banded (< 1 cm thick bands) and composed of dense-layered ice lenses. At the interlayers, fine lenses and vertical ice veins are obvious. The sediment is brownish-grey silty fine-sand, sporadically with iron oxide patches. Surrounding at 28 m height a.s.l. larger organic patches occur and reveal cryoturbated paleosol. The ice content of the frozen part of Buo-02-A is around 70 wt % (Fig. 5-7).

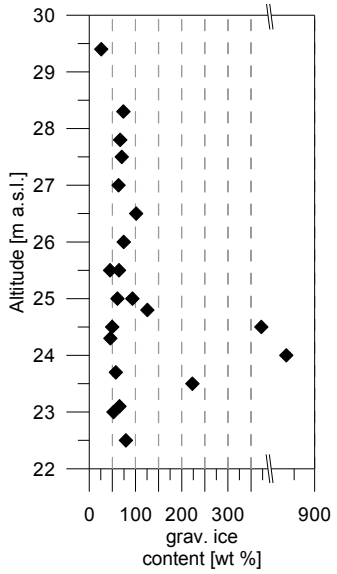

Figure 5-7: Gravimetric ice content of Buo-02.

The sub profile Buo-02-B (Fig. 5-8b) is located on the other side of the same thermokarst mound. At uppermost part of sub profile B, concentric organic-rich patches and plant detritus indicate a paleocryosol. Around these organic patches the sediment is grey-brown and silty fine-sandy with vertical filament roots. The cryostructure in the upper part of sub profile Buo-02-B is banded (Fig. 5-9), especially in 26.5 m height. In the lower part, lens-like to massive cryostructures are obvious. Here at 25 m a.s.l., a paleocryosol with tongues of light-brown material occur (Fig. 5-10). The gravimetric ice content at Buo-02-B ranges between 50 and 100 wt % (Fig. 5-7).

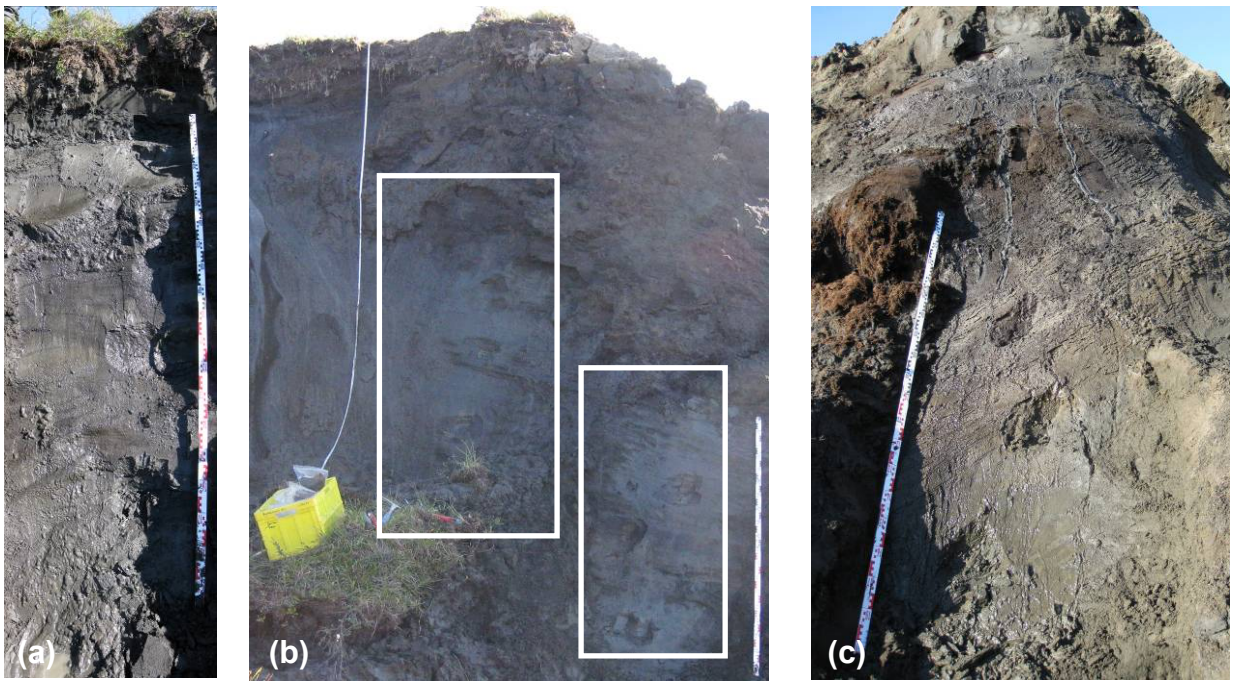

Figure 5-8: (a) Sub profile Buo-02-A; (b) Buo-02-B; (c) Buo-02-D (Photos by J. Strauss, August 2010).

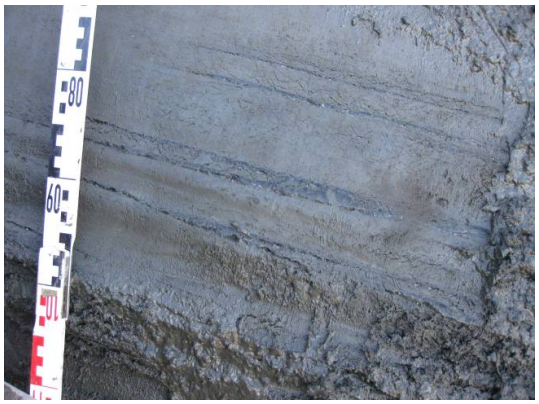

Figure 5-9: Uplifted ice bands, next to sample Buo-02-B-09 (by J. Strauss, August 2010).

Figure 5-10: Cryoturbated paleocryosol, next to sample Buo-02-B-12 (by J. Strauss, August 2010).

The sub profile Buo-02-C and D are located at the same thermokarst mound. A discordant peat layer was visible along the whole thaw slump (Fig. 5-5b) and the thermokarst mound Buo-02-C/-D comprises this layer. The thermokarst mound is apparently slumped and rotated. For this reason, sub profile Buo-02-C is stratigraphically included in Buo-02-D.
Buo-02-C is composed of grey to brownish fine sand. The uppermost sample is ice saturated (125 wt %, Fig. 5-7) with up to 10 mm thick ice veins. At the underlying parts down to 23.1 m, coarse to fine lens-like cryostructures are obvious. The gravimetric ice content amounts 45 to 65 wt % (Fig. 5-7).
At Buo-02-D, a remarkable heterogeneity of sediment composition is obvious. In the upper part at 25.5 m a.s.l. the sediment is composed of silty greyish material with brown patches and larger plant fragments. From 24 to 24.5 m a.s.l., a peat layer and peat inclusions appear. Vertical and diagonal ice veins are included and the gravimetric ice content is up to 865 wt % (Fig. 5-7). Below the peat layer, the sediment are characterised by brownish silty sand with several plant fragments. The cryostructure is micro lens-like with some ice veins. Directly below the peat layer, the gravimetric ice content (23.5 m a.s.l.) is very high (223 wt %) but decreases further down to about 52 to 79 wt % (Fig. 5-7).

5.3.3 Profile Buo-03

The short profile Buo-03 (Fig. 5-11a and b) is located south of the thaw slump of Buo-02. On the surface high-centred polygons occur.
The sampled part was exposed from 28 to 30 m height (Fig. 5-11b). A horizon with plant detritus layers are obvious (Fig. 5-11a). The uppermost sample is unfrozen and composed of light grey clayish silt. Several plant fragments are visible. A frozen peat layer in 28.7 and 29.2 m a.s.l. is 20 to 30 cm thick and ice supersaturated (249 and 259 wt %, Fig. 5-11c). The part lower 28.5 m a.s.l. consists of light greyish silty fine sand.
These deposits are most likely sediments from a shallow lake environment. Above the lake deposits, the terrain surface with thermokarst mounds increase approximately 10 m to its highest point. Possibly this indicates the occurrence of Ice Complex deposits.
Two preliminary interpretations of the origin of this well-stratified sequence are considered. Firstly these sediments could be overlain by late Pleistocene Ice Complex deposits and were accumulated in an interglacial (for example Eemian) lake. Secondly, a thermokarst depression could be frontal cut by the sea coast. This question will be answered by radiocarbon dating.

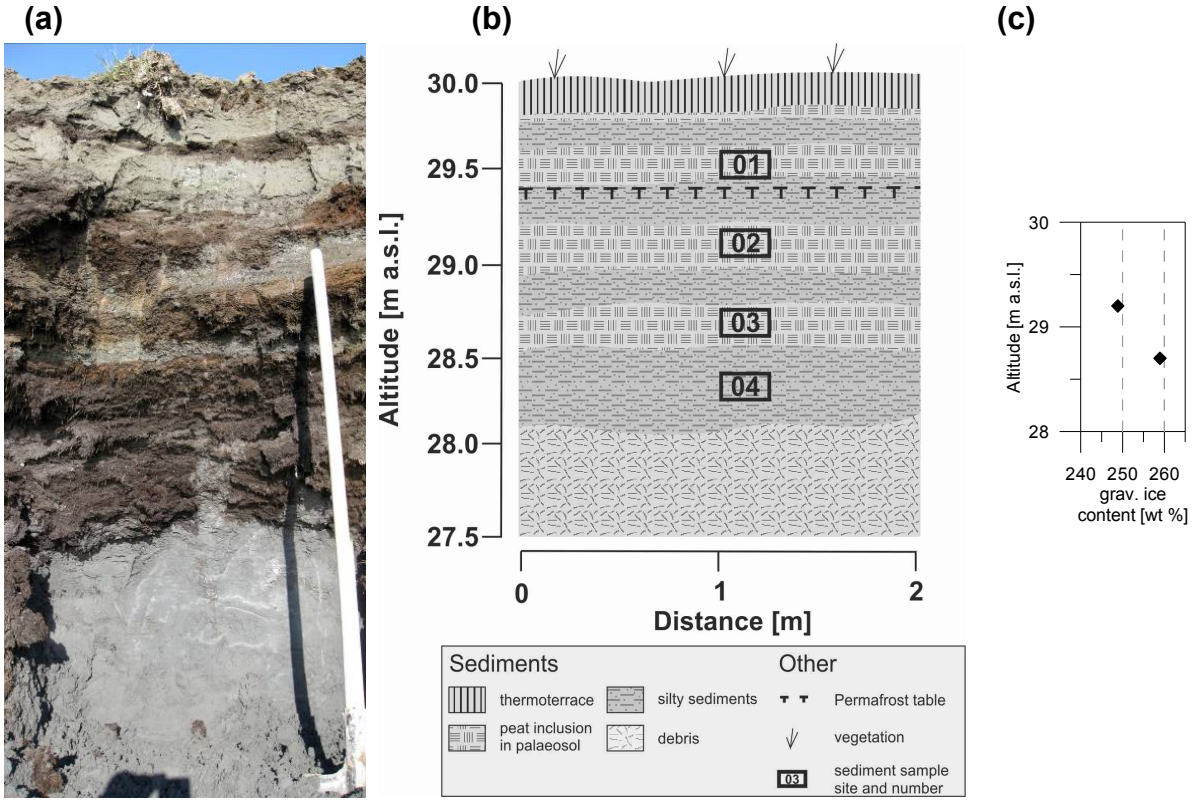

Figure 5-11: (a) Photo (by J. Strauss, August 2010), (b) scheme and (c) gravimetric ice content of profile Buo-03.

5.3.4 Profile Buo-04

A second composite profile covering Ice Complex deposits was studied in a thaw slump about 1 km north of Buo-01 (Fig. 5-1). A about 20 m long sequence was surveyed downwards starting in front of a steep wall at the cliff edge (sub profile Buo-04 A), crossing the thermo terrace for sub profile Buo-04-B and ending at a large thermokarst mound (Buo-04-C) at beach level (Fig. 5-12 and Fig. 5-13). The height of the cliff edge is not the highest point of the Yedoma hill, whose top is shaped by large thermokarst mounds (Fig. 6-12). As at Buo-02 this is an indication of degradation processes and of a stratigraphically incomplete outcrop.

The uppermost sub profile Buo-04-A is exposed between 13.6 and 18.5 m a.s.l. at a steep wall between two longitudinal cut ice wedges (Fig. 5-14). The uppermost sample was taken in the unfrozen active layer in the zone of recent vegetation and roots. The frozen Ice Complex of Buo-04-A consists of greyish-brown silty fine-sand with a lens-like cryostructure and in several parts with horizontal ice bands. Except the uppermost frozen sample (90 wt %), the gravimetric ice content ranges from 45 to 65 wt % (Fig. 5-13b). The sediments and the ice bands are bended to both sides to the ice wedges.

The nearby studied syngenetic ice wedge is diagonal cut (10 m width). Here 21 samples were taken in 0.5 mm distance. This ice wedge was sampled for ^{36}Cl dating as well. The light-grey ice wedge contains gas bubbles and several mm wide sediment stripes.

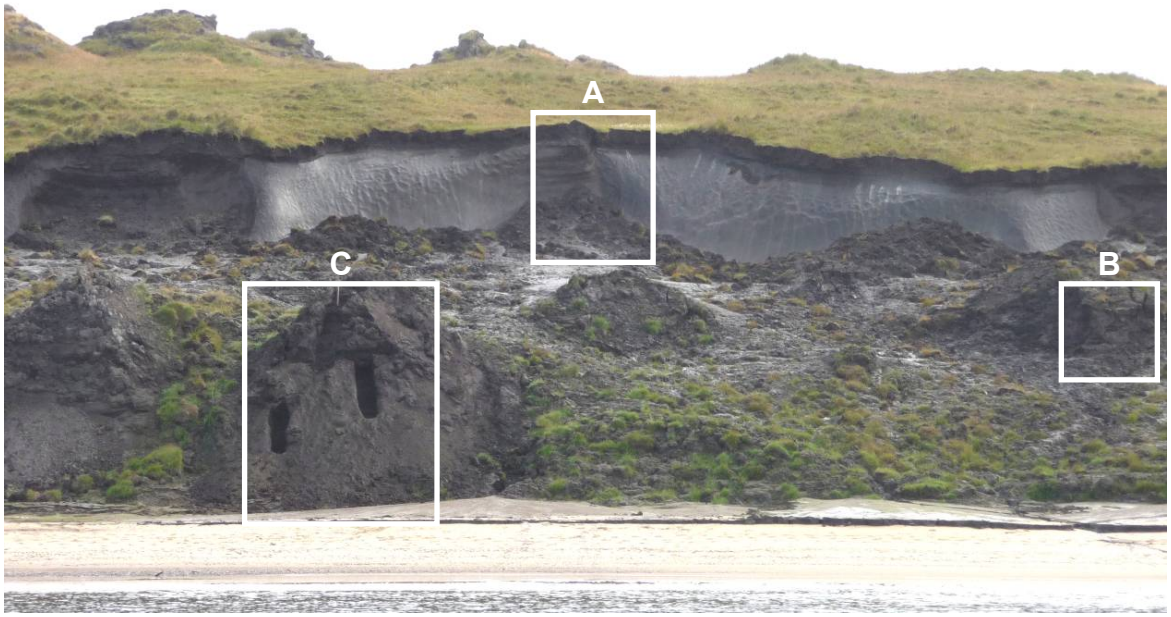

Figure 5-12: Photo of the thaw slump Buo-04 (by Frank Guenther, August 2010).

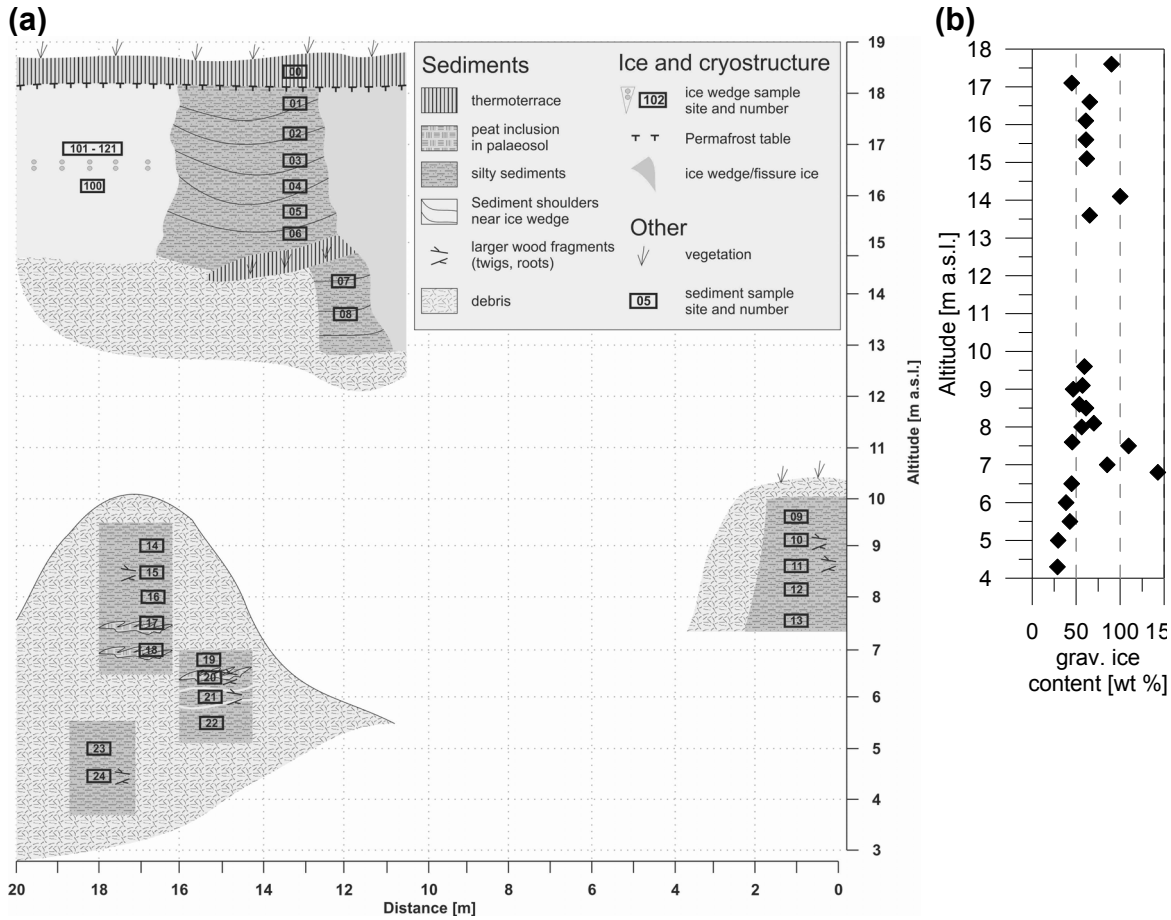

Figure 5-13: (a) Scheme and (b) ice content of profile Buo-05.

The sediments of sub profile Buo-04-B (Fig. 5-15) consist of greyish-brown silty fine-sand. The cryostructure is layered with ice bands (< 2 mm thick) composed of ice lenses. Between these ice bands horizontal orientated ice lenses are obvious. The gravimetric ice content is between 45 and 70 wt % (Fig. 5-13b). Coarse plant and wood fragments are visible at 9 m a.s.l.
The lowermost thermokarst mound was sampled in three parts (Fig. 5-12 and Fig. 5-16a, b, c). The uppermost part of sub profile Buo-04-C between 7.0 and 9.0 (Fig. 5-16a) m a.s.l. is characterised by greyish-brown silty fine sand and the occurrence of plant detritus, much root material and smaller plant stems.

Figure 5-14: Photo of sub profile Buo-04-A (by J. Strauss, August 2010).

Figure 5-15: Sub profile Buo-04-B (by J. Strauss, August 2010).

At 8.5 m a.s.l. the cryostructure is characterised by coarse lens-like ice bands. These bands appear in 5 cm distance and ice lenses (< 1 mm thick 0.5 to 1 cm long) in the sediment interlayers are reticular orientated. At 8 m a.s.l., a matrix of greyish-brown silty fine sand contained a peaty cryoturbated paleosol.
Several ice lenses cause increased gravimetric ice content between 85 to 110 wt % at 7.0 to 7.5 m a.s.l. (Fig. 5-13b). Moreover, plant detritus is layered in 7 m a.s.l.

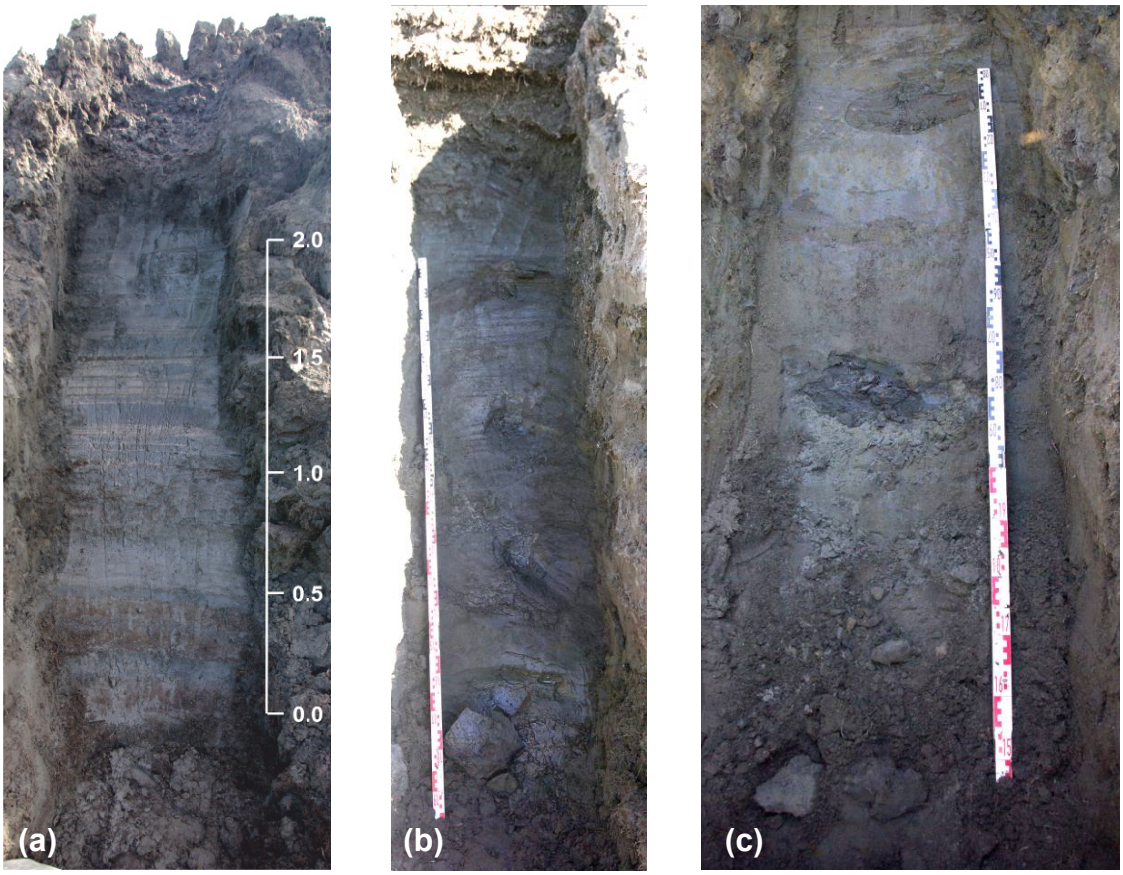

Figure 5-16: Buo-04-C upper part (a), middle part (b) and lower part (c) (by J. Strauss, August 2010).

The middle part of Buo-04-C (Fig. 5-16b) is exposed between 5.5 and 6.8 m a.s.l.. The sediment becomes sandier with depth. The peaty and horizontal bedded layers of the upper part of Buo-04-C are continued. In addition, coarse plant and wood fragments are obvious at 6.0 to 6.5 m a.s.l.. In 6.8 m height, the deposits are ice super saturated (143 wt %, Fig. 5-13b) and the cryostructure is composed of coarse ice lenses surrounding plant fragments. Smaller than 0.5 to 4 mm thickness ice bands occur. The gravimetric ice content at 5.5 to 6.5 m a.s.l. is between 39 and 45 wt % (Fig. 5-13b)
The lowest part of Buo-04-C (4.4 to 5.0 m a.s.l., Fig. 5-16c) is more sandy and dry (29 wt % ice content, Fig. 5-13b). Here a yellowish light grey matrix with iron oxide spots and broken ice lenses as well as horizontal ice fissures indicates a disturbance of the deposits.

5.3.5 Profile Buo-05

One profile, exposing lake deposits of the behind located thermokarst depression, was studied close to the first alas sequence Buo-01 (Fig. 5-1 and Fig. 5-17).
The lake sequence is covered by a peat layer, which is composed of brown peat with roots and bigger wood fragments.
At the uppermost sub profile Buo-05-A (Fig. 5-18a), the frozen deposit is characterised by greyish-brown silty to sandy sediments with partly brown spots. At 8.7 m a.s.l. a cryoturbated paleosol occur. The cryostructure is fine to coarse lens-like, partly with diagonal orientated ice lenses (width 1 mm, length 1 to 2 cm). In the lower part of Buo-05-A ice bands are obvious. The gravimetric ice content is high and ranges between 86 and 104 wt % (Fig. 5-18c).

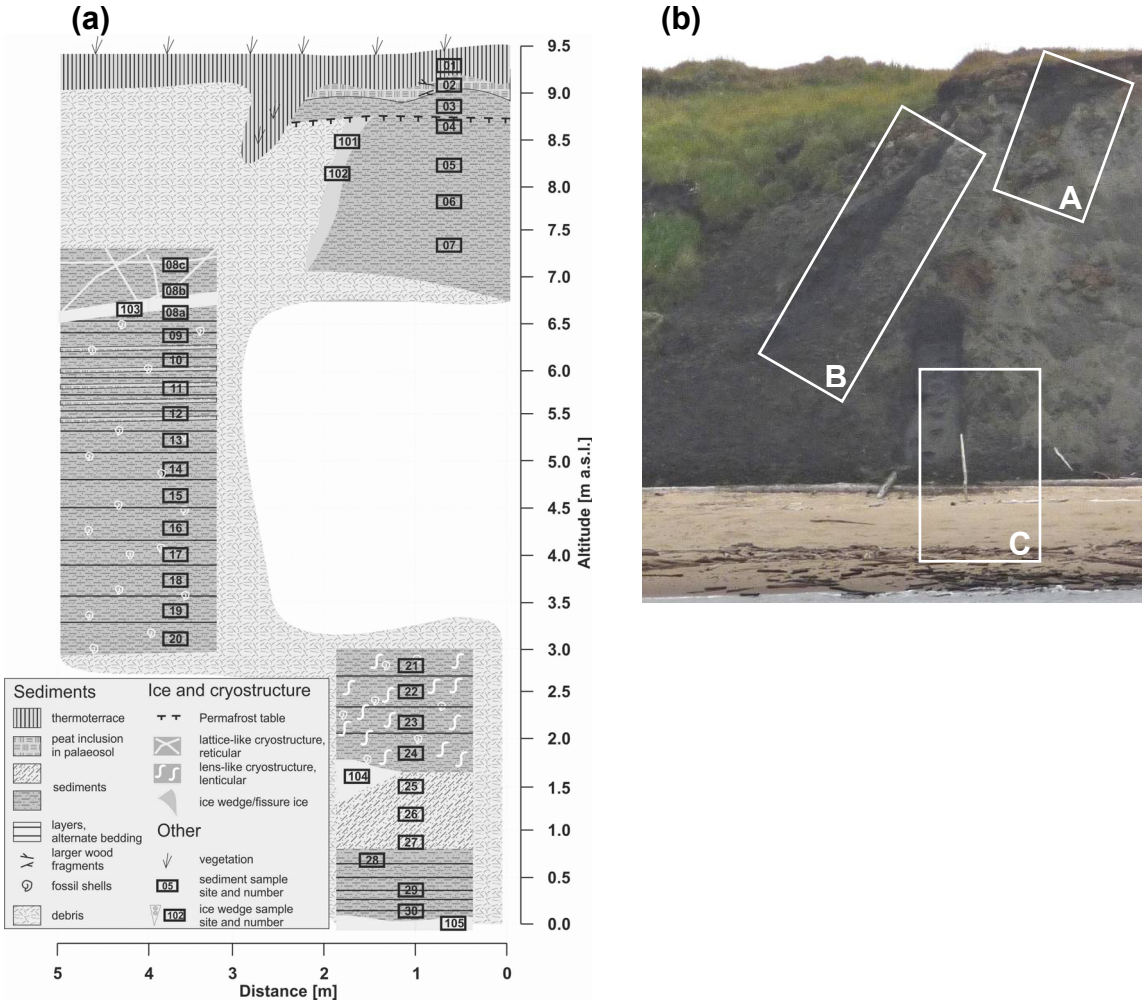

Figure 5-17: (a) Scheme and (b) photo (by J. Strauss, August 2010) of the alas lake sediment profile Buo-05.

The sub profile Buo-05-B (Fig. 5-18b), exposed between 3 and 7.5 m a.s.l. is dominantly alternate bedded with plant detritus layers (Fig. 5-19). From 5.5 to

7.1 m a.s.l. the sediments are mostly grey and silty. The cryostructure is complex, from reticulated at 7 m a.s.l. to sediment parallel banded ice lenses around 6 m a.s.l.. Molluscs appear along the whole sub profile Buo-05-B. The gravimetric ice content ranges between 30 to 51 wt %. Just at the uppermost two samples at 6.9 to 7.1 m a.s.l. the content is with 68 wt % or 82 wt % rather higher (Fig. 5-18d).

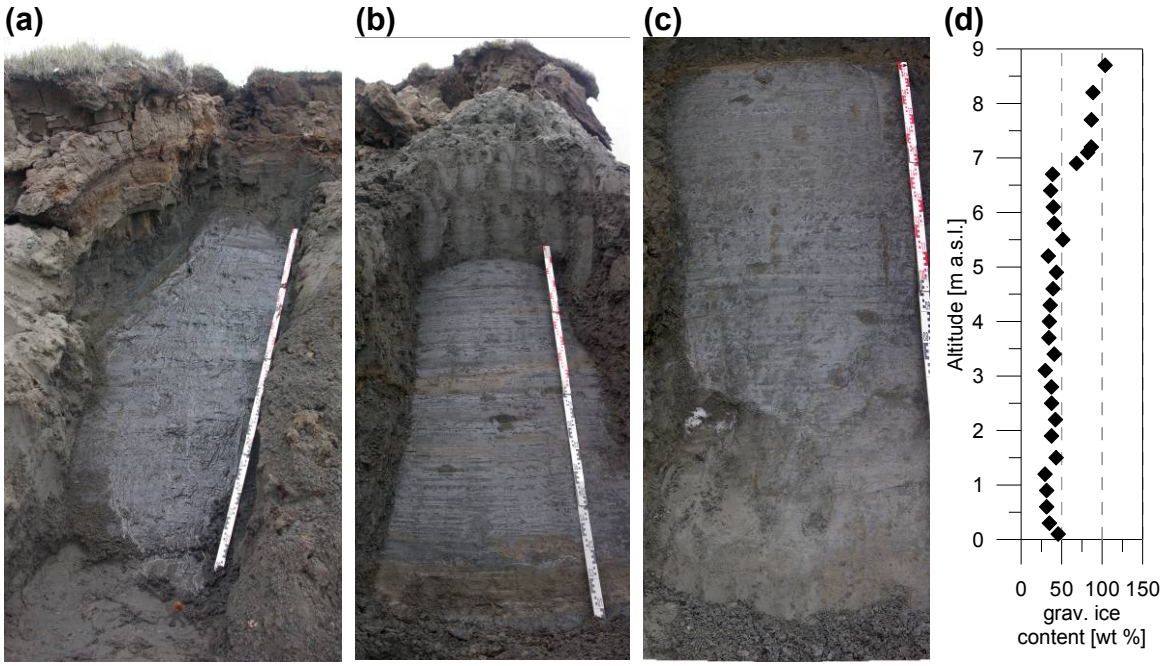

Figure 5-18: Sub profiles (a) Buo-05-A, (b) Buo-05-B, (c) Buo-05-C and (d) gravimetric ice content of Buo-05 (Photos by J. Strauss, August 2010).

Figure 5-19: Buo-05-B, alternate bedding, near sample Buo-05-B-14 (by J. Strauss, August 2010).

The upper part of sub profile Buo-05-C between 1.9 and 2.8 m a.s.l. (Fig. 5-18c) is the overlapping continuation of Buo-05-B. The sediment are characterised by grey clayey deposits which alternate bedding of several plant detritus rich layers. The cryostructure is diagonal oriented coarse lens-like (Fig. 5-20a).

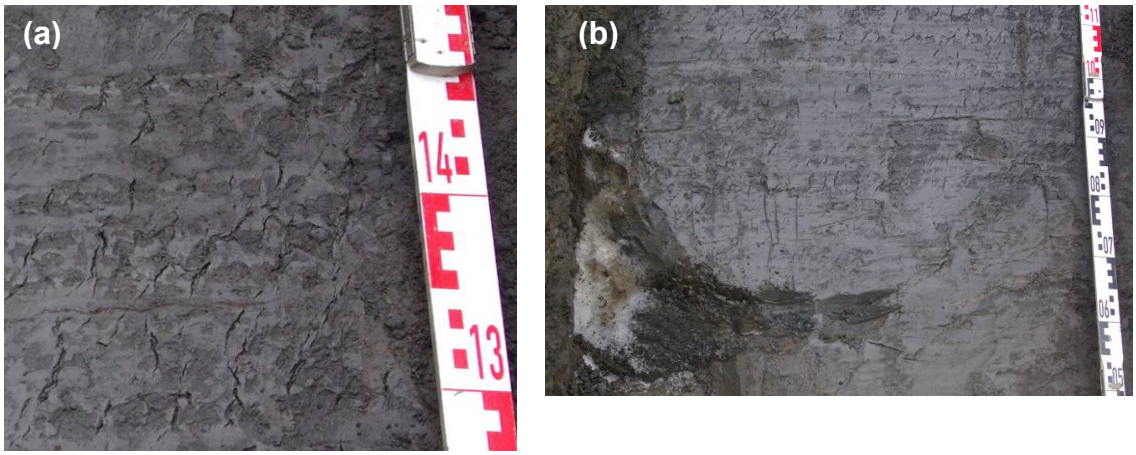

Figure 5-20: (a) coarse diagonal ice lenses near sample Buo-05-C-23 and (b) ground ice inclusion near samples Buo-05-C-24 and 25 (Photos by J. Strauss, August 2010).

Directly below a buried icy snow patch (Fig. 5-20b, 0.9 to 1.5 m a.s.l.), the sediments are different. Here, the deposits become greyish with Fe-oxide spots (10 x 5 cm), the bedding disappears and the sediment is sandy and seems drier. Moreover disturbed/washing structures are obvious. Around ice veins and horizontal ice lenses more brownish parts occur.
From the surface level up to 0.6 m a.s.l. the fine layered sediments are obvious again, but the sediments remain sandier than at the top of the sub profile Buo-05-C. Molluscs and vivianite are an additional evidence for a lake environment. At this part, the cryostructure is composed of several horizontally and vertically oriented ice lenses. The gravimetric ice content in sub profile Buo-05-C is more or less similar between 29 and 46 wt % (Fig. 5-18d).

5.4 Mammal bones

Paleoenvironmental studies of late Pleistocene and Holocene deposits at the Buor Khaya Peninsula included the collection of large fossil mammal bones. All participants of the expedition helped to collect bone material during their field trips collecting altogether 137 bones and teeth. As in previous expeditions of the Russian-German science cooperation SYSTEM LAPTEV SEA the bones and bone fragments were photographed and registered in order to obtain statistics of species composition.
The bones were collected from the different outcrops Buo-02, Buo-04 and Buo-05. A larger collecting point (99 specimens) was found in front of an Ice Complex outcrop at the bank of a large thermokarst lake approximately 2 km inland. Moreover, several bones were collected along the beach.

As a first assessment the majority of the bones belong to mammoth and bison skeletons (Appendix 3). The identification of the collection was carried out by Dr. Tatyana Kuznetsova (Moscow State University).

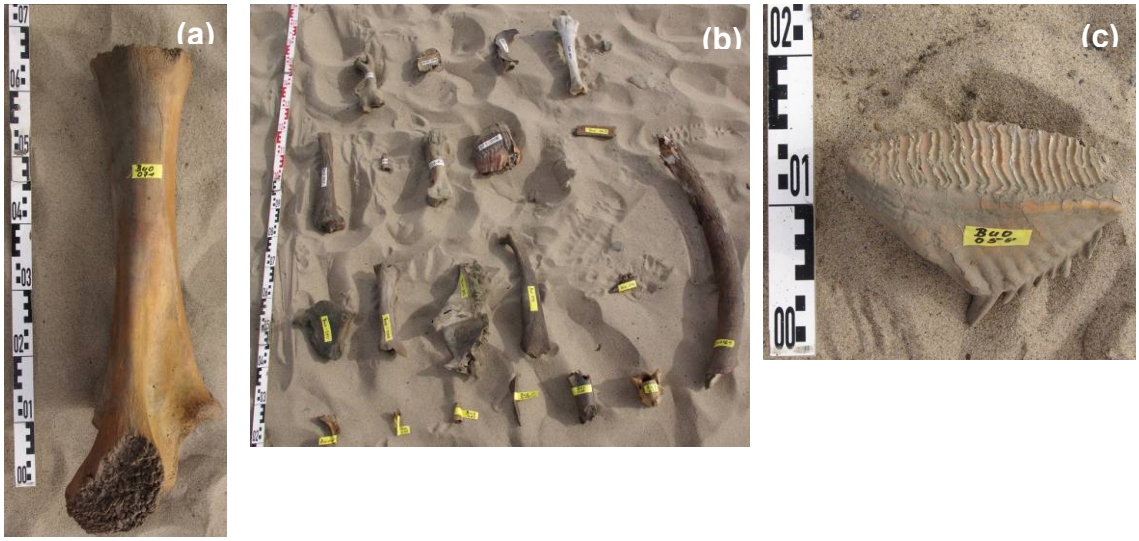

Figure 5-21: Examples of collected bones, (a) mammoth leg, (b) collection of different bones and (c) mammoth tooth (Photos by J. Strauss, August 2010).

6. MARINE SURFACE SEDIMENTS

Aleksandr Sandakov & Mikhail Grigoriev

6.1 Scientific background and objectives

The aim of our field research was to determine how much organic carbon enters the Laptev Sea, with the destruction of the Ice Complex west coast of the Peninsula Buor Khaya (Fig. 6-1), and how organic carbon is redistributed through the underwater coastal slope. The heightened interest in the coast consists of Ice Complex due to the fact that the Ice Complex is one of the main suppliers of organic carbon in the Laptev Sea (Grigoriev et al., 2004).

Figure 6-1: Outcrop of Ice Complex on Buor Khaya Penisnula.

6.2. Material and methods

During the field period in August 2010 along the western coast of the Peninsula Buor Khaya we have been sampled coastal and bottom sediments. Samples were selected from 7 profiles (Fig. 6-2). The average length of each profile was 3 km. From the Ice Complex, samples were collected at height intervals from 1 to 10 m. From the sea bottom samples were collected at depth intervals from 0.5 to 2 m with a bottom sampler. As a result, 134 samples have been obtained from 7 profiles (Tab. 6-1). Later, we will analyze the samples for organic carbon content in the Limnological Institute SB RAS and for grain size distribution at the Permafrost Institute SB RAS.

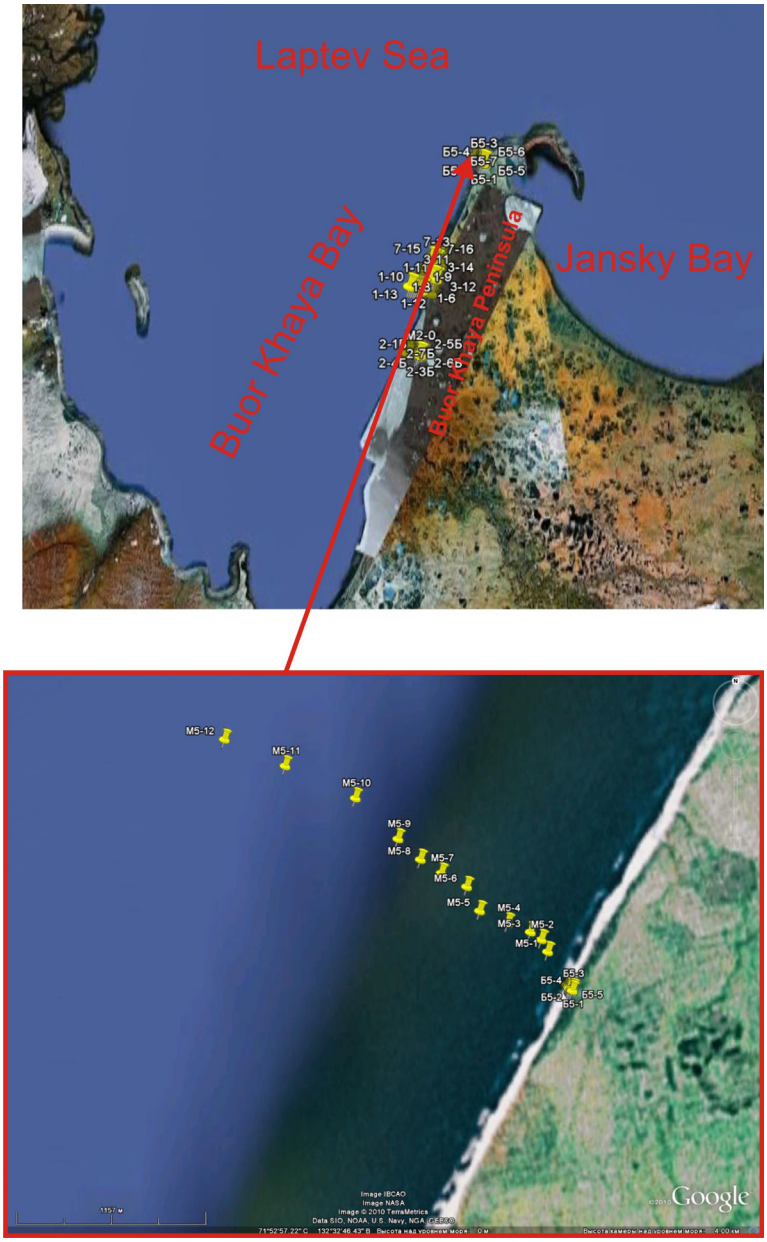

Figure 6-2: Plan of the location of profiles.

Table 6-1: Catalogue of the samples.

№	№ sample	N	E	Depth [m]	Date	Material	Selection place
1	1-1	71°33‘59.8“	132°11’ 07.9’’	- 2.7	4.08.10	sand	sea bottom
2	1-2	71°34‘07.8“	132°10’ 03.4’’	- 4.2	4.08.10	fine-grained sand	sea bottom
3	1-3	71°34‘11.8“	132°09’ 35.0’’	- 5.6	4.08.10	sandy loam	sea bottom
4	1-4	71°34’17.2“	132°08’ 58.0’’	- 6.7	4.08.10	sandy loam	sea bottom
5	1-5	71°34’21.2“	132°08’ 31.7’’	- 7.6	4.08.10	sandy loam	sea bottom
6	1-6	71°34’25.4’’	132°07’ 50.6’’	- 8.7	4.08.10	sandy loam	sea bottom
7	1-7	71°34’31.4’’	132°07’ 05.2’’	- 9.7	4.08.10	sandy loam	sea bottom
8	1-8	71°34’41.0’’	132°06’ 17.3’’	- 11.0	4.08.10	sandy loam	sea bottom
9	1-9	71°34’46.3’’	132°05’19.6’’	- 11.5	4.08.10	sandy loam	sea bottom
10	1-10	71°34’47.8’’	132°04’35.7’’	- 11.5	4.08.10	sandy loam	sea bottom
11	1-11	71°34’51.0’’	132°03’39.6’’	- 12	4.08.10	sandy loam	sea bottom
12	1-12	71°34’53.9’’	132°02’48.3’’	- 12	4.08.10	sandy loam	sea bottom
13	1-13	71°34’58.6’’	132°01’53.2’’	0.2	4.08.10	medium-grained sand	beach
14	1-14	71°33’59.4’’	132°11’35.4’’	0	4.08.10	medium-grained sand	coastline
15	2-1Б	71°25’07.7’’	132°06’15.8’’	32.0	6.08.10	silt with organic inclusion	top of the slope
16	2-2Б	71°25’07.7’’	132°06’15.8’’	27.0	6.08.10	silt	slope
17	2-3Б	71°25’07.7’’	132°06’15.8’’	26.0	6.08.10	peat	slope
18	2-4Б	71°25’07.7’’	132°06’15.8’’	16.0	6.08.10	silt with organic inclusion	slope
19	2-5Б	71°25’07.7’’	132°06’15.8’’	11.0	6.08.10	silt with organic inclusion	slope
20	2-6Б	71°25’07.7’’	132°06’15.2’’	6.0	6.08.10	silt	slope
21	2-7Б	71°25’07.4’’	132°06’14.1’’	2.0	6.08.10	silt	slope
22	M2-0	71°25’08.4’’	132°06’14.2’’	1.0	6.08.10	silt	alluvial cone
23	2-8Б	71°25’07.7’’	132°06’12.8’’	0	6.08.10	medium-grained sand	coastline
24	M2-1	71°25’10.0’’	132°06’00.1’’	- 1	6.08.10	medium-grained sand	sea bottom
25	M2-2	71°25’10.0’’	132°05’53.6’’	- 2	6.08.10	fine-grained sand	sea bottom
26	M2-3	71°25’09.6’’	132°05’41.1’’	- 2.8	6.08.10	sandy loam	sea bottom
27	M2-4	71°25’07.1’’	132°05’27.1’’	- 3.5	6.08.10	sandy loam	sea bottom
28	M2-5	71°25’06.5’’	132°05’11.8’’	- 4	6.08.10	sandy loam	sea bottom
29	M2-6	71°25’06.8’’	132°04’48.1’’	- 4.5	6.08.10	sandy loam	sea bottom
30	M2-7	71°25’05.0’’	132°04’33.4’’	- 5	6.08.10	sandy loam	sea bottom
31	M2-8	71°25’03.9’’	132°04’16.3’’	- 5.5	6.08.10	sandy loam	sea bottom
32	M2-9	71°25’05.1’’	132°04’00.5’’	- 6	6.08.10	sandy loam	sea bottom
33	M2-10	71°25’07.4’’	132°03’39.8’’	- 6.6	6.08.10	sandy loam	sea bottom
34	M2-11	71°25’10.4’’	132°03’19.8’’	- 7	6.08.10	sandy loam	sea bottom
35	M2-12	71°25’13.6’’	132°03’02.6’’	- 7.5	6.08.10	sandy loam	sea bottom
36	M2-13	71°25’13.9’’	132°02’39.7’’	- 8	6.08.10	sandy loam	sea bottom

№	№ sample	N	E	Depth [m]	Date	Material	Selection place
37	M2-14	71°25’18.5’’	132°02’16.9’’	- 8.5	6.08.10	sandy loam	sea bottom
38	M2-15	71°25’19.9’’	132°01’52.7’’	- 9.1	6.08.10	sandy loam	sea bottom
39	M2-16	71°25’19.0’’	132°01’32.9’’	- 9.5	6.08.10	sandy loam	sea bottom
40	M2-17	71°25’19.8’’	132°01’16.1’’	- 10	6.08.10	sandy loam	sea bottom
41	M2-18	71°25’19.5’’	132°01’04.1’’	- 11	6.08.10	silt	sea bottom
42	3-1	71°36’02.1’’	132°13’42.0’’	26	07.08.10	sandy loam	slope top
43	3-2	71°36’02.5’’	132°13’39.3’’	23	07.08.10	silt	slope
44	3-3	71°35’59.7’’	132°13’33.3’’	14	07.08.10	silt	slope
45	3-4	71°36’00.3’’	132°13’32.5’’	11	07.08.10	silt with inclusion	slope
46	3-5	71°36’02.6’’	132°13’33.8’’	9	07.08.10	silt with organic inclusion	slope
47	3-6	71°36’02.9’’	132°13’33.9’’	8	07.08.10	silt with organic inclusion	slope
48	3-7	71°36’02.9’’	132°13’33.1’’	5	07.08.10	peat	slope
49	3-8	71°36’03.5’’	132°13’32.3’’	0.5	07.08.10	silt	the lower part of slope
50	3-9	71°36’03.9’’	132°13’29.8’’	0	07.08.10	medium-grained sand	coastline
51	3-10	71°36’01.6’’	132°13’22.8’’	- 1.0	07.08.10	medium-grained sand	sea bottom
52	3-11	71°36’03.2’’	132°13’14.9’’	- 2.0	07.08.10	medium-grained sand	sea bottom
53	3-12	71°36’06.1’’	132°13’04.5’’	- 3.0	07.08.10	sandy loam	sea bottom
54	3-13	71°36’07.4’’	132°12’31.5’’	- 4.0	07.08.10	sandy loam	sea bottom
55	3-14	71°36’11.0’’	132°11’55.7’’	- 5.0	07.08.10	sandy loam	sea bottom
56	3-15	71°36’10.9’’	132°11’15.3’’	- 6.0	07.08.10	sandy loam	sea bottom
57	3-16	71°36’13.3’’	132°10’35.8’’	- 7.0	07.08.10	sandy loam	sea bottom
58	3-17	71°36’09.8’’	132°10’07.3’’	- 8.0	07.08.10	sandy loam	sea bottom
59	3-18	71°36’09.5’’	132°09’32.9’’	- 9.0	07.08.10	sandy loam	sea bottom
60	3-19	71°36’11.7’’	132°08’42.2’’	- 10.0	07.08.10	silt	sea bottom
61	3-20	71°36’14.4’’	132°07’26.4’’	- 11.0	07.08.10	sandy loam	sea bottom
62	3-21	71°36’15.8’’	132°06’39.2’’	- 12.5	07.08.10	sandy loam	sea bottom
63	4-1	71°35’03.3’’	132°12’39.2’’	10.0	08.08.10	peat	slope top
64	4-2	71°35’03.4’’	132°12’39.3’’	8.0	08.08.10	silt with organic inclusion	slope
65	4-3	71°35’03.4’’	132°12’38.9’’	5.5	08.08.10	silt	slope
66	4-4	71°35’03.5’’	132°12’38.7’’	3.5	08.08.10	silt	slope
67	4-5	71°35’03.2’’	132°12’38.0’’	1.0	08.08.10	silt	slope
68	4-6	71°35’03.8’’	132°12’34.9’’	0	08.08.10	medium-grained sand	coastline
69	4-7	71°35’04.1’’	132°12’20.5’’	- 1.5	15.08.10	fine-grained sand	sea bottom
70	4-8	71°35’04.2’’	132°12’18.6’’	- 2.0	15.08.10	fine-grained sand	sea bottom
71	4-9	71°35’05.5’’	132°12’07.8’’	- 3.0	15.08.10	sandy loam	sea bottom
72	4-10	71°35’06.6’’	132°11’40.1’’	- 4.0	15.08.10	sandy loam	sea bottom

№	№ sample	N	E	Depth [m]	Date	Material	Selection place
73	4-11	71°35'03.5''	132°11'04.7''	- 5.0	15.08.10	sandy loam	sea bottom
74	4-12	71°35'10.1''	132°10'50.1''	- 6.0	15.08.10	sandy loam	sea bottom
75	4-13	71°35'09.7''	132°10'16.1''	- 7.0	15.08.10	sandy loam	sea bottom
76	4-14	71°35'17.9''	132°09'12.4''	- 8.0	15.08.10	sandy loam	sea bottom
77	4-15	71°35'18.3''	132°08'32.5''	- 9.0	15.08.10	sandy loam	sea bottom
78	4-16	71°35'21.9''	132°07'57.9''	- 10.0	15.08.10	sandy loam	sea bottom
79	4-17	71°35'23.7''	132°07'11.9''	- 11.0	15.08.10	sandy loam	sea bottom
80	Б5-1	71°52'48.2''	132°34'44.2''	32.0	12.08.10	silt with organic inclusion	slope top
81	Б5-2	71°52'48.2''	132°34'44.3''	28.0	12.08.10	silt with organic inclusion	slope
82	Б5-3	71°52'48.6''	132°34'44.4''	22.0	12.08.10	silt	slope
83	Б5-4	71°52'48.6''	132°34'43.9''	17.0	12.08.10	silt	slope
84	Б5-5	71°52'48.7''	132°34'42.6''	7.0	12.08.10	sandy loam	slope
85	Б5-6	71°52'49.0''	132°34'41.9''	2.0	12.08.10	silt	slope
86	Б5-7	71°52'49.2''	132°34'41.5''	0.5	12.08.10	sandy loam	alluvial cone
87	Б5-8	71°52'49.4''	132°34'41.0''	0	12.08.10	medium-grained sand	coastline
88	М5-1	71°52'55.9''	132°34'29.0''	- 1.0	10.08.10	medium-grained sand	sea bottom
89	М5-2	71°52'58.3''	132°34'25.0''	- 4.0	10.08.10	sandy loam	sea bottom
90	М5-3	71°52'59.8''	132°34'18.1''	- 5.0	10.08.10	sandy loam	sea bottom
91	М5-4	71°53'01.6''	132°34'03.7''	- 6.0	10.08.10	sandy loam	sea bottom
92	М5-5	71°53'04.0''	132°33'45.9''	- 7.0	10.08.10	sandy loam	sea bottom
93	М5-6	71°53'08.8''	132°33'37.7''	- 8.0	10.08.10	sandy loam	sea bottom
94	М5-7	71°53'11.5''	132°33'21.5''	- 9.0	10.08.10	sandy loam	sea bottom
95	М5-8	71°53'14.2''	132°33'08.2''	- 10.0	10.08.10	sandy loam	sea bottom
96	М5-9	71°53'18.3''	132°32'53.9''	- 11.0	10.08.10	sandy loam	sea bottom
97	М5-10	71°53'26.4''	132°32'26.7''	- 13.0	10.08.10	sandy loam	sea bottom
98	М5-11	71°53'32.8''	132°31'41.8''	- 15.0	10.08.10	sandy loam	sea bottom
99	М5-12	71°53'38.1''	132°31'03.0''	- 17.0	10.08.10	sandy loam	sea bottom
100	6-1	71°38'51.3''	132°16'14.8''	32.0	17.08.10	silt	slope top
101	6-2	71°38'50.8''	132°16'14.0''	28.0	17.08.10	silt with organic inclusion	slope
102	6-3	71°38'52.3''	132°16'16.0''	22.0	17.08.10	silt with organic inclusion	slope
103	6-4	71°38'52.3''	132°16'14.7''	17.0	17.08.10	silt with organic inclusion	slope
104	6-5	71°38'51.3''	132°16'12.4''	12.0	17.08.10	peat	slope
105	6-6	71°38'53.3''	132°16'13.5''	7.0	17.08.10	silt with organic inclusion	slope
106	6-7	71°38'51.5''	132°16'10.4''	1.5	17.08.10	peat	slope
107	6-8	71°38'51.7''	132°16'10.0''	0.5	17.08.10	sandy loam	alluvial cone
108	6-9	71°38'51.8''	132°16'09.3''	0	17.08.10	medium-grained sand	coastline

№	№ sample	N	E	Depth [m]	Date	Material	Selection place
109	6-10	71°38’51.7’’	132°16’04.7’’	- 1.0	17.08.10	medium-grained sand	sea bottom
110	6-11	71°38’53.6’’	132°15’53.6’’	- 2.0	17.08.10	fine-grained sand	sea bottom
111	6-12	71°38’55.2’’	132°15’37.0’’	- 3.0	17.08.10	sandy loam	sea bottom
112	6-13	71°38’55.0’’	132°15’20.8’’	- 4.0	17.08.10	sandy loam	sea bottom
113	6-14	71°38’55.8’’	132°14’50.9’’	- 5.0	17.08.10	sandy loam	sea bottom
114	6-15	71°38’57.5’’	132°14’15.9’’	- 6.0	17.08.10	sandy loam	sea bottom
115	6-16	71°39’02.5’’	132°13’35.9’’	- 7.0	17.08.10	sandy loam	sea bottom
116	6-17	71°39’08.3’’	132°13’14.3’’	- 8.0	17.08.10	sandy loam	sea bottom
117	6-18	71°39’16.2’’	132°12’48.0’’	- 9.0	17.08.10	sandy loam	sea bottom
118	6-19	71°39’22.0’’	132°11’57.6’’	- 10.0	17.08.10	sandy loam	sea bottom
119	7-1	71°38’08.5’’	132°15’36.7’’	7.5	17.08.10	peat	slope top
120	7-2	71°38’08.3’’	132°15’36.7’’	5.5	17.08.10	silt	slope
121	7-3	71°38’08.1’’	132°15’36.8’’	3.5	17.08.10	silt	slope
122	7-4	71°38’08.3’’	132°15’36.8’’	0.5	17.08.10	silt	slope
123	7-5	71°38’08.1’’	132°15’36.9’’	0	17.08.10	fine-grained sand	coastline
124	7-7	71°38’06.7’’	132°15’19.8’’	- 1.0	17.08.10	fine-grained sand	sea bottom
125	7-8	71°38’08.5’’	132°15’08.5’’	- 2.0	17.08.10	fine-grained sand	sea bottom
126	7-9	71°38’10.5’’	132°15’04.5’’	- 3.0	17.08.10	sandy loam	sea bottom
127	7-10	71°38’15.1’’	132°14’46.8’’	- 4.0	17.08.10	sandy loam	sea bottom
128	7-11	71°38’23.1’’	132°14’10.6’’	- 5.0	17.08.10	sandy loam	sea bottom
129	7-12	71°38’30.0’’	132°13’33.9’’	- 6.0	17.08.10	sandy loam	sea bottom
130	7-13	71°38’35.0’’	132°13’12.4’’	- 7.0	17.08.10	medium-grained sand	sea bottom
131	7-14	71°38’42.3’’	132°12’45.2’’	- 8.0	17.08.10	sandy loam	sea bottom
132	7-15	71°38’49.8’’	132°12’12.1’’	- 9.0	17.08.10	sandy loam	sea bottom
133	7-16	71°38’45.7’’	132°11’35.2’’	- 10.0	17.08.10	sandy loam	sea bottom
134	1-рек	71°33’56.0’’	132°11’59.9’’	0.3	08.08.10	sandy loam	River Orto-Stan
135	2-рек	71°33’28.1’’	132°11’15.7’’	0.4	08.08.10	sand	Orto-Stan River mouth

7. GEOELECTRICAL PROFILING IN THE NEAR SHORE ZONE OF THE BUOR KHAYA PENINSULA

Paul Overduin & Sebastian Wetterich

7.1 Scientific background and objectives

Geoelectric surveys offer the chance to measure the bathymetry, to detect the depth of penetration of the salt front into the sediment, and to detect the upper surface of the ice-bonded permafrost within the sediment profile. Coupled with a geophysical method suitable for observing structure within the sediment, such as seismic surveys, our aim is to use geoelectric surveys to investigate processes involved in permafrost degradation in the near-shore zone, including the effects of sea ice, storm events, sedimentation and sea water dynamics on the permafrost. An overarching goal at the Buor Khaya site was to characterize drill sites for a proposed drilling campaign, which, conversely, will provide verification for geophysical observations and improve the applicability of these geophysical techniques for permafrost investigations in the coastal zone.
Our objectives in the field were, therefore, to observe the apparent resistivity of the sediment, collect surface sediment samples for laboratory determination of resistivity as a function of temperature and salinity, to log the temperature and salinity at the sea bed during the summer high temperature period and to characterize the proposed drilling site in terms of bathymetry and permafrost depth, via inversion of observed apparent resistivity. Logistical difficulties made it impossible to include seismic survey equipment in this field excursion (the device planned for the expedition was irreparably damaged shortly before the expedition freight was to be shipped).
The western coast of the Buor Khaya Peninsula is influenced by the Lena River´s nival discharge regime. As a result, the salinity and temperature of the water in the Buor Khaya Bay can be expected to be lower and warmer than more exposed marine coastal zones, as well as to vary strongly with season. The bathymetry available for this coastline is from the 1940s to 1970s, and shows a, for the Laptev Sea, steep inclination of the sea bed, so that water depth commonly reach 10 m at less than 2 km offshore.

7.2 Sub-bottom geoelectric Surveys

The geoelectric system used was the Syscal Pro Deep Marine system with 10 channels, an injection voltage of up to 36 V and about 10 A. A Wenner-Schlumberger array (also called a reciprocal Schlumberger array) and a dipole-

dipole array were employed. The former is the standard floating electrode array employed by the Syscal system, and measures quasi-symmetric voltages around a current injection dipole of 5 m size. The potential electrodes were graphite electrodes about 7 cm in length and 6 cm in diameter. The injection electrodes were non-corroding metal tubes of ca. 25 cm length and similar diameter. The dipole-dipole configuration employed a 5 m injection dipole separated from the potential electrode chain by 50 m (Fig. 7-1).

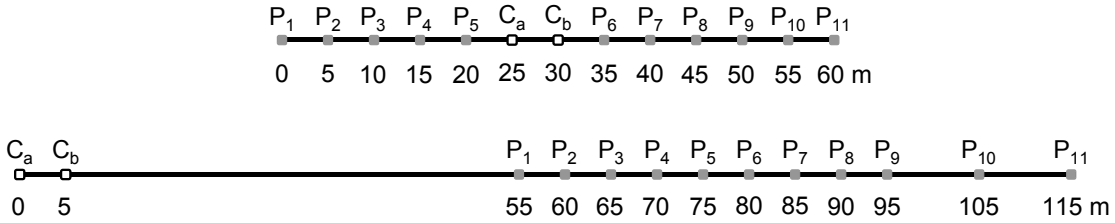

Figure 7-1: Electrode arrays used in this investigation, where C_a and C_b indicate current injection electrodes and P_i indicate potential electrodes. We refer to the upper array as the reciprocal Schlumberger, and to the lower as dipole-dipole. Neither array is symmetrical.

Measured apparent resistivities are generally assigned to a subsurface pseudo-depth. The pseudo-depth can be calculated in different ways, but is generally a reflection of the depth within the subsurface at which sensitivity reaches a maximum or median value for a homogeneous half-space. In the latter case, it is the depth to which half of the observed variation in resistivity can be ascribed. Figure 7-2 compares the 2D distribution of the sensitivity index for both electrode arrays. Both arrays are highly sensitive to variations in resistivity near the surface, so that inversions of apparent resistivity data are sensitive to inaccuracies in water resistivity and bathymetry. The pseudo-depths ascribed to the apparent resistivites range from 2.6 to 11.2 m for the reciprocal Schlumberger array, and from 13.5 to 26.8 m for the dipole-dipole array.

Through the use of two electrode arrays, we attempted to use the equipment available in the field to penetrate as deeply as possible into the sediment, a reaction to the observed steep inclination of what was interpreted from apparent resistivity variations with depth as the top of the ice-bearing permafrost.

The geoelectric system was employed around two locations along the western coast of the Buor Khaya Peninsula, one north and south of the base camp position at the mouth of the Orto-Stan River, and the second 14 to 16 km to the south, at a proposed drilling site. 71 soundings and profiles that extended for more than 54 km were surveyed. Simultaneous recording of bathymetry for these profiles was complemented by alongshore bathymetric profiles along 52 km of coastline.

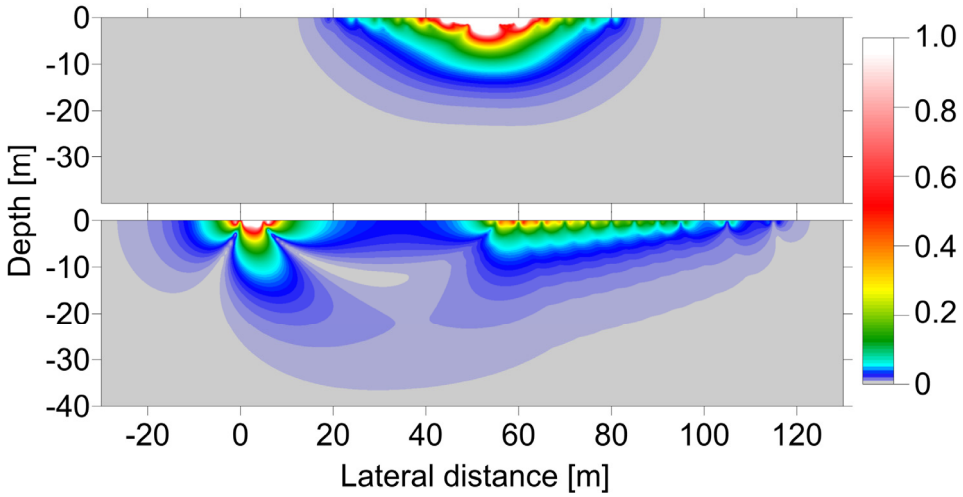

Figure 7-2: Net relative sensitivities of the two electrode arrays (upper graph: reciprocal Schlumberger; lower graph: dipole-dipole) are shown, calculated for a homogeneous half-space. The distributed cumulative sensitivity shown here gives the sensitivity of the measured potential to changes in resistivity of a point in the subsurface. The actual sensitivity will be affected by changes in the spatial distribution of resistivity in the subsurface. Nonetheless, the sensitivities shown here give an indication of the relative strengths and weaknesses of the two electrode arrays.

7.3 Bottom-moored measurements of salinity, temperature and water depth

Dataloggers (Miniloggers) from UIT Umwelttechnik GmbH were anchored on the seabed with metal plates at two locations in 2 and 4 m water depth and measured electrical conductivity, temperature and pressure sensors. Hourly data was collected between August 6, 2010 04:00 (GMT) and August 16, 2010 04:00 (GMT), and recorded one storm event during this period. Recovery of the loggers was made difficult by the amount of sediment, a mix of sand and silt, deposited on the anchor plates. At least 5 cm had been deposited on the logger at 4 m water depth. Recovery of the logger at 2 m water depth was made difficult due to sediment loading of the plate, but no value for the amount of deposition can be given.

Table 7-1: Details of the CTD datalogger deployment.

Position	Water depth	Inventory and serial numbers
71° 25' 07.5" N 132° 05' 51.2" E	2 m	AWI 102903 SN: 56.300/108
71° 25' 10.8" N 132° 05' 13.9" E	4 m	AWI 102902 SN: 56.300/107

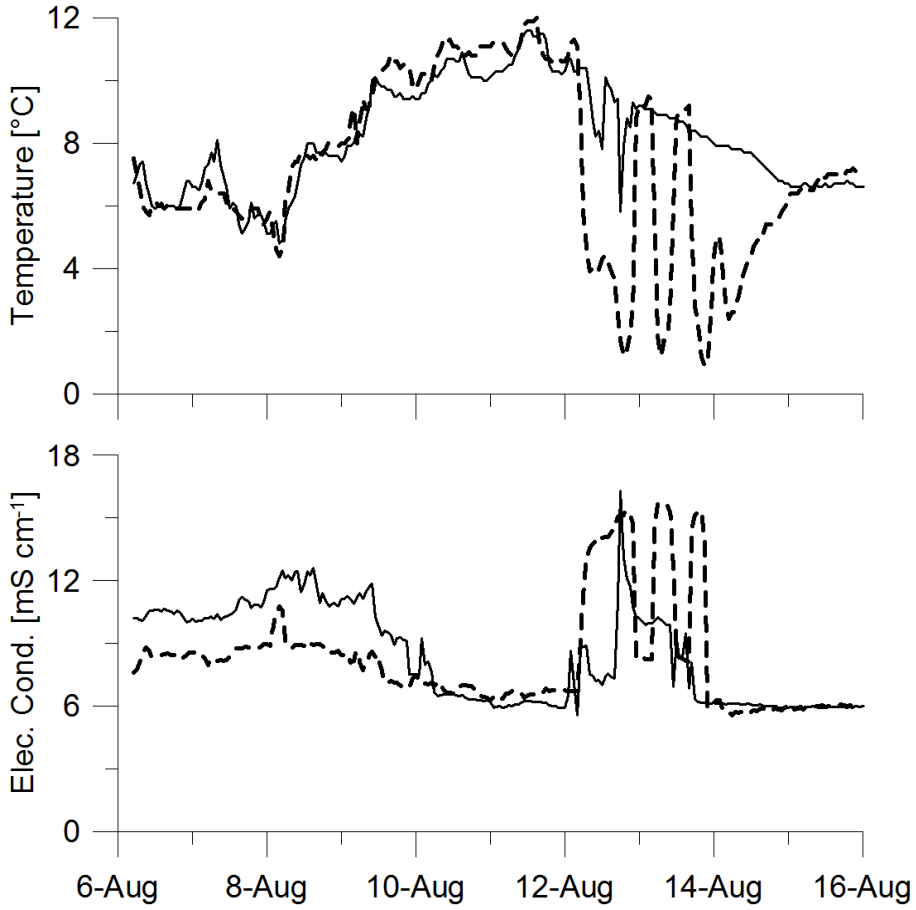

Figure 7-3: Water temperature and electrical conductivity at two water depths: 2 m (solid) and 4 m (dashed).

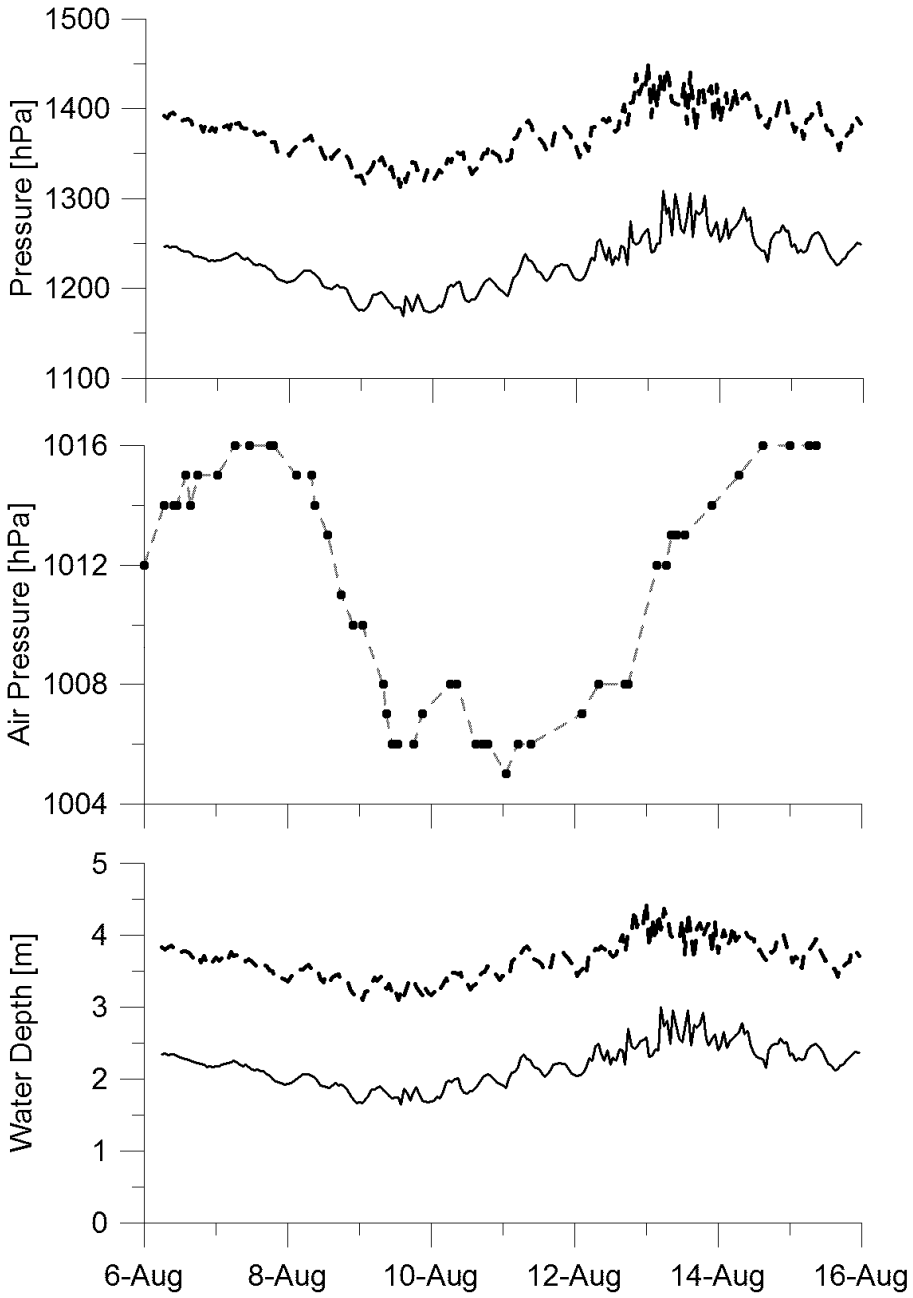

Figure 7-4: Observed pressure at two locations on the sea bed (top; solid line: approx. 2 m water depth; dashed line: approx. 4 m depth), air pressure [hPa] at sea level measured using a Suunto wristband barometer (middle) and water depths adjusted for variations in air pressure (bottom).

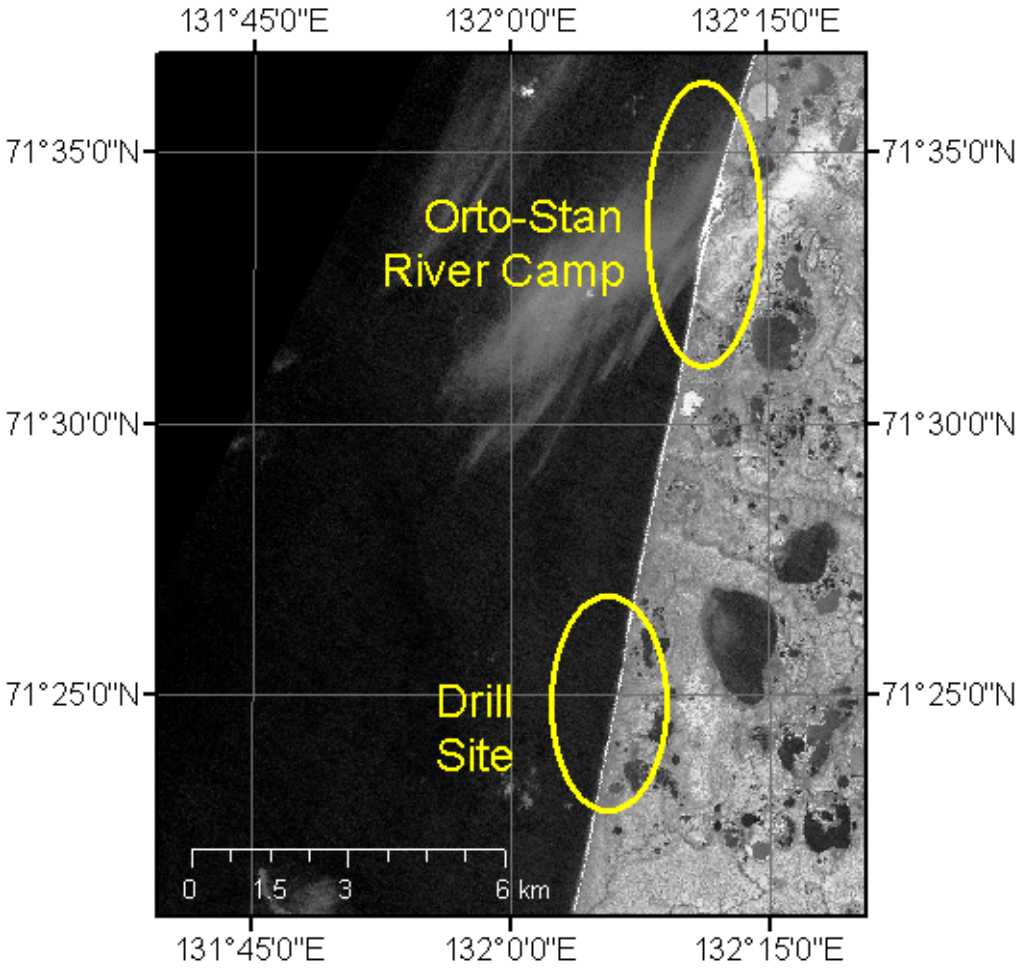

Figure 7-5: Geo-electrical investigations centred around two locations: from the Orto-Stan campsite northward and the drill site, at which coastal erosion rates were measured in 1999 (Rachold, 2000).

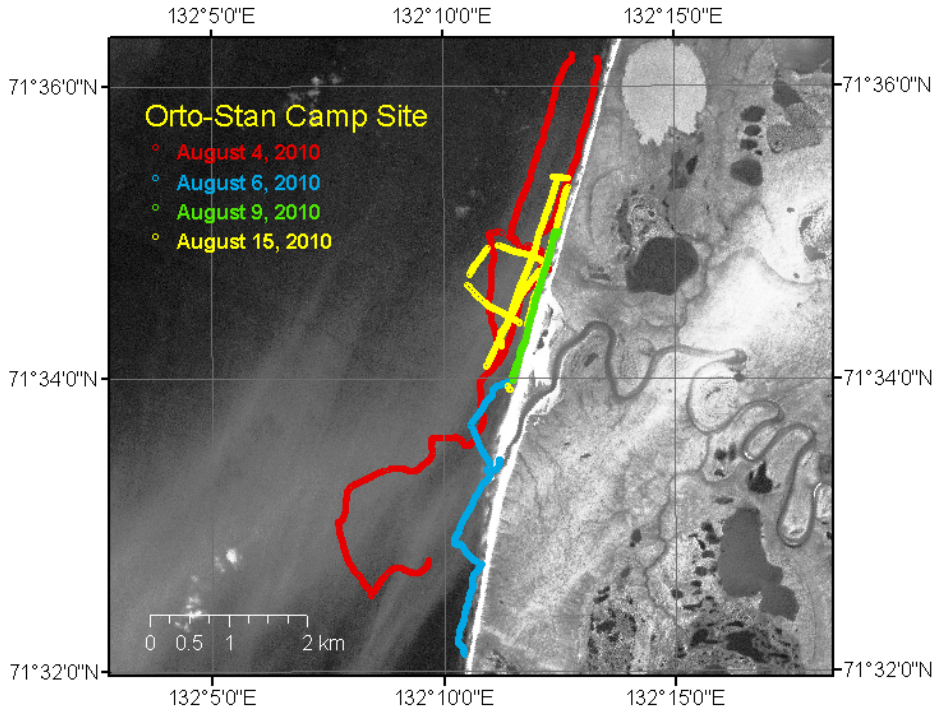

Figure 7-6: ERT data were collected around the Orto-Stan campsite on four days as shown above. On August 4th and 6th, the reciprocal Schlumberger array was used, on August 15th the dipole-dipole array, and on August 9th, both arrays were tested along the same stretch of shoreline (Tab. 7-2).

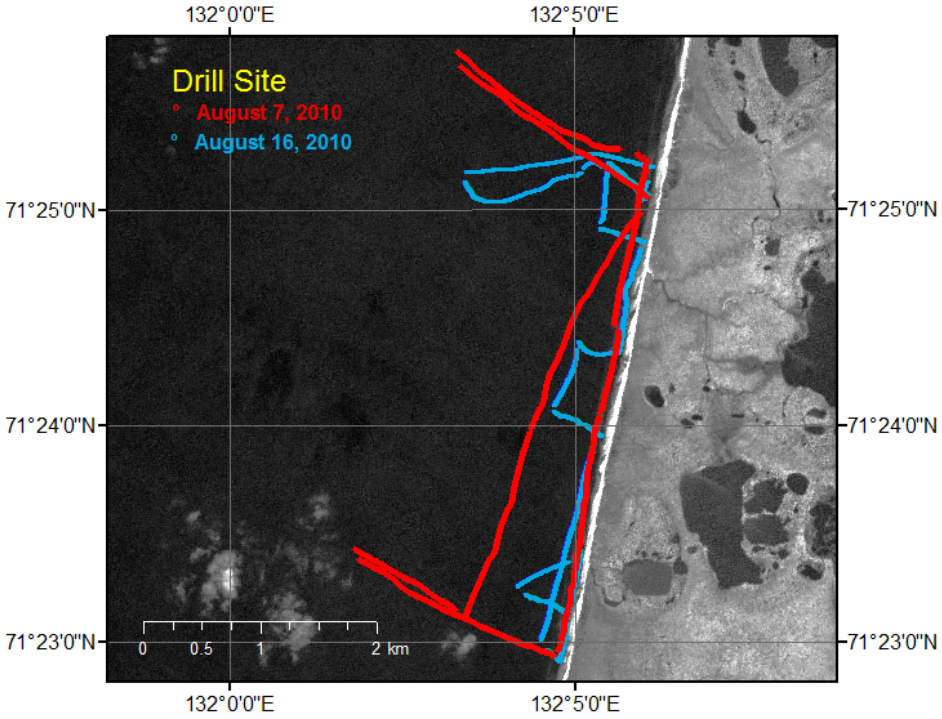

Figure 7-7: The drill site was surveyed on two days: on August 7th with the reciprocal Schlumberger array, and on August 16th with the dipole-dipole array.

Table 7-2: Description of geoelectric profiles measured around the mouth of the Orto-Stan River.

Date	Length [m]	# Meas.	Electrode Array	Start Coordinates		End Coordinates		Filename
				°N	°E	°N	°E	
04.08.2010	sounding	1	RS					*01_BuorKhayaCamp04_firsttest.bin*
	832	287	RS	71.5426636	132.139954	71.5561295	132.145416	*02_BuorKhayaCamp04_afterturning.bin*
	1111	181	RS	71.5563202	132.147293	71.5594788	132.1772	*03_BuorKhayaCamp04_towardscamp.bin*
	2004	302	RS	71.5601349	132.178345	71.5780411	132.184174	*04_BuorKhayaCamp04_para_2m_S2N.bin*
	737	131	RS	71.5784988	132.18425	71.5790939	132.205109	*05_BuorKhayaCamp04_para_2m_S2Ncont…*
	2346	403	RS	71.5830994	132.201721	71.6031418	132.222321	*06_BuorKhayaCamp04_para_2m_S2Ncon_…*
	2571	440	RS	71.6035233	132.213593	71.5806961	132.202484	*07_BuorKhayaCamp04_para_3point5m_N2…*
	1437	237	RS	71.5803833	132.202896	71.5684891	132.187027	*08_BuorKhayaCamp04_para_2point0m_N2…*
06.08.2010	sounding	1	RS					*01_Waterline_AB2AB.bin*
	sounding	1	RS					*02_Waterline_A45_B40.bin*
	156	30	RS	71.5664444	132.191391	71.5658569	132.187378	*03_FromCamp2RiverMouth.bin*
	995	175	RS	71.5657959	132.186844	71.5569229	132.18364	*04_FromCamp2RiverMouth_parallel.bin*
	144	37	RS	71.5565491	132.183594	71.5572739	132.186966	*05_UpThe River.bin*
	316	58	RS	71.5563126	132.184815	71.5539856	132.179703	*06_FromRiverSouthward_1m.bin*
	730	129	RS	71.5537415	132.179489	71.5478058	132.170792	*07_FromRiverSouthward_1mcontd.bin*
	407	74	RS	71.5477524	132.171509	71.5454865	132.180542	*08_back2shore.bin*
	sounding	1	RS					*09_Waterline_S_of_River.bin*
	291	54	RS	71.5454636	132.180664	71.5430832	132.177307	*10_Waterline_S_of_River_Contd_1m.bin*
	858	154	RS	71.5428848	132.177261	71.5352402	132.174286	*11_Waterline_S_of_River_Contd_1m_cont…*
	sounding	1	RS					*12_Alas_Waterline.bin*
09.08.2010	sounding	1	RS					*01_Waterline_at_low_water_at_camp.bin*
	1935	775	RS	71.5667877	132.19162	71.5833282	132.208466	*02_knietief_nach_N.bin*
	sounding	1	RS					*03_Waterline_1st_alas_N_low_water_leve…*
	sounding	1	RS					*04_Waterline_1st_alas_N_wieder.bin*
	sounding	1	DD					*05_extended_cable_out_front_1st_alas_N…*
	sounding	1	DD					*06_better_waterline_1st_alas_N.bin*
	1966	790	DD	71.5833282	132.208359	71.5664673	132.191849	*07_back_S.bin*
	sounding	1	DD					*08_waterline_at_camp_with_wet_boots.bin*

Table 7-2: Description of geoelectric profiles measured around the mouth of the Orto-Stan River (continuation).

Date	Length [m]	# Meas.	Electrode Array	Start Coordinates		End Coordinates		Filename
				°N	°E	°N	°E	
15.08.2010	sounding	1	DD					*01_waterline_at_camp_extended_cable.bin*
	55	10	DD					*01_waterline_at_camp_extended_crossco…*
	2546	436	DD	71.567955	132.18219	71.5893173	132.208008	*03_camp to yedoma.bin*
	203	38	DD	71.5896378	132.206299	71.589447	132.212021	*04_crosscoast_alas.bin*
	16	4	DD					*04_crosscoast_alas_a.bin*
	1810	317	DD	71.5884399	132.211762	71.5728531	132.197189	*06_alas to camp.bin*
	815	139	DD	71.5729675	132.194443	71.5772552	132.175705	*07_crosscoast_campsite.bin*
	404	70	DD	71.5785141	132.176239	71.5814972	132.182724	*08_along yedoma_5m.bin*
	680	127	DD	71.5818787	132.186539	71.5795822	132.204422	*09_acrosscoast_yedoma.bin*
	1066	195	DD	71.5788651	132.201386	71.5703201	132.187729	*10_along campsite_2point5m.bin*
	295	54	DD					*crosscoast_01.bin*

Table 7-3: Description of geoelectric profiles measured around the proposed drill site.

Date	Length [m]	# Meas.	Electrode Array	Start Coordinates		End Coordinates		Filename
				°N	°E	°N	°E	
07.08.2010	sounding	1	RS					*01_felixsite_Waterline.bin*
	1574	263	RS	71.4178391	132.101166	71.418869	132.056946	*02_felixsite_bathymetry_E2W.bin*
	1595	270	RS	71.4196014	132.057419	71.4199982	132.102356	*03_felixsite_bathymetry_W2E.bin*
	sounding	1	RS					*04_felixsite_waterline_sandbar.bin*
	160	56	RS	71.4188156	132.101288	71.4174652	132.099747	*05.bin*
	413	140	RS	71.4174957	132.100601	71.4201126	132.092362	*06.bin*
	507	115	RS	71.4202423	132.092041	71.4157486	132.089722	*07_to_new_offshore_positision.bin*
	396	148	RS	71.4152069	132.089615	71.4141769	132.100296	*08.bin*
	448	165	RS	71.4136276	132.099258	71.4097595	132.095825	*09_along shore in knee deep water and alas.bin*
	426	162	RS	71.409584	132.095825	71.4057922	132.094345	*10_along shore in knee deep water and alas to…*
	356	58	RS	71.405632	132.09407	71.4065094	132.084427	*11_perp_from_grave.bin*
	511	93	RS	71.405899	132.083542	71.4016113	132.07843	*12_parallel_6m_N of the big wreck.bin*
	461	140	RS	71.4011536	132.078384	71.3992462	132.089874	*13_perp2zedoma_N of wreck.bin*
	1682	428	RS	71.3981247	132.087784	71.3835831	132.075043	*14_zurueck_zu_lutz_und_jens.bin*
	144	50	RS	71.382782	132.076798	71.3819427	132.079849	*15_perp_alas_litz_jacke.bin*
	965	372	RS	71.3819275	132.079956	71.3904572	132.08461	*16_S2.bin*
	481	72	RS	71.3895721	132.081833	71.3877106	132.069626	*17_perp_las_river.bin*
	379	101	RS	71.3870926	132.071442	71.3856888	132.081131	*18_back to bazderakhs.bin*
16.08.2010	sounding	1	DD					*01_waterline_extended_felixsite.bin*
	74	19	DD	71.420723	132.100296	71.4211197	132.098312	*02_perpendicular_extended_felixsite.bin*
	1609	280	DD	71.4214249	132.093872	71.4288635	132.054962	*03_perpendicular_extd_felixsite_nochmals.bin*
	1954	344	DD	71.4277649	132.055649	71.4176712	132.100708	*04_perp_2shore_felix_extd.bin*
	2065	363	DD	71.4163971	132.098923	71.3998718	132.072586	*05_alongshore_felix2S_extd.bin*
	1680	303	DD	71.3995743	132.07225	71.3853378	132.05661	*06_alongshore_wreck2S_extd.bin*
	1011	165	DD	71.38591	132.054276	71.3905869	132.029907	*07_i_think_sebs_handsigns_meant_perp.bin*
	1871	266	DD	71.389801	132.030945	71.3823318	132.078095	*08_perp_2shore_drillsite1_extd.bin*
	sounding		DD					*09_waterline_sandbar_drillpoint1.bin*
	2039	285	DD	71.3827286	132.078964	71.4007568	132.088913	*10_drillpoint1_2_felix_extd.bin*
	720	104	DD	71.4010773	132.089233	71.4073715	132.093735	*11_Nofwreck_2_felix_extd_ca1m.bin*
	1437	207	DD	71.4078293	132.092743	71.4204788	132.100708	*12_Nofgrave_2_felix_extd_ca1m.bin*

Date: August 4, 2010, Orto-Stan campsite

Profile 01

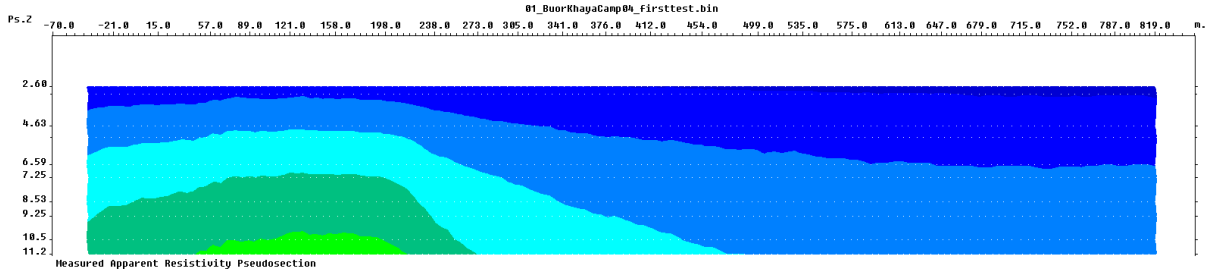

Profile 02

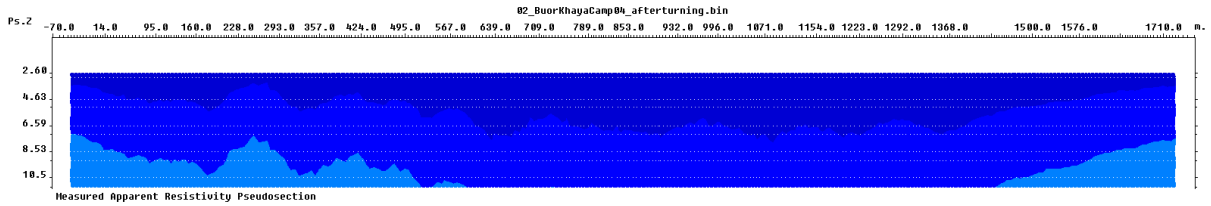

Profile 03

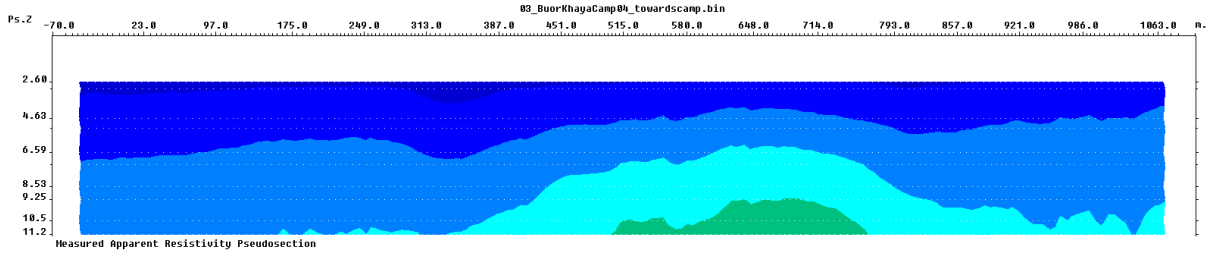

Profile 04

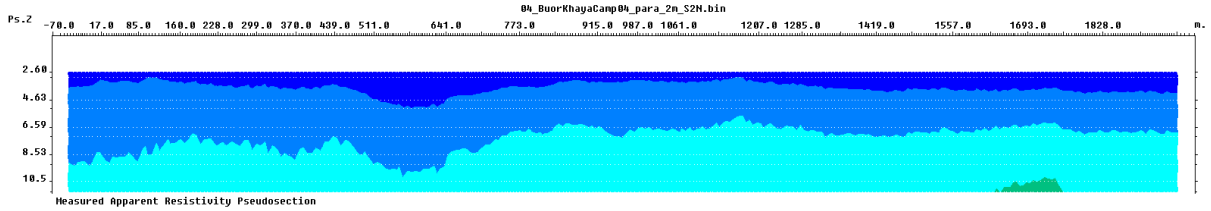

Profile 05

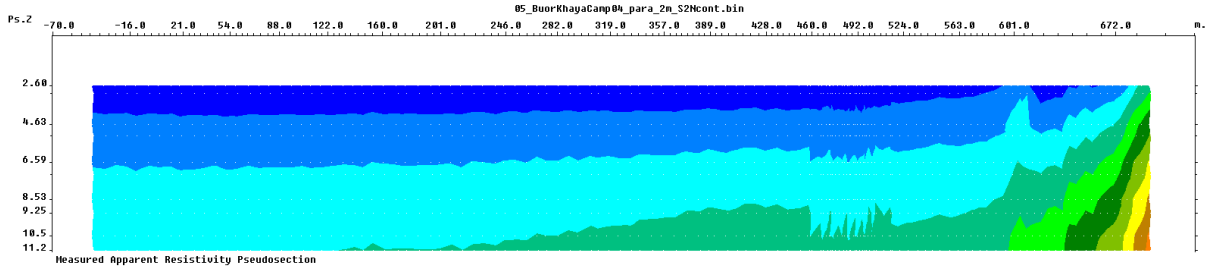

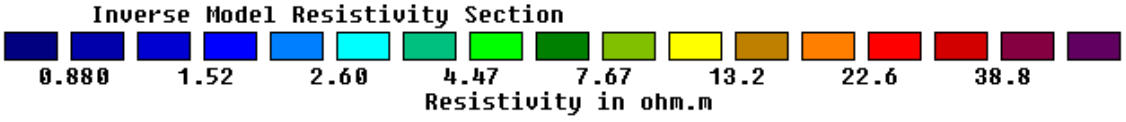

Date: August 4, 2010, Orto-Stan campsite (continued)

Profile 06

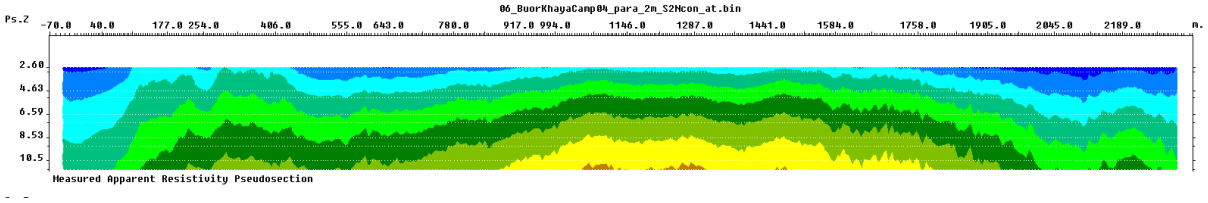

Profile 07

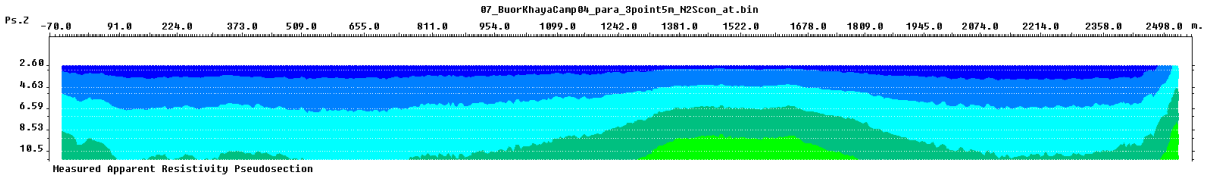

Profile 08

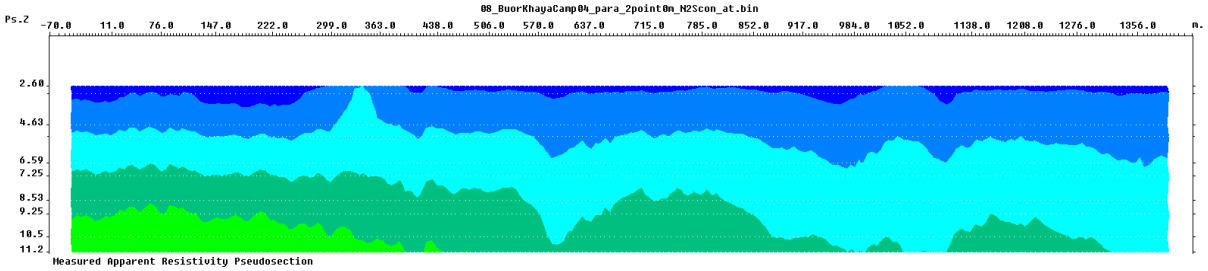

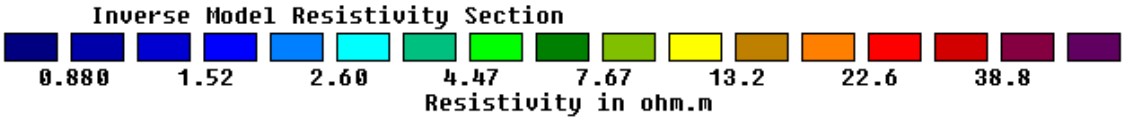

Date: August 6, 2010, Orto-Stan campsite

Profile 03

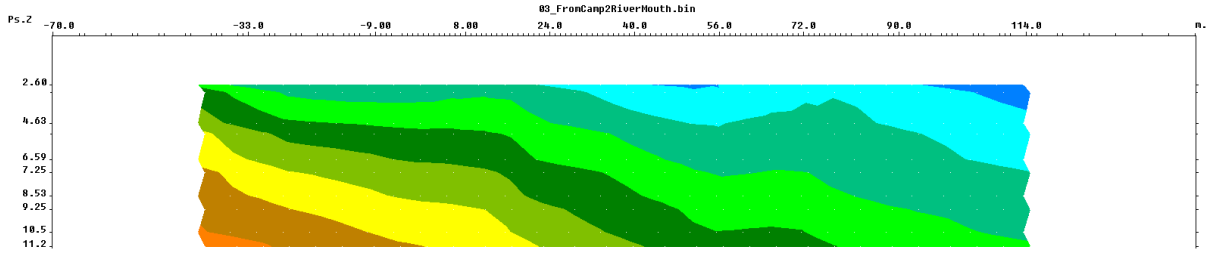

Profile 04

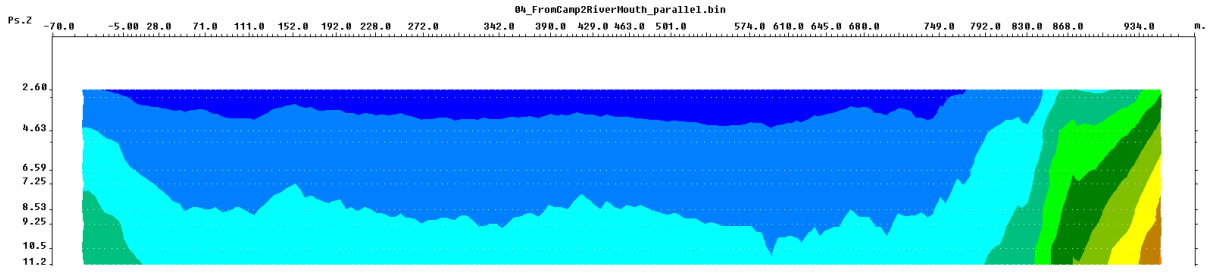

Profile 05

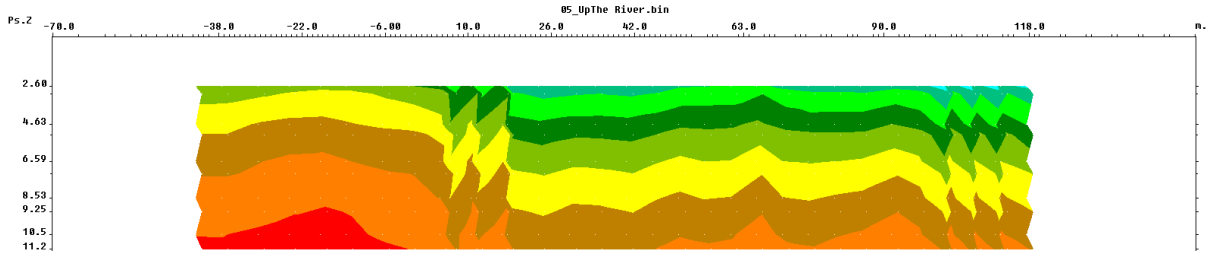

Profile 06

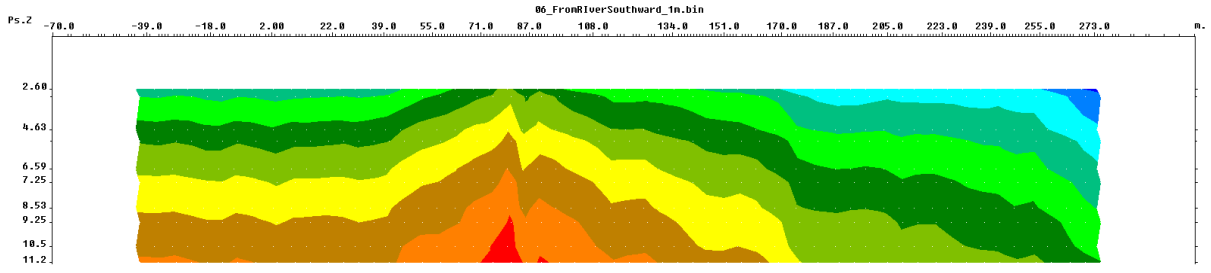

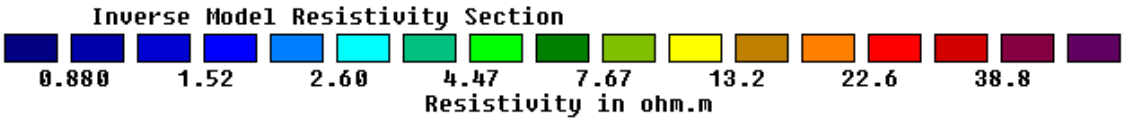

Date: August 6, 2010 (continued)

Profile 07

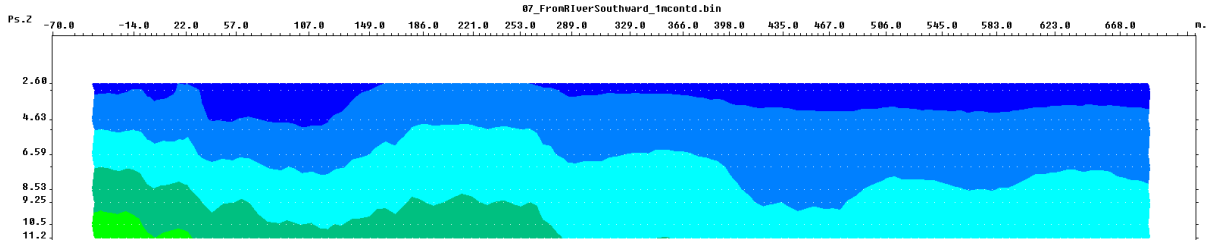

Profile 08

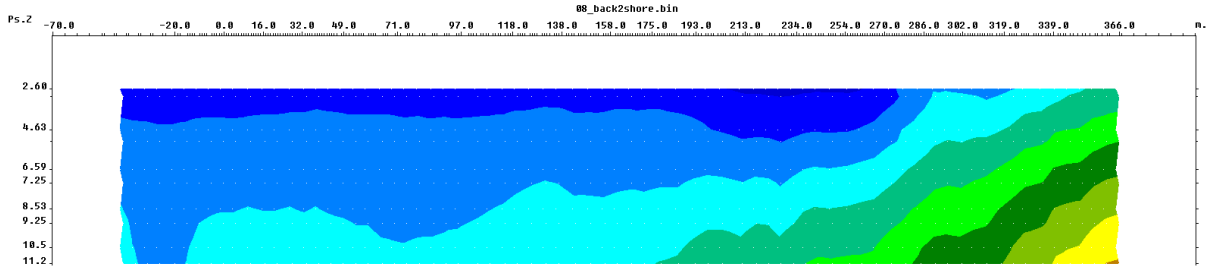

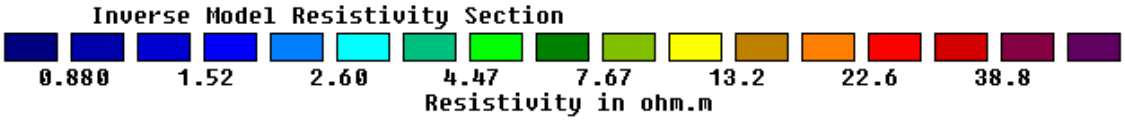

Date: August 7, 2010, drill site

Profile 02

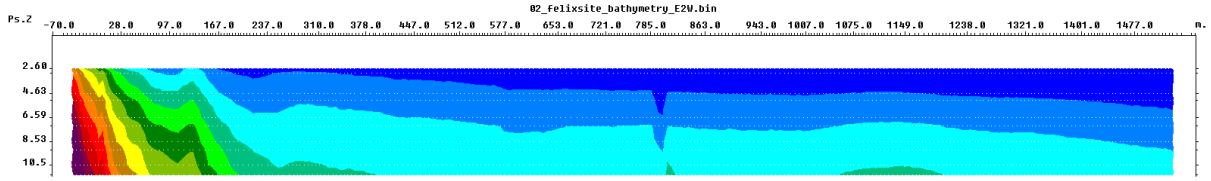

Profile 03

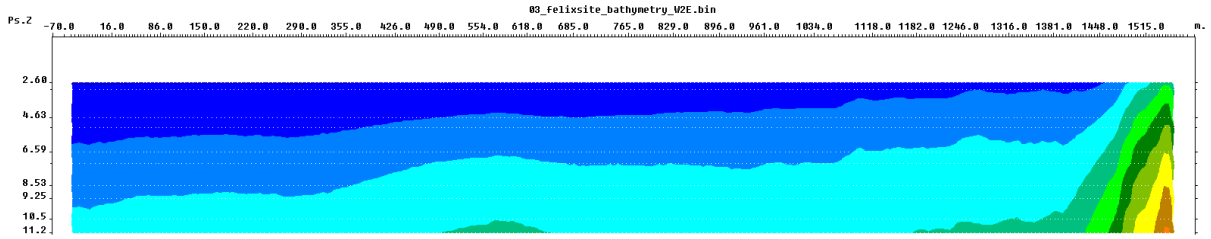

Profile 05

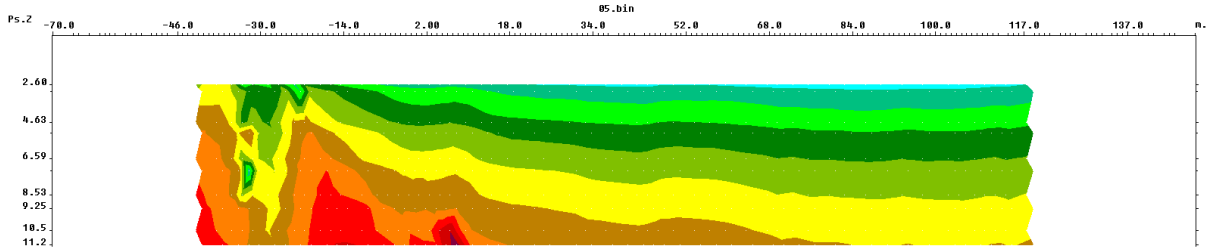

Profile 06

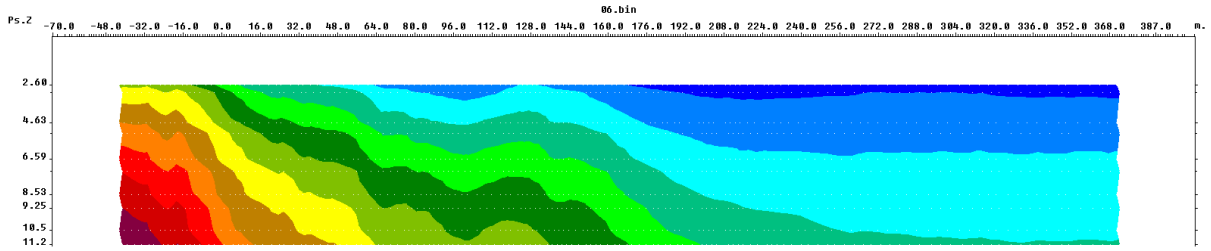

Profile 07

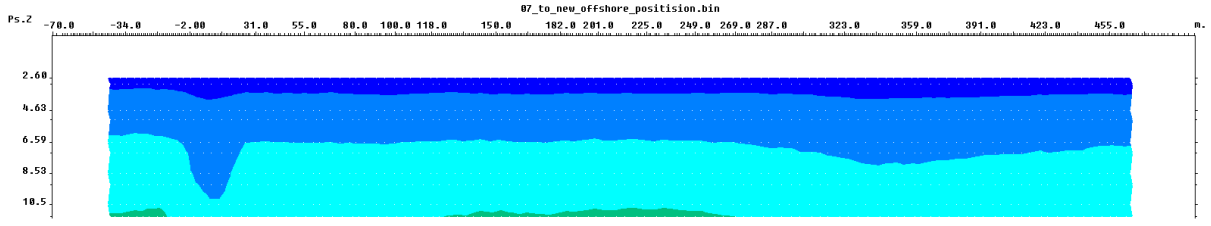

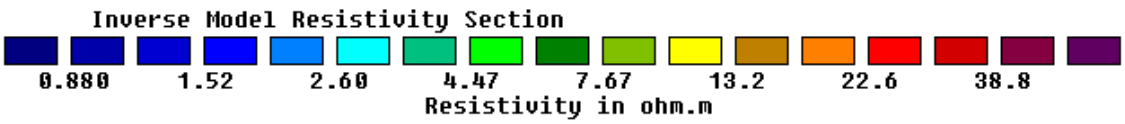

Date: August 7, 2010, drill site (continued)

Profile 08

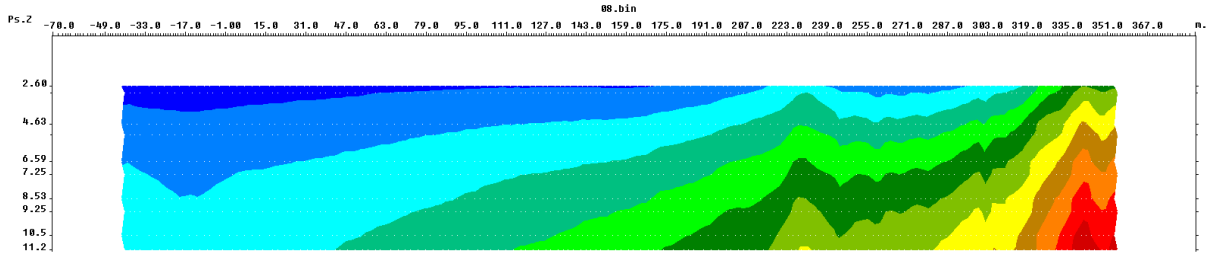

Profile 09

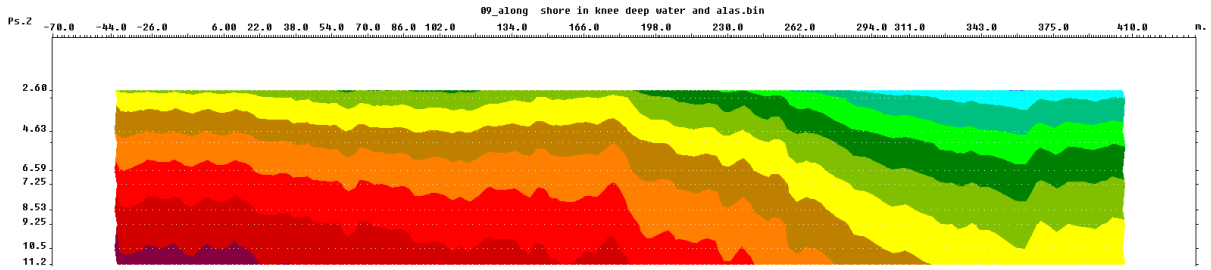

Profile 11

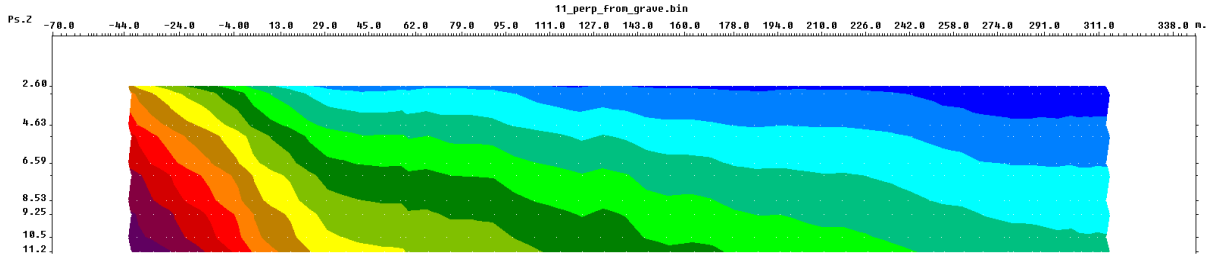

Profile 12

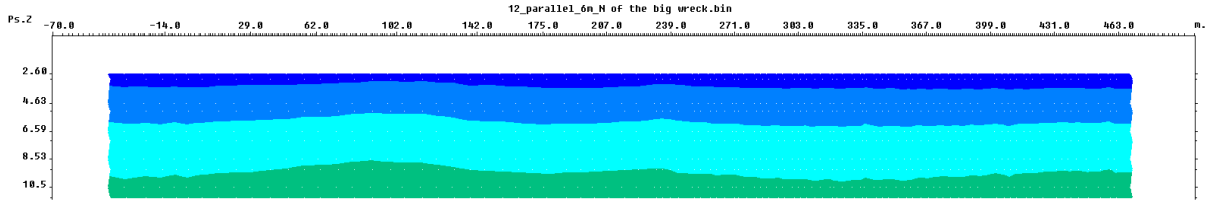

Profile 13

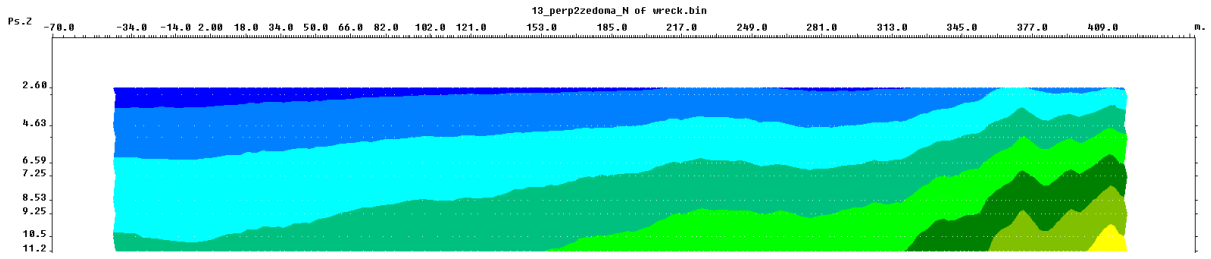

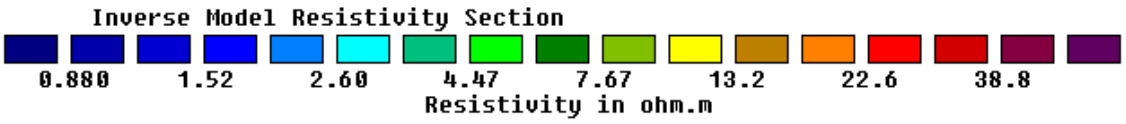

Date: August 7, 2010, drill site (continued)

Profile 14

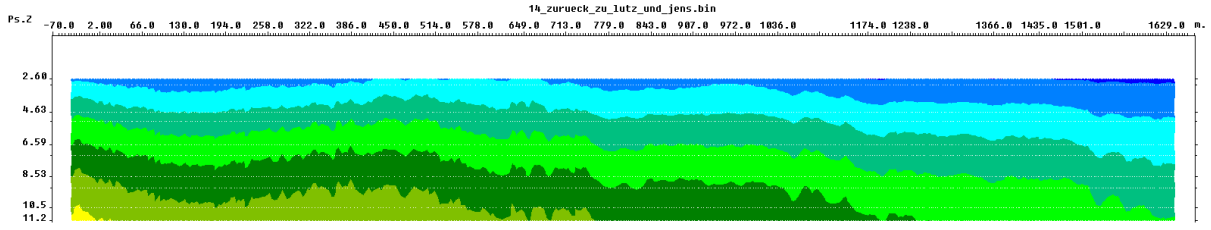

Profile 15

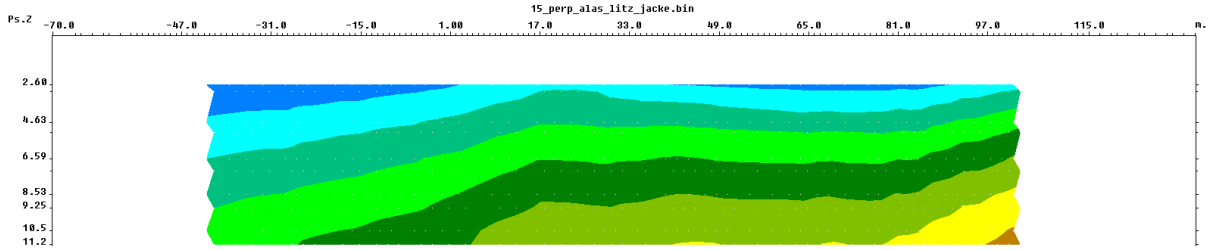

Profile 16

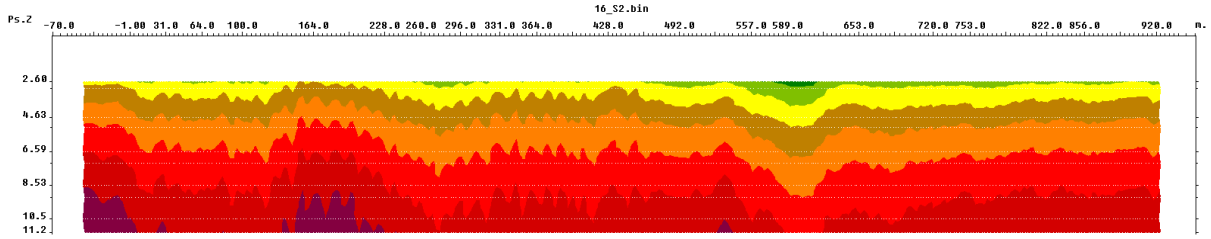

Profile 17

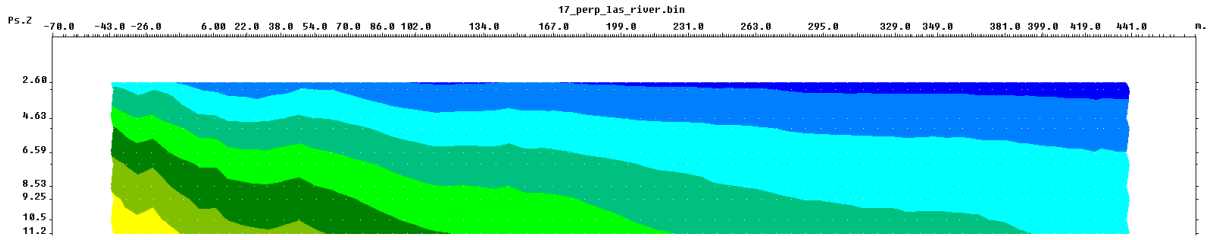

Profile 18

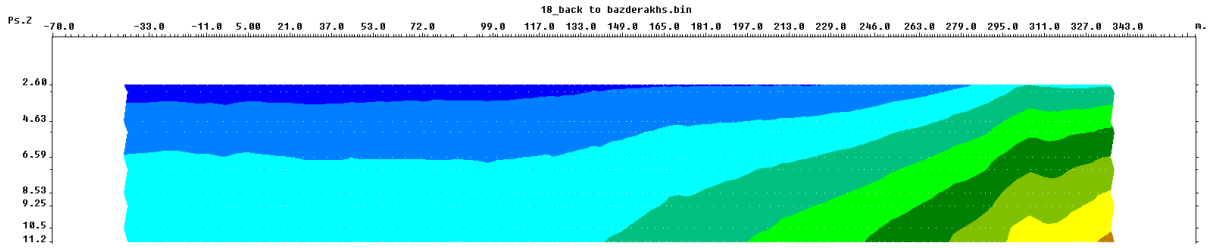

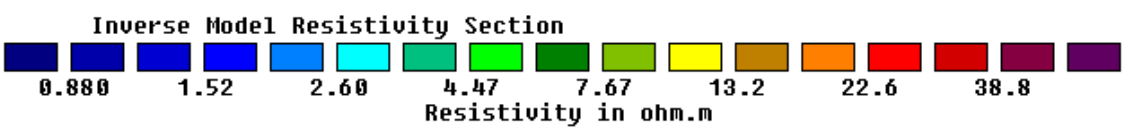

Date: August 9, 2010, Orto-Stan campsite

Profile 02

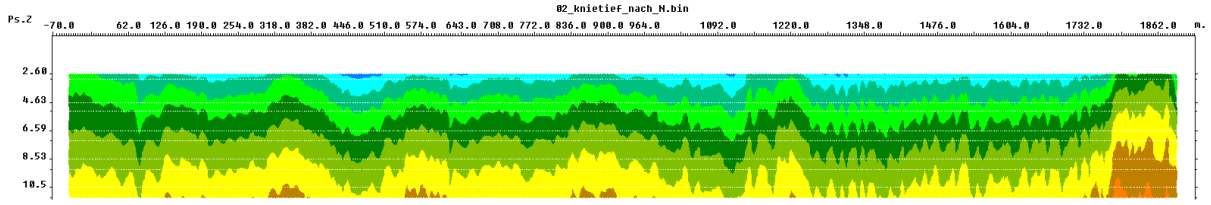

Profile 07

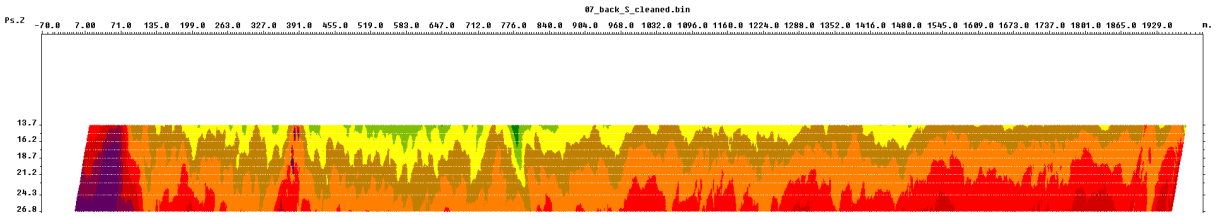

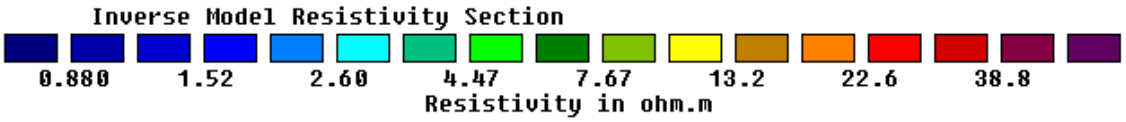

Date: August 15, 2010, Orto-Stan campsite

Profile 03

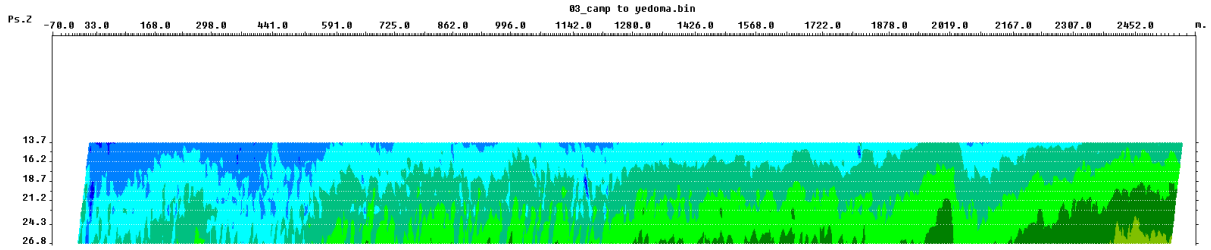

Profile 04

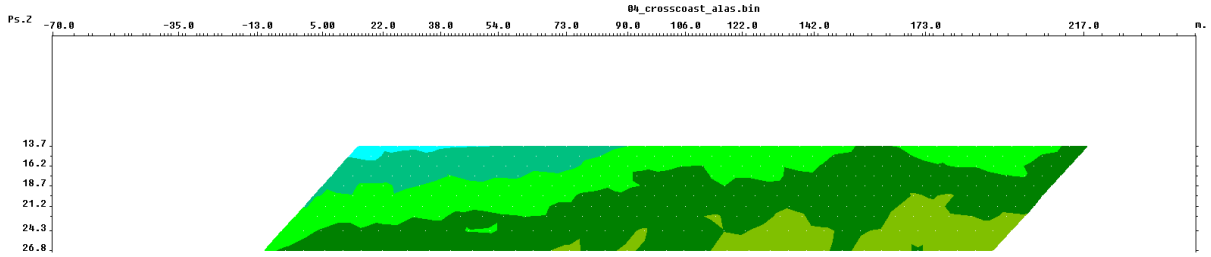

Profile 06

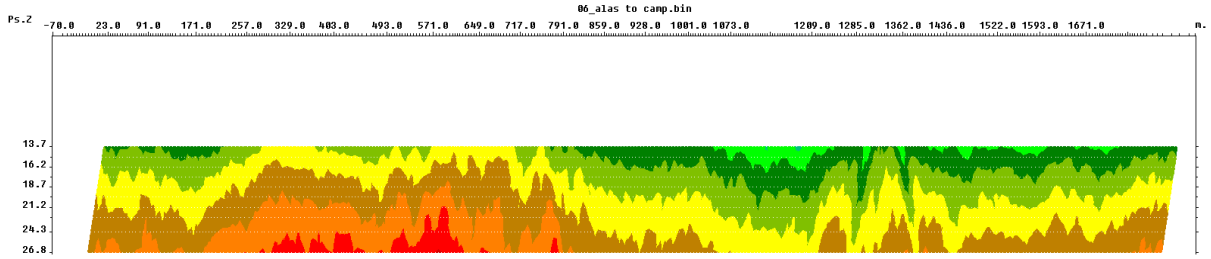

Profile 07

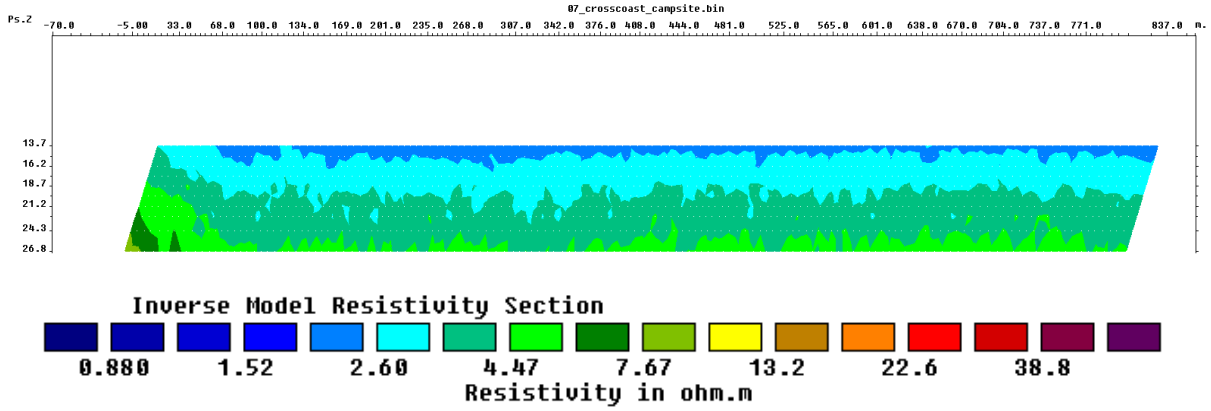

Date: August 15, 2010, Orto-Stan campsite (continued)

Profile 08

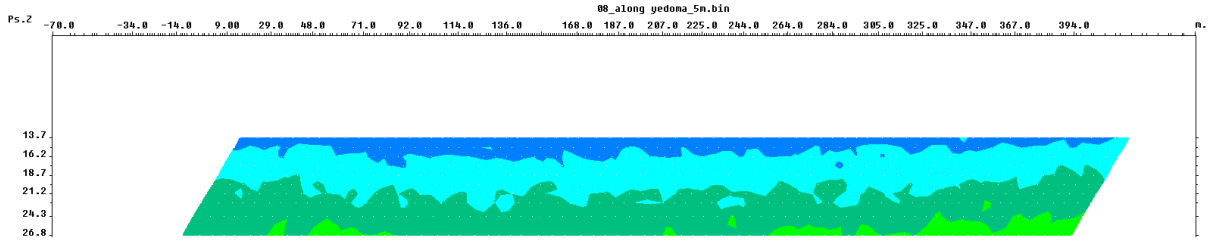

Profile 09

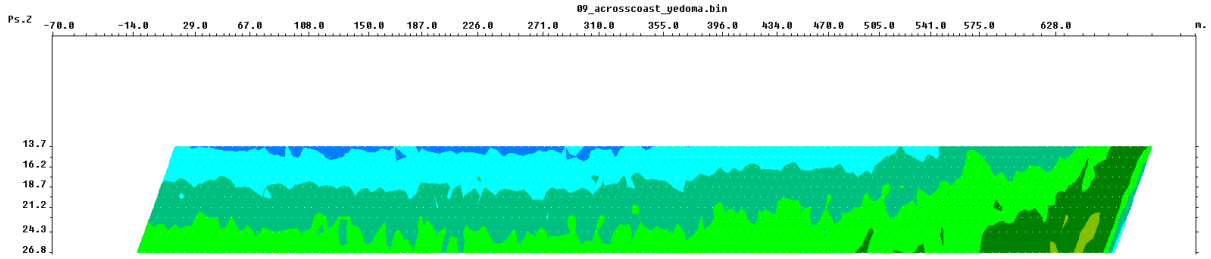

Profile 10

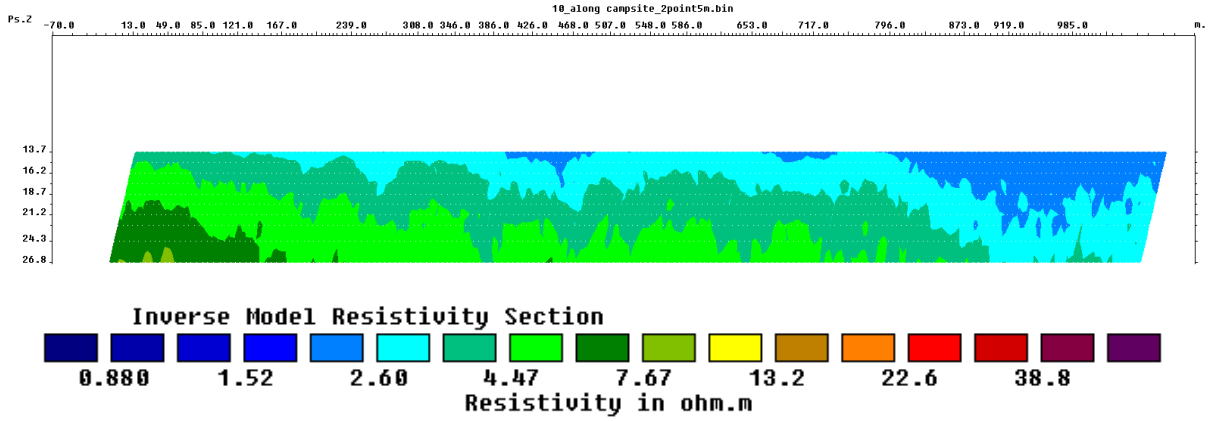

Date: August 16, 2010, drill site

Profile 02

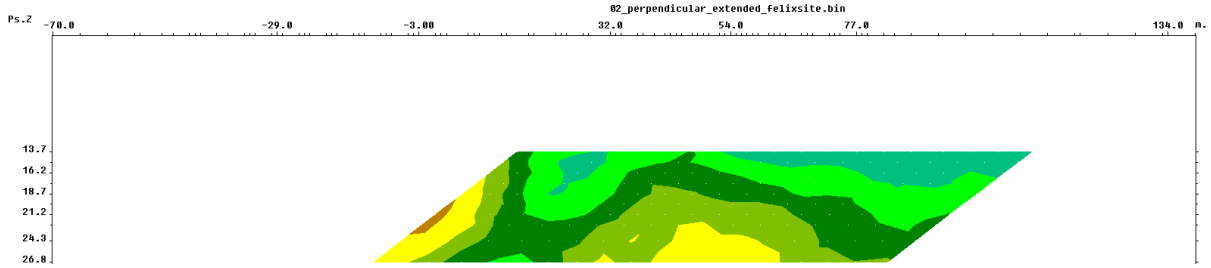

Profile 03

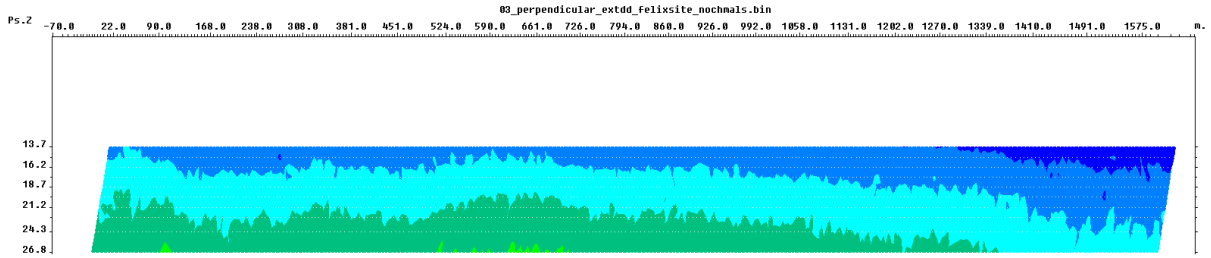

Profile 04

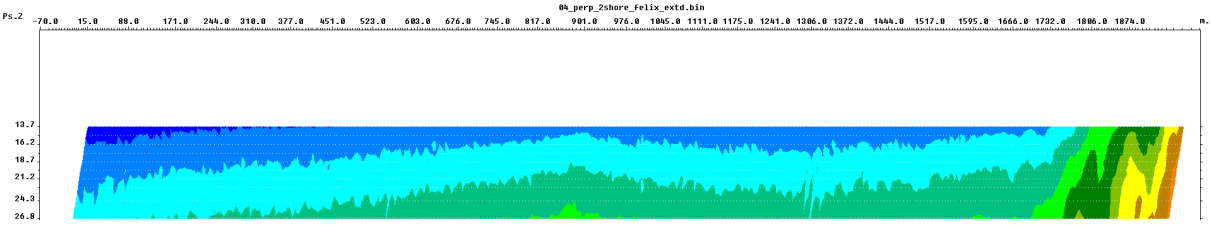

Profile 05

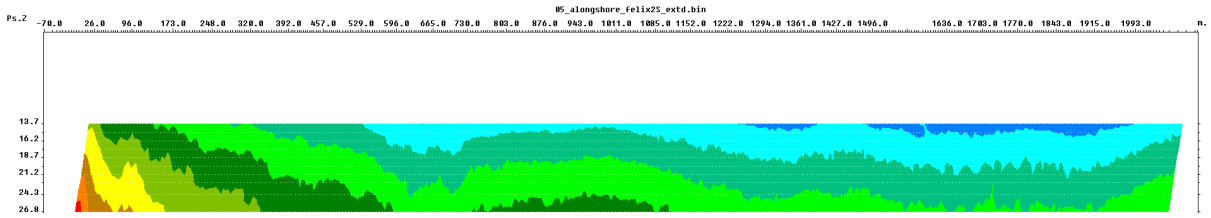

Profile 06

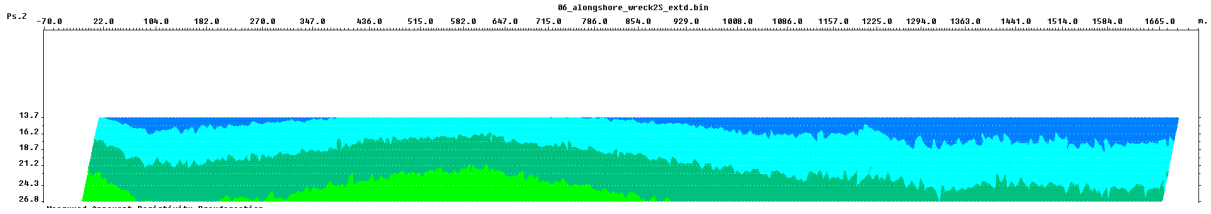

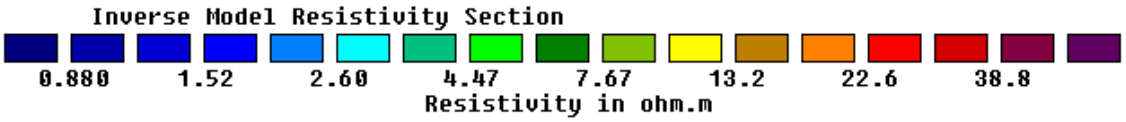

Date: August 16, 2010, drill site (continued)

Profile 07

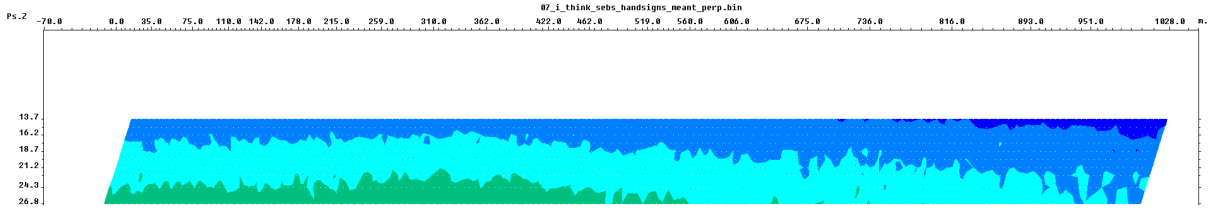

Profile 08

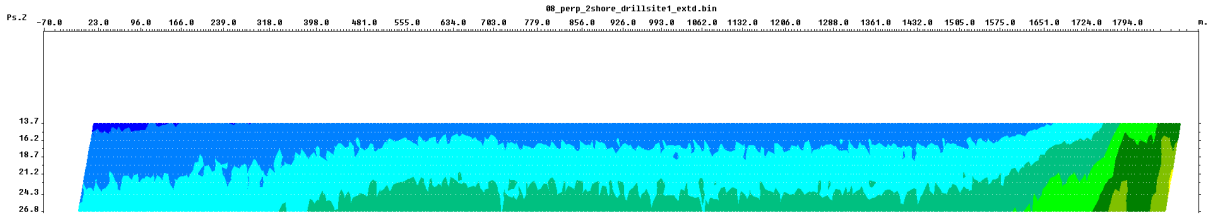

Profile 10

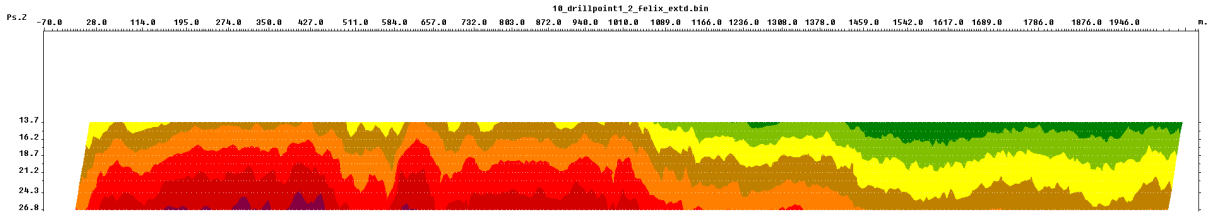

Profile 11

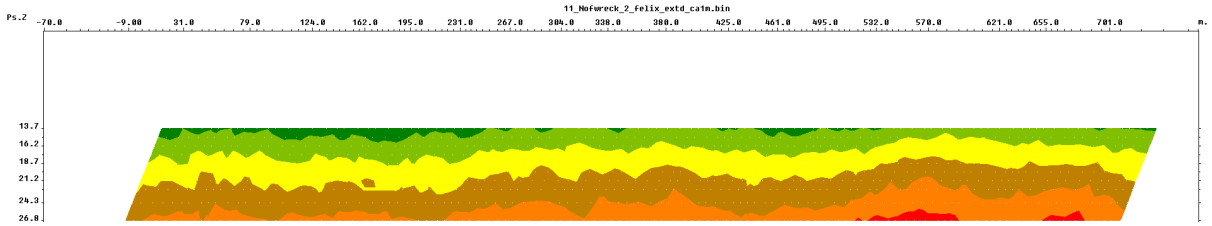

Profile 12

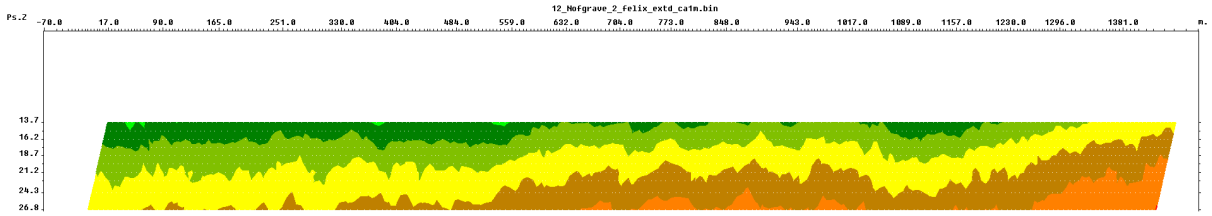

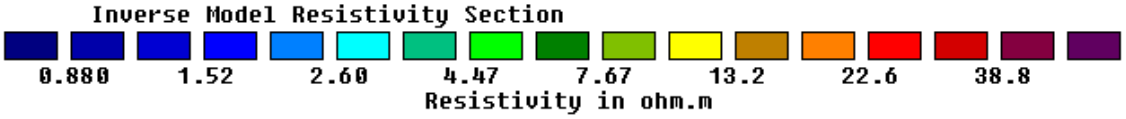

REFERENCES

Are, F.E., Grigoriev, M.N., Hubberten, H.-W., Rachold, V., Razumov, Schneider, W. (2000). Coastal erosion studies in the Laptev Sea. In: Rachold, V., Grigoriev, M.N. (eds.). Russian-German Cooperation SYSTEM LAPTEV SEA 2000: The Expedition LENA 1999. *Reports on Polar and Marine Research* 354: 65-74.

Desyatkin, R.V. (2009). *Pochvy Yakutii (Soils of Yakutia)*. In: Desyatkin, R.V., Okoneshnikova, M.V., Desyatkin, A.R. (eds.) Pochvy Yakutii (Soils of Yakutia).Yakutsk, Bichik, pp. 9-10. (original in Russian).

Dobrovol'sky G.V. (ed., 1979). *Pochvy SSSR (Soils of the USSR)*. Moscow, Mysl'. pp.15-18. (original in Russian).

Gilichinsky, D. A., Nolte, E., Basilyan, A.E., Beer, J., Blinov, A., Lazarev, V., Kholodov, A., Meyer, H., Nikolsky, P.A., Schirrmeister, L., and Tumskoy, V. (2007). Dating of syngenetic ice wedges in permafrost with 36Cl and 10Be. *Quaternary Science Reviews* 26: 1547-1556.

Grigoriev M.N., Vasiliev A.A., Rachold V. (2004). Siberian Arctic coasts: sediment and organic carbon fluxes in connection with permafrost degradation. American Geophysical Union 2004 Fall Meeting, St. Francisco. *Eos Transactions* 85(47): Abstract C13A-0261

Rachold, V. (ed., 2000). Expeditions in Siberia in 1999. *Reports on Polar Research* 354.

van Everdingen, R.O. (1998). *Multi-language glossary of permafrost and related ground-ice terms*. Boulder, CO: National Snow and Ice Data Center/World Data Center for Glaciology, 233 pp.

Viehberg, F.A. (2002). A new and simple method for qualitative sampling of meiobenthos communities. *Limnologica* 32: 350-351.

Wetterich, S., Schirrmeister, L., Meyer, H., Viehberg, F.A., Mackensen, A. (2008). Arctic freshwater ostracods from modern periglacial environment in the Lena River Delta Siberian Arctic, Russia): Geochemical applications for palaeoenvironmental reconstructions. *Journal of Paleolimnology* 39: 427-449.

Wetterich, S., Schirrmeister, L. (2009). Limnological studies in the Dmitry Laptev Strait region. In: Boike, J., Bol'shiyanov, D.Yu., Schirrmeister, L., Wetterich, S. (eds.). The Expedition LENA - NEW SIBERIAN ISLANDS 2007 during the International Polar Year (IPY) 2007/2008. *Reports on Polar and Marine Research* 584: 155-163.

Wetterich, S., Schirrmeister, L. (submitted). Limnological studies in modern periglacial waters on the lower Kolyma plain. In: Schirrmeister, L., Wetterich, S., Kholodov, A.L. (eds.). The joint Russian-German Expedition BERINGIA/KOLYMA 2008 during the International Polar Year (IPY) 2007/2008. *Reports on Polar and Marine Research*, 6 pp.

Yelovskaya, L.G. (1987). *Klassifikaciya i diagnostika merzlotnyh pochv Yakutii (Classification and diagnosis of permafrost soils of Yakutia)*. Yakutsk. 172 pp. (original in Russian).

APPENDIX 1

List of sediment samples with sedimentological and cryolithological sample characteristics

Abbreviations

a.s.l.	–	above surface level
b.s.	–	below surface
ice abs.	–	absolute ice content
ice grav.	–	gravimetric ice content
TI	–	texture ice samples
a.l.	–	active layer
frag.	–	fragments

Sample	Depth	Height	Cryotexture	Sediment	Organic	ice grav.	ice abs.	TI	Remarks
	m b.s.	m a.s.l.				wt %	wt %		
Buo-01, N 71.58146°, E 132.20801°, 06/08/2010									
Buo-01-A-00	0.3	9.1	unfrozen, a.l.	Ah-horizon, sandy grey, greyish-brown, spotty, dry	modern roots	NA	NA		above ice wedge
Buo-01-A-01	0.5	8.9	ice veins, micro lens-like	grey, silty fine-sand	filament roots	79.0	44.1	x	
Buo-01-A-02	0.7	8.7	fine lens-like	light-grey, peat	peat inclusion (ø 0.2m), moss	646.5	86.6		
Buo-01-A-03	1.3	8.1	Ice bands (0.5-1 cm width) and 1-2 cm long lenses (1mm width)	iron-oxide patches, grey-brown, silty fine-sand		45.3	31.2	x	
Buo-01-A-04	1.8	7.6	Ice bands (0.5-1 cm width) and 1-2 cm long lenses (1mm width)	iron-oxide patches, grey-brown, silty fine-sand		76.1	43.2	x	
Buo-01-A-05	2.3	7.1	Ice bands (0.5-1 cm width) and 1-2 cm long lenses (1mm width)	iron-oxide patches, grey-brown, silty fine-sand		45.2	31.1		
Buo-02, N 71.38361°, E 132.08397°, 07/08/2010									
Buo-02-A-01	0.3	29.7	unfrozen, a.l.	brownish, sandy	modern roots, a.l.	NA	NA		
Buo-02-A-02	0.6	29.4	unfrozen, a.l.	dark-brown, silty fine-sand, several iron-oxide patches	several small roots	26.0	20.6		
Buo-02-A-03	0.7	29.3	massive, 1 cm thick ice bands	dark-grey, silty fine-sand	several larger plant frag.	NA	NA	x	directly under p. table

Sample	Depth	Height	Cryotexture	Sediment	Organic	ice grav.	ice abs.	TI	Remarks
	m b.s.	m a.s.l.				wt %	wt %		
Buo-02-A-04	1.2	28.8	horizontal banded, up to 1 cm thick ice bands, composed of dense-layered ice lenses; fine lens-like in sediment interlayers, vertical ice veins (fissure ice ?)	brownish-grey, silty fine-sand	plant remains	NA	NA	x	
Buo-02-A-05	1.7	28.3	horizontal banded, coarse-lenses; sediment interlayers: lens-like reticulated, diagonal oriented lenses	larger organic patches, cryoturbated paleosol	filament roots, larger organic patches	73.9	42.5	x Rhizon	
Buo-02-A-06	2.2	27.8	horizontal banded, coarse lenses; sediment interlayers: lens-like reticulated, diagonal oriented lenses	larger organic patches, cryoturbated paleosol	filament roots, larger organic patches	67.0	40.1		
Buo-02-B-07	2.5	27.5	lens-like, some times banded, 20 cm distance	cryoturbated paleosol with concentric organic-rich patches, grey-brown	filament roots, plant detritus	70.3	41.3		
Buo-02-B-08	3.0	27.0	ice bands	grey-brown, silty fine-sand	vertical filament roots	63.4	38.8	x	
Buo-02-B-09	3.5	26.5	ice bands, 2-10 mm thick diagonal	grey-brown, silty fine sand	vertical filament roots	101.4	50.4	x	
Buo-02-B-10	4.0	26.0	no ice bands	grey-brown, silty fine-sand	vertical filament roots	74.6	42.7	x	
Buo-02-B-11	4.5	25.5	lens-like, isolated	grey-brown, silty fine sand	several filament roots	64.5	39.2	x	
Buo-02-B-12	5.0	25.0	massive	grey-brown to light brown, cryoturbated paleosol "tongues"	no macro plant remains	61.0	37.9		
Buo-02-B-13	5.5	24.5	fine lens-like	light greyish-brown	no visible	49.7	33.2	x	

Sample	Depth	Height	Cryotexture	Sediment	Organic	ice grav.	ice abs.	TI	Remarks
	m b.s.	m a.s.l.				wt %	wt %		
Buo-02-C-14	5.2	24.8	up to 10 mm thick ice veins,	greyish, silty fine sand	plant detritus	125.7	55.7	x	
Buo-02-C-15	5.7	24.3	coarse lens-like	brownish, fine sand		45.7	31.4	x	
Buo-02-C-16	6.3	23.7	coarse lens-like, linear oriented	dark-brown fine sand		57.5	36.5	x	
Buo-02-C-17	6.9	23.1	fine lens-like, 1-2 mm long, lamented	silty		65.4	39.5	x	
Buo-02-D-18	4.5	25.5	massive to fine lens-like	greyish, brown patches, silty	plant fragm.	44.9	31.0		
Buo-02-D-19	5.0	25.0	ice-rich, ice bands, fine lens-like	greyish, brown patches, silty	many plant and wood frag., < 5mm ø	93.4	48.3	x	
Buo-02-D-20	5.5	24.5	diagonal ice veins	peat	moss	372.2	78.8		
Buo-02-D-21	6.0	24.0	vertical and diagonal ice veins, ice-rich	peat	moss peat, large plant frag.	865.6	89.6		
Buo-02-D-22	6.5	23.5	fine lens-like, laminated, partly larger lenses	brownish, silty sand	below the peat layer, larger plant frag.	223.1	69.1	x	suppos-able repetition of profile C
Buo-02-D-23	7	23.0	micro lenses and ice veins	brownish, silty sand	several plant frag.	52.5	34.4	x	
Buo-02-D-24	7.5	22.5	micro lenses and ice veins	brownish, silty sand	several plant frag.	79.3	44.2	x	
Buo-03, 07/08/2010									
Buo-03-A-01	0.5	29.5	unfrozen, a.l.	light-grey, clayish silt, not layered, 10-20 cm thick	plant frag.	NA	NA		Cliff at landing point, smells like Yedoma
Buo-03-A-02	0.8	29.2	ice rich	up to 30 cm thick peaty horizon	peat	248.9	71.3		Yedoma smell
Buo-03-A-03	1.3	28.7	ice rich	peat, 10-20 cm thick	moss peat	258.9	72.1		Yedoma smell
Buo-03-A-04	1.6	28.4	coarse lenses	light greyish silty fine sand		NA	NA		Yedoma smell
Buo-04, N 71.60048°, E 132.22670°, 08/08/2010 and 10/08/2010 (sub profile C)									
Buo-04-A-00	0.1	18.5	unfrozen, a.l.		modern roots	NA	NA		
Buo-04-A-01	1.0	17.6	lens-like to micro lens like	greyish-brown silty fine sand		90.2	47.4	x	

Sample	Depth	Height	Cryotexture	Sediment	Organic	ice grav.	ice abs.	TI	Remarks
	m b.s.	m a.s.l.				wt %	wt %		
Buo-04-A-02	1.5	17.1	ice veins <1mm thick, distance 15 cm, between micro lens-like and compact orientated	greyish-brown silty fine sand	filament roots	44.9	31.0	x	
Buo-04-A-03	2.0	16.6	no ice veins, micro lens-like and compact orientated	greyish-brown silty fine sand		65.4	39.6	x	
Buo-04-A-04	2.5	16.1	micro lens-like and compact orientated	greyish-brown silty		61.0	37.9	x	
Buo-04-A-05	3.0	15.6	ice veins <1mm thick, distance 5 cm, between micro lens-like and compact orientated	greyish-brown silty fine sand	several plant detritus	61.2	37.9		
Buo-04-A-06	3.5	15.1	ice veins <1mm thick, distance 5 cm, between micro lens-like and compact orientated	greyish-brown silty fine sand	several plant detritus	62.0	38.3		
Buo-04-A-07	4.5	14.1	micro lens-like	greyish-brown silty	several plant detritus	100.0	50.0	x	
Buo-04-A-08	5.0	13.6	coarse ice lenses	greyish-brown silty	several plant detritus	65.4	39.5	x	
Buo-04-B-09	8.0	9.6	ice rich, layered, bands composed of ice lenses, between band lenses horizontal orientated	dark greyish-brown silty	filament roots, plant detritus	59.4	37.3	x	
Buo-04-B-10	8.5	9.1	banded, micro-lenses	greyish-brown silty fine sand	coarse plant and wood frag.	57.1	36.4		
Buo-04-B-11	9.0	8.6	ice band up to 2mm thick	greyish-brown silty fine sand	many plant frag.	53.7	34.9		
Buo-04-B-12	9.5	8.1	ice band up to 2mm thick	greyish-brown silty fine sand	plant frag.	70.1	41.2	x	
Buo-04-B-13	10.0	7.6	ice band up to 2mm thick	greyish-brown silty fine sand	several filament roots	45.5	31.3	x	

Sample	Depth	Height	Cryotexture	Sediment	Organic	ice grav.	ice abs.	TI	Remarks
	m b.s.	m a.s.l.				wt %	wt %		
Buo-04-C-14	9.5	9.0	horizontal ice bands, 0.5-1cm thick and lens-like	greyish-brown silty fine sand	several filament roots	46.6	31.8	x	
Buo-04-C-15	10.0	8.5	ice band composed of coarse lenses, bands in 5 cm distance, in the sediment in between ice lenses <1mm tick 0.5-1cm long, reticular orientated	greyish-brown silty fine sand	several filament roots	61.1	37.9	x	
Buo-04-C-16	10.5	8.0	several ice veins, several micro-lenses	peaty, cryoturbated paleosol	plant detritus, much root material, plant stems	56.3	36.0		
Buo-04-C-17	11.0	7.5	several ice-lenses	greyish-brown silty fine sand	fine distributed organic detritus	109.5	52.3	Rhizon	
Buo-04-C-18	11.5	7.0	ice lenses, bigger around plant detritus	silty fine sand	layered plant detritus	85.3	46.0		
Buo-04-C-19	11.7	6.8	coarse lenses around plant detritus	greyish-brown silty fine sand	peaty, horizontal layered	142.9	58.8	x	
Buo-04-C-20	12.0	6.5	Ice bands	dark greyish silty fine sand	coarse plant and wood frag.	44.8	31.0	x	
Buo-04-C-21	12.5	6.0	between 4mm thick ice bands	sandy, diagonal structures	coarse plant detritus	38.5	27.8		possibly reworked material, slope deposits
Buo-04-C-22	13.0	5.5	weakly ice bands, 0.5 cm thick	sandy, yellowish-light-grey iron oxide spots		42.9	30.0	x	slope deposits
Buo-04-C-23	13.5	5.0	broken ice lenses	sandy, yellowish-light-grey iron oxide spots		29.5	22.8		
Buo-04-C-24	14.2	4.3	horizontal ice fissures	sandy	coarse plant fragment and roots	28.7	22.3		

Sample	Depth	Height	Cryotexture	Sediment	Organic	ice grav.	ice abs.	TI	Remarks
	m b.s.	m a.s.l.				wt %	wt %		
Buo-05, N 71.58241°, E 132.20941°, 14/08/2010									
Buo-05-A-01	0.2	9.3	unfrozen, a.l.	greyish-brown, sandy	modern roots	NA	NA		
Buo-05-A-02	0.3	9.2	unfrozen, a.l.	brown, horizontal layered peat	peat and roots, bigger wood frag.	NA	NA		
Buo-05-A-03	0.6	8.9	unfrozen, a.l.	greyish, partly brown spots, sandy	filament roots	NA	NA		
Buo-05-A-04	0.8	8.7	micro-lenses	cryoturbated paleosol, silty fine sand	plant detritus	103.7	50.9	x	directly under perma-frost table
Buo-05-A-05	1.3	8.2	micro-lenses to lenses, diagonal orientated, more ice than above	grey, silty	several plant detritus and plant detritus layers	88.7	47.0	x	
Buo-05-A-06	1.8	7.7	coarse lens-like, diagonal orientated, width 1 mm, length 1 to 2 cm, banding	greyish-brown silty	fine distributed organic detritus	86.7	46.4	x	
Buo-05-A-07	2.3	7.2	coarse lens-like, banded	greyish-brown silty	layers of plant detritus layers, plant inclusions	86.6	46.4	x	detailed photo
Buo-05-B-08c	2.4	7.1	reticular coarse lens-like, contact of the ice lenses	silty fine sand, no layers, but some molluscs		82.2	45.1	x	border to 8b pure ice, ice wedge/vein Buo-05-B-102
Buo-05-B-08b	2.6	6.9	lens-like, ice rich, horizontal	silty fine sand, dark grey, silty fine sand, weakly layered	plant detritus	68.3	40.6	x	
Buo-05-B-08a	2.8	6.7	reticular coarse lens-like, contact of the ice lenses	silty fine sand	several plant detritus	38.8	28.0		over pure ice layer, facies change?
Buo-05-B-09	3.1	6.4	ice lenses parallel to sedimentlayers	dark grey silty, fine layered, molluscs	plant detritus layers	36.5	26.7		
Buo-05-B-10	3.4	6.1	ice lenses parallel to sediment layers	dark grey silty, fine layered, molluscs	clearly visible plant detritus layers	39.7	28.4	x Rhizon	

Sample	Depth	Height	Cryotexture	Sediment	Organic	ice grav.	ice abs.	TI	Remarks
	m b.s.	m a.s.l.				wt %	wt %		
Buo-05-B-11	3.7	5.8	ice lenses parallel to sediment layers	dark grey silty, fine layered, molluscs	plant detritus layers	40.9	29.0		
Buo-05-B-12 + u	4.0	5.5	massive to several ice lenses, at the lens borders Fe-oxide and plant detritus brown.	sandy, brown, fine layered	plant detritus around ice lenses	51.5	34.0		additional unfrozen sample (u) from the right side of the profile
Buo-05-B-13 + u	4.3	5.2	massive to very thin long ice lenses	greyish brown, more clayey, Fe-oxide fissures (likely melted ice lenses)	several plant fragment	33.5	25.1	x Rhizon	see Buo-05-B-12 + u
Buo-05-B-14 + u	4.6	4.9	several ice lenses, parallel to the horizontal sediment layers	alternate bedding of sandy layers and plant detritus layers, mollusc	plant detritus layers	43.6	30.3		see Buo-05-B-12 + u
Buo-05-B-15 + u	4.9	4.6	several ice lenses, parallel to the horizontal sediment layers	alternate bedding of sandy layers and plant detritus layers, mollusc	plant detritus layers	39.4	28.2		see Buo-05-B-12 + u
Buo-05-B-16 + u	5.2	4.3	several diagonal ice lenses, width <1mm	many molluscs, partly brown, fine layered	plant detritus layers	35.8	26.4	x Rhizon	see Buo-05-B-12 + u
Buo-05-B-17 + u	5.5	4.0	ice bands and several diagonal ice lenses, width <1 mm	many molluscs, partly brown, fine layered, Fe-oxide	plant detritus layers	34.8	25.8		see Buo-05-B-12 + u
Buo-05-B-18 + u	5.8	3.7	massive	brownish, sandy, Fe-oxide spots, fine layered		34.2	25.5		see Buo-05-B-12 + u
Buo-05-B-19 + u	6.1	3.4	vertical and diagonal ice lenses	dark grey, sandy silty, fine layered	plant detritus layers	40.9	29.0	x Rhizon	see Buo-05-B-12 + u
Buo-05-B-20 + u	6.4	3.1	vertical and diagonal ice lenses	dark grey, sandy silty, fine layered	plant detritus layers	29.8	23.0		see Buo-05-B-12 + u
Buo-05-C-21	6.7	2.8	diagonal coarse ice lenses	grey clayey, alternate bedding, molluscs, fine layered	plant detritus rich layers	37.4	27.2		

Sample	Depth	Height	Cryotexture	Sediment	Organic	ice grav.	ice abs.	TI	Remarks
	m b.s.	m a.s.l.				wt %	wt %		
Buo-05-C-22	7.0	2.5	diagonal coarse ice lenses	same like Buo-05-B-20	same like Buo-05-B-20	37.6	27.3		
Buo-05-C-23	7.3	2.2	diagonal coarse ice lenses	same like Buo-05-B-20	same like Buo-05-B-20	42.3	29.7	x Rhizon	
Buo-05-C-24	7.6	1.9	diagonal coarse ice lenses	same like Buo-05-B-20	same like Buo-05-B-20	37.5	27.3		
Buo-05-C-25	8.0	1.5	ice veins, horizontal ice lenses	greyish with Fe-oxide spots (10x5cm), sandy, disturbed / washed structures, more brownish parts	plant detritus, filament roots	43.1	30.1		detailed photo
Buo-05-C-26	8.3	1.2	ice veins, horizontal ice lenses	greyish with Fe-oxide spots, sandy	plant detritus, filament roots	29.4	22.7	x Rhizon	
Buo-05-C-27	8.6	0.9	ice veins, horizontal ice lenses, less ice content	Fe-oxide spots, drier than above	plant detritus, filament roots	31.5	23.9		
Buo-05-C-28	8.9	0.6	several horizontal and vertical ice lenses	grey, sandy, alternate bedding, molluscs, fine layered, vivianite	plant detritus layers, macro detritus, roots	31.5	23.9		
Buo-05-C-29	9.2	0.3	several lenses, vertical orientated	grey, dry, sandy, fine layered	plant detritus layers	34.9	25.9	n	
Buo-05-C-30	9.4	0.1	diagonal and vertical oriented ice lenses	dark grey, less sandy, fine layered	plant detritus layers	45.7	31.3		

APPENDIX 2

List of ice wedge and precipitation samples

Abbreviations a.s.l. – above surface level
b.s. – below surface
EC – electrical conductivity

No	Sample	Depth	Height	Sample distance	Remarks	Hydro-chemistry	pH	EC
		m b.s.	m a.s.l.	m				µS/cm
Ice wedge near profile Buo-01, N 71.58146°, E 132.20801°								
1	Buo-01-A-100	0.7	8.7		sample for ^{36}Cl dating			
2	Buo-01-A-101	0.5	8.9	0.15	vertical cut, milky-white, gas bubbles < 1 mm, less sedi-ment, 0.9 m wide on top, 0.3 m wide in 1 m depth			75
2	Buo-01-A-102	0.5	8.9	0.15	see Buo-01-A-101			52
3	Buo-01-A-103	0.5	8.9	0.15	see Buo-01-A-101	x		
4	Buo-01-A-104	0.5	8.9	0.15	see Buo-01-A-101			50
5	Buo-01-A-201	1	8.4	0.3	diagonal cut, 3 m width visible, milky-white, 4m right of Buo.01-A-101 to104, surface with high centre polygons			
6	Buo-01-A-202	1	8.4	0.3	see Buo-01-A-201			
7	Buo-01-A-203	1	8.4	0.3	see Buo-01-A-201			
8	Buo-01-A-204	1	8.4	0.3	see Buo-01-A-201			
9	Buo-01-A-205	1	8.4	0.3	see Buo-01-A-201			
Ice wedge near profile Buo-04, N 71.60048°, E 132.22670°								
10	Buo-04-A-100	2	16.6		in the area of Buo-04-B-12, sample for ^{36}Cl dating			128
11	Buo-04-A-101	2	16.6	0.5	diagonal cut, 10 m width visible, mm big bubbles, sediment veins included, light-grey ice			
12	Buo-04-A-102	2	16.6	0.5	see Buo-04-A-101			
13	Buo-04-A-103	2	16.6	0.5	see Buo-04-A-101			
14	Buo-04-A-104	2	16.6	0.5	see Buo-04-A-101			
15	Buo-04-A-105	2	16.6	0.5	see Buo-04-A-101			
16	Buo-04-A-106	2	16.6	0.5	see Buo-04-A-101			
17	Buo-04-A-107	2	16.6	0.5	see Buo-04-A-101			
18	Buo-04-A-108	2	16.6	0.5	see Buo-04-A-101	x	7.8	124
19	Buo-04-A-109	2	16.6	0.5	see Buo-04-A-101			
20	Buo-04-A-110	2	16.6	0.5	see Buo-04-A-101			
21	Buo-04-A-111	2	16.6	0.5	see Buo-04-A-101			

No	Sample	Depth	Height	Sample distance	Remarks	Hydro-chemistry	pH	EC
		m b.s.	m a.s.l.	m				µS/cm
22	Buo-04-A-112	2	16.6	0.5	see Buo-04-A-101			
23	Buo-04-A-113	2	16.6	0.5	see Buo-04-A-101			
24	Buo-04-A-114	2	16.6	0.5	see Buo-04-A-101			
25	Buo-04-A-115	2	16.6	0.5	see Buo-04-A-101			
26	Buo-04-A-116	2	16.6	0.5	see Buo-04-A-101	x	7.5	158
27	Buo-04-A-117	2	16.6	0.5	see Buo-04-A-101			
28	Buo-04-A-118	2	16.6	0.5	see Buo-04-A-101			
29	Buo-04-A-119	2	16.6	0.5	see Buo-04-A-101			
30	Buo-04-A-120	2	16.6	0.5	see Buo-04-A-101			
31	Buo-04-A-121	2	16.6	0.5	see Buo-04-A-101			
Ground ice near Buo-05, N 71.58241°, E 132.20941°								
32	Buo-05-A-101	0.8	8.7		isolated thick ice vein with sediment veins		7.05	123
33	Buo-05-A-102	0.8	8.7		see Buo-05-A-101			
34	Buo-05-B-103	2.8	6.7		ice wedge, ice vein, width 2 cm, bubbles and milky colour	x	7.12	118
35	Buo-05-C-104	7.4	2.3		looks like firn/snow, milky coarse grained ice	x	6.5	72
36	Buo-05-C-105	9.6	0.0		ice wedge?, end of the profile, close to the beach level	x	6.4	83
Precipitation samples, N 71.56667°, E 132.19631°								
37	Buo-rain-01				10/08/10, 04:00			
38	Buo-rain-02				12/08/10, 09:00			
39	Buo-rain-03				12/08/10, 13:00			
40	Buo-rain-04				13/08/10, 09:00			
41	Buo-rain-05				13/08/10, 22:00			
42	Buo-rain-06				14/08/10, 08:00			
43	Buo-rain-07				15/08/10, 09:30			
44	Buo-rain-08				17/08/10, 08:00			
45	Buo-rain-09				18/08/10, 09:00			
46	Buo-rain-10				13/08-16/08/10			

APPENDIX 3

List of collected mammal bones

Sample	Taxon	Skeleton element	Preservation	Locality	Coordinates	Note
Buo 001	*Equus* sp.	humerus	damaged	beach between camp and 2nd Yedoma		
Buo 002	*M. primigenius*	tooth	fragment			
Buo 003	Large herbivore animal	pelvis	fragment			
Buo 004	*R. tarandus*	tibia		thermoterrace Yedoma exposure	N 71,38361° E 132,08397°	
Buo 005	*R. tarandus*	tibia	damaged			
Buo 006	*R. tarandus* ?	ph I		beach between camp and 2nd Yedoma		
Buo 007	*Equus* sp.	humerus	damaged	beach		
Buo 008	*M. primigenius*	tooth	fragment			
Buo 009	Large herbivores animal	costa?	fragment			
Buo 010						
Buo 011	*R. tarandus* ?	tibia	fragment			
Buo 012	*M. primigenius*?	skull	fragment	thermoterrace near the polygon pond site BK 5		
Buo 013	*M. primigenius*	costa	fragment	beach		
Buo 014	*R. tarandus*	mandible with two teeth	fragment	beach		
Buo 015	*M. primigenius*	tusk				
Buo 016	*Lepus* sp.?	lumbar vertebra	damaged			juv.
Buo 017	R. tarandus	ph I				
Buo 018						
Buo 019						
Buo 020	*Equus* sp.	cervical vertebra	damaged			
Buo 021	*M. primigenius*	tusk	fragment	at profile Buo-05	N 71,58241 E 132,20941	
Buo 022	*M. primigenius* ?	costa	fragment	in front of the Yedoma exposure, next to a thermokarst lake	N 71° 36,120' E 132° 15,597'	
Buo 023	*M. primigenius* ?	costa	fragment			
Buo 024	*M. primigenius* ?	costa	fragment			juv.
Buo 025	*M. primigenius* ?	costa	fragment			
Buo 026	*M. primigenius* ?	costa	fragment			
Buo 027	*M. primigenius* ?	costa	fragment			
Buo 030	*M. primigenius* ?	costa	fragment			juv.
Buo 031	*M. primigenius* ?	costa	fragment			
Buo 032	*M. primigenius* ?	costa	fragment			
Buo 035	*M. primigenius* ?	costa	fragment			
Buo 036	*M. primigenius* ?	costa	fragment			juv.
Buo 037	*M. primigenius* ?	costa	fragment			
Buo 038	*M. primigenius* ?	costa	fragment			juv.
Buo 039	*M. primigenius* ?	costa	fragment			juv.
Buo 040	*M. primigenius* ?	costa	fragment			juv.
Buo 041	*M. primigenius* ?	costa	fragment			
Buo 042	*M. primigenius*	1-st costa	fragment			juv.

Sample	Taxon	Skeleton element	Preservation	Locality	Coordinates	Note
Buo 043	*M. primigenius* ?	costa	fragment			
Buo 045	*R. tarandus*	scapula	fragment			
Buo 046	*M. primigenius* ?	costa	fragment			
Buo 047	Mammalia	vertebra				
Buo 048	*M. primigenius*	cervical vertebra	damaged			juv.
Buo 049	*M. primigenius*	vertebra	fragment			
Buo 050	*M. primigenius*	7-th cervical vertebra	damaged			juv.
Buo 051	Mammalia	sacrum vertebra				
Buo 052	*M. primigenius*	sacrum	fragment			
Buo 053	*M. primigenius* ?	skull	fragment			
Buo 054	*M. primigenius*	tooth	fragment			
Buo 055	Mammalia	skull	fragment			
Buo 056	*M. primigenius*	tooth	fragment			
Buo 057						
Buo 058	*M. primigenius*	tooth				
Buo 059	*M. primigenius*	tooth	fragment			
Buo 060	*M. primigenius*	tooth	damaged			
Buo 061	*M. primigenius*	skull with tooth	fragment			
Buo 062	*M. primigenius* ?	lumbar vertebra	fragment			juv.
Buo 063	*M. primigenius* ?	skull	fragment			
Buo 064						
Buo 065	*M. primigenius* ?	skull	fragment			
Buo 066	*M. primigenius*	mandible, left stem	fragment			
Buo 067	*M. primigenius*	pelvis	fragment			
Buo 068	*M. primigenius*	pelvis	fragment			
Buo 069	Large herbivore animal	pelvis	fragment			
Buo 070	Large herbivore animal	pelvis	fragment			
Buo 071	*M. primigenius*	ulna	fragment			juv.
Buo 072	*M. primigenius*	tibia	fragment			juv.
Buo 073	*M. primigenius*	costa?	fragment			
Buo 074	*R. tarandus*	skull with antler	fragment			
Buo 075	*M. primigenius*	calcaneus				
Buo 076						
Buo 077	*Equus* sp.	tibia	distal fragment			
Buo 078	*M. primigenius*	tibia				juv.
Buo 079	Mammalia	vertebra	damaged			juv.
Buo 080	*M. primigenius*	astrogalus				
Buo 081	Large herbivore animal	limb bone				
Buo 082	*M. primigenius*	metapodium	damaged			juv.
Buo 083	*M. primigenius*	thorax vertebra	fragment			juv.
Buo 084	*M. primigenius*	sacrum	fragment			juv.
Buo 085	*M. primigenius*	humerus				juv.
Buo 086	*M. primigenius* ?	limb bone				
Buo 087	*M. primigenius*	humerus	distal fragment			juv. ?
Buo 088	*M. primigenius*	femur	distal fragment			juv. ?

Sample	Taxon	Skeleton element	Preservation	Locality	Coordinates	Note
Buo 089						
Buo 090	Large herbivore animal	sacrum	fragment			
Buo 091	*M. primigenius*	femur	distal fragment			juv. ?
Buo 092	*Equus* sp.	Mt III				
Buo 093						
Buo 094	*M. primigenius*	scull	fragment			
Buo 095						
Buo 096	Mammalia	vertebra	fragment			
Buo 097						
Buo 098	Large herbivore animal	scapula?	fragment			
Buo 099	*M. primigenius*	costa	fragment			juv.
Buo 100	*M. primigenius*	metapodium	damaged			juv.
Buo 101	Mammalia	vertebra	fragment			
Buo 102	*M. primigenius*	vertebra				juv.
Buo 103	*M. primigenius*	limb bone	fragment			juv.
Buo 104	*M. primigenius*	humerus				juv. ?
Buo 105	*M. primigenius*	humerus	distal fragment			juv. ?
Buo 106	*M. primigenius*	radius				juv. ?
Buo 107						
Buo 108	*M. primigenius* ?	skull	fragment			
Buo 109 A						
Buo 109 B	*M. primigenius* ?	skull	fragment			
Buo 110	*M. primigenius*	tibia ?	fragment			juv. ?
Buo 112	*M. primigenius* ?	skull	fragment			
Buo 113	*M. primigenius* ?	skull	fragment			
Buo 114						
Buo 115 A						
Buo 115 B						
Buo 116						
Buo 117	*M. primigenius* ?	skull ?	fragment			
Buo 118	*M. primigenius* ?	skull	fragment			
Buo 119						
Buo 120				thermo-terrace, 3rd Yedoma	N 71° 38,524'; E 132° 16,153'	
Buo 121						
Buo 122						
Buo 123	*M. primigenius*	vertebra	fragment			
Buo 124	*M. primigenius* ?	costa?	fragment			
Buo 125	*M. primigenius*	mandible, left stem	fragment			
Buo 126	M. primigenius	epistropheus	damaged			
Buo 127	*M. primigenius* ?	skull ?	fragment			
Buo 128	*M. primigenius* ?	skull ?	fragment			
Buo 129	*Equus* sp.	scupula	damaged			
Buo 130	*M. primigenius*	skull	fragment			
Buo 131						

Sample	Taxon	Skeleton element	Preservation	Locality	Coordinates	Note
Buo 132	*M. primigenius*	pelvis	fragment			
Buo 133	*M. primigenius*	skull	fragment			
Buo 134	*M. primigenius*	1-st costa	damaged			
Buo 135	*M. primigenius*	skull	fragment			

Die "Berichte zur Polar- und Meeresforschung" (ISSN 1866-3192) werden beginnend mit dem Heft Nr. 569 (2008) ausschließlich elektronisch als Open-Access-Publikation herausgegeben. Ein Verzeichnis aller Hefte einschließlich der Druckausgaben (Heft 377-568) sowie der früheren **"Berichte zur Polarforschung** (Heft 1-376, von 1982 bis 2000) befindet sich im Internet in der Ablage des electronic Information Center des AWI (**ePIC**) unter der URL http://epic.awi.de. Durch Auswahl "Reports on Polar- and Marine Research" auf der rechten Seite des Fensters wird eine Liste der Publikationen in alphabetischer Reihenfolge (nach Autoren) innerhalb der absteigenden chronologischen Reihenfolge der Jahrgänge erzeugt.

To generate a list of all Reports past issues, use the following URL: http://epic.awi.de and select the right frame to browse "Reports on Polar and Marine Research". A chronological list in declining order, author names alphabetical, will be produced, and pdf-icons shown for open access download.

Verzeichnis der zuletzt erschienenen Hefte:

Heft-Nr. 617/2010 — "The Expedition of the Research Vessel 'Polarstern' to the Amundsen Sea, Antarctica, in 2010 (ANT-XXVI/3)", edited by Karsten Gohl

Heft-Nr. 618/2010 — "Sozialhistorische Studie zur Polarforschung anhand von deutschen und österreich-ungarischen Polarexpeditionen zwischen 1868-1939", by Ursula Rack

Heft-Nr. 619/2010 — "Acoustic ecology of marine mammals in polar oceans", by Ilse Van Opzeeland

Heft-Nr. 620/2010 — "Cool Libraries in a Melting World - Proceedings of the 23rd Polar Libraries Colloquy 2010, June 13-18, 2010, Bremerhaven, Germany", edited by Marcel Brannemann and Daria O. Carle

Heft-Nr. 621/2010 — "The Expedition of the Research Vessel 'Polarstern' to the Arctic in 2010 (ARK-XXV/3)", edited by Volkmar Damm

Heft-Nr. 622/2010 — "Environmentally induced responses of *Donax obesulus* and *Mesodesma donacium* (Bivalvia) inhabiting the Humboldt Current System", by Daniel Carstensen

Heft-Nr. 623/2010 — "Research in the Laptev Sea region - Proceedings of the joint Russian-German workshop, November 8-11, 2010, St. Petersburg, Russia", edited by Sebastian Wetterich, Paul Pier Overduin and Irina Fedorova

Heft-Nr. 624/2010 — "The Expedition of the Research Vessel 'Polarstern' to the Arctic in 2010 (ARK-XXV/2)", edited by Thomas Soltwedel

Heft-Nr. 625/2011 — "The Expedition of the Research Vessel 'Polarstern' to the Arctic in 2010 (ARK-XXV/1)", edited by Gereon Budéus

Heft-Nr. 626/2011 — "Towards data assimilation in ice-dynamic models: the (geo)physical basis", by Olaf Eisen

Heft-Nr. 627/2011 — "The Expedition of the Research Vessel 'Polarstern' to the Arctic in 2007 (ARK-XXII/1a-c)", edited by Michael Klages & Jörn Thiede

Heft-Nr. 628/2011 — "The Expedition of the Research Vessel 'Polarstern' to the Antarctic in 2010 (ANT-XXVII/1)", edited by Karl Bumke

Heft-Nr. 629/2011 — "Russian-German Cooperation SYSTEM LAPTEV SEA: The expedition Eastern Laptev Sea - Buor Khaya Peninsula 2010" edited by Sebastian Wetterich, Pier Paul Overduin and Mikhail Grigoriev